(1)

SYSTEMS, SCIENCE AND SOFTWARE

DRAFT

SSS-R-81-4668

SYNTHESIS OF Lg IN EASTERN UNITED STATES CRUSTAL MODELS WITH FREQUENCY INDEPENDENT Q

T. C. BACHE
H. SWANGER
B. SHKOLLER

SEMI-ANNUAL TECHNICAL REPORT

SPONSORED BY
ADVANCED RESEARCH PROJECTS AGENCY
ARPA ORDER No. 3291-32

This research was supported by the Advanced Research Projects Agency of the Department of Defense and was monitored by the Air Force Office of Scientific Research under Contract No. F49620-80-C-0019.

S³ PROJECT No. 11127

SEPTEMBER 1980

P. O. BOX 1620, LA JOLLA, CALIFORNIA 92038, TELEPHONE (714) 453-0060

ARPA Order No. 3291-32, Program Code No. 0D60

Contractor: Systems, Science and Software

Effective Date of Contract: 1 October 1979

Contract Expiration Date: 30 September 1980

Amount of Contract: $88,024

Contract No: F49620-80-C-0019

Principal Investigator and Phone No:
Dr. Thomas C. Bache, (714) 453-0060, Ext. 337

Program Manager and Phone No:
Dr. Thomas C. Bache, (714) 453-0060, Ext. 337

Title: Theoretical Basis for Regional Discrimination

Unclassified

SECURITY CLASSIFICATION OF THIS PAGE (When Data Entered)

REPORT DOCUMENTATION PAGE

READ INSTRUCTIONS BEFORE COMPLETING FORM

1. REPORT NUMBER (19): (18) AFOSR TR-81-0145
2. GOVT ACCESSION NO.: AD-A096
3. RECIPIENT'S CATALOG NUMBER: 340

4. TITLE (and Subtitle): (6) SYNTHESIS OF Lg IN EASTERN UNITED STATES CRUSTAL MODELS WITH FREQUENCY INDEPENDENT Q
5. TYPE OF REPORT & PERIOD COVERED: INTERIM
6. PERFORMING ORG. REPORT NUMBER

7. AUTHOR(s): (10) Thomas C. Bache, H. Swanger, B. Shkoller
8. CONTRACT OR GRANT NUMBER(s): (15) F49620-80-C-0019, ARPA Order-3291

9. PERFORMING ORGANIZATION NAME AND ADDRESS: Systems, Science & Software, P.O. Box 1620, La Jolla, CA 92038
10. PROGRAM ELEMENT, PROJECT, TASK AREA & WORK UNIT NUMBERS: 61102F (16) 3291 (17) 32

11. CONTROLLING OFFICE NAME AND ADDRESS: AFOSR/ NP, Bolling AFB, DC 20332
12. REPORT DATE: (11) September, 1980
13. NUMBER OF PAGES: 120 (12) 121

14. MONITORING AGENCY NAME & ADDRESS (if different from Controlling Office): (9) Semi-annual technical rept.
15. SECURITY CLASS. (of this report): unclassified
15a. DECLASSIFICATION DOWNGRADING SCHEDULE

16. DISTRIBUTION STATEMENT (of this Report): (14) SSS-R-81-4668

Approved for public release; distribution unlimited.

17. DISTRIBUTION STATEMENT (of the abstract entered in Block 20, if different from Report)

18. SUPPLEMENTARY NOTES

19. KEY WORDS (Continue on reverse side if necessary and identify by block number)

Lg, synthetic seismograms, nuclear explosion detection

388507

20. ABSTRACT (Continue on reverse side if necessary and identify by block number)

The parametric dependence of short period Lg on characteristics of the source and travel path is studied using synthetic seismograms computed by modal superposition. The earth models are plane-layered and laterally homogeneous with a frequency-independent Q, and are meant to represent the eastern United States. The Q and velocity structure of the 34 km thick crust are varied with the upper mantle being represented by a halfspace.

Synthetic seismograms that qualitatively match many observed features of eastern United States Lg are computed with 35 to 50 modes in models that include

UNCLASSIFIED

some lower velocity sediments and low Q near the surface. The observations are represented by the LRSM short period recordings of the SALMON nuclear explosion in Mississippi. Three quantitative data features not reproduced by the synthetics are: (1) There is not enough energy at group velocities less than 2.9 km/sec; (2) The synthetic spectra fall off more rapidly above 2.5 Hz than observed spectra from SALMON; (3) the amplitude attenuation with range is much faster than observed in the eastern United States. While some of this may be due to not including the multipathing and scattering that must be present at these high frequencies, the requirement for frequency-dependent Q is strongly indicated.

Since many qualitative features of Lg are reproduced by the synthetic seismograms, they are computed for double-couple sources at several orientations to delineate the gross dependence of Lg on source depth. Strike-slip and 45 degree dip-slip earthquakes show a similar uniform amplitude decrease with depth. Vertical dip-slip sources show the opposite trend, with amplitude increasing with depth between 1 and 25 km depths in an eastern United States model.

TABLE OF CONTENTS

TABLE OF CONTENTS (continued)

LIST OF FIGURES

LIST OF FIGURES (continued)

LIST OF FIGURES (continued)

ABSTRACT

The parametric dependence of short period Lg on characteristics of the source and travel path is studied using synthetic seismograms computed by modal superposition. The earth models are plane-layered and laterally homogeneous with a frequency-independent Q, and are meant to represent the eastern United States. The Q and velocity structure of the 34 km thick crust are varied with the upper mantle being represented by a halfspace.

Synthetic seismograms that qualitatively match many observed features of eastern United States Lg are computed with 35 to 50 modes in models that include some lower velocity sediments and low Q near the surface. The observations are represented by the LRSM short period recordings of the SALMON nuclear explosion in Mississippi. Three quantitative data features not reproduced by the synthetics are: (1) There is not enough energy at group velocities less than 2.9 km/sec; (2) The synthetic spectra fall off more rapidly above 2.5 Hz than observed spectra from SALMON; (3) The amplitude attenuation with range is much faster than observed in the eastern United States. While some of this may be due to not including the multipathing and scattering that must be present at these high frequencies, the requirement for frequency-dependent Q is strongly indicated.

Since many qualitative features of Lg are reproduced by the synthetic seismograms, they are computed for double-couple sources at several orientations to delineate the gross dependence of Lg on source depth. Strike-slip and 45° dip-slip earthquakes show a similar uniform amplitude decrease with depth. Vertical dip-slip sources show the opposite trend, with amplitude increasing with depth between 1 and 25 km depths in an eastern United States model.

THIS PAGE LEFT BLANK

I. INTRODUCTION AND SUMMARY

The objective of this contract is to apply theoretical seismogram methods to determine the dependence of the important regional phases, especially Lg, on characteristics of the source and travel path. Our approach is to construct synthetic seismograms that resemble the data, to delineate the parametric dependence of these seismograms, and then to attempt to explain observed features of the data, using the models as a guide. Such an approach has been quite successful in improving understanding of teleseismic data, but has scarcely been attempted for regional data. There seem to be two reasons for this. One is that the regional data characteristics have not been studied very thoroughly, but this deficiency is rapidly being corrected. The second is that the construction of realistic synthetic seismograms at regional distances is relatively difficult and convenient techniques have not been available. We have developed a set of programs for superposition of the normal modes for an earth model which provide a convenient synthesis tool, and these programs are applied in the research described in this report.

The main body of this report includes three sections and we will summarize the main results from each. In Section II we describe our modal superposition method for computing synthetic seismograms and compare with results from a direct wave-number integration program that computes the total solution. Section III is concerned with the synthesis of Lg for shallow explosions. We consider crustal models that represent the eastern United States and study the effect of realistic parameter variations on the characteristics of synthetic Lg compared to observations. Using one of the "best" crustal models of Section III, we compute the theoretical dependence of Lg on source depth for point double-couple representations for earthquakes. The results are described in Section IV.

In this report we are only concerned with synthesizing Lg. All the earth models to be discussed include the upper mantle as a

halfspace. Therefore, the cutoff velocity for the modal calculations is about 4.5 km/sec, the shear velocity of the upper mantle, and energy travelling with greater velocities is not included in the modal solution. But how well do the modes represent the total solution for apparent velocities less than 4.5 km/sec? This can only be determined (for complex structures) by comparing with total solutions.

In Section II we compare the modal seismograms with seismograms computed with the direct wave-number integration program PROSE (Apsel, 1979). The comparison has some uncertainties, but does indicate that the modes include most of the important features of the seismogram in the included group velocity window. More complete and unambiguous comparisons are being done with PROSE and with a direct wave-number integration program recently developed at S-Cubed, and these will be described in our next report.

Most of the important results are included in our rather lengthy Section III. The question addressed in that Section can be framed as follows: Using plane-layered, laterally homogeneous crustal models with frequency-independent Q, can the main observed characteristics of Lg in the eastern United States be reproduced? The observations are represented by the SALMON nuclear explosion in Mississippi. These observations are consistent with the trends observed for eastern United States earthquakes, but are especially convenient for synthetic seismogram studies because we know the source function rather well. We emphasize that we are not trying to model the SALMON recordings in detail, but are using them to represent a broad class of eastern U.S. Lg observations.

The results of Section III can be quickly summarized. Standard earth models give synthetic Lg seismograms with a realistic appearance as long as they include some lower velocity, low Q material near the surface (within a kilometer or so). If this is not included, an unrealistic fundamental model dominates the seismogram. We can probably think of the low velocity, low Q layers near

the surface as representing, in a crude way, the lateral heterogeneity that must be quite strong over the multi-hundred kilometer paths studied.

There are three basic features of the data that we are unable to reproduce. These are:

1. The synthetics do not include the high frequency energy arriving with apparent velocities slower than 2.9 km/sec that is a prominent feature of the observations.

2. The synthetic spectra fall off more rapidly at high frequencies than the observed SALMON spectra.

3. The amplitude attenuation with range is much faster than is observed in the eastern United States for earthquakes or explosions.

The first deficiency may be to some degree explained by arguing that the late arriving high frequency energy must be associated with multipathing and scattering by lateral heterogenities. This can never be reproduced with the laterally homogeneous models used. If this is the primary reason for the first deficiency, we could focus our attention on the portion of the wavetrain before 2.9 km/sec and not be much concerned with the rest.

The second two deficiencies (and, probably, some of the first) are almost certainly due to deficiencies in our model for Q. In Section II we describe some parameter studies that suggest that no frequency-independent Q model will be able to match all aspects of the data. A frequency-dependent Q is strongly suggested. We will be describing results from such models in our next report.

The better crustal models used in Section III do reproduce many important features of the Lg observations. Therefore, they should be able to delineate the gross dependence of Lg on source depth. In Section IV we compute synthetic seismograms to plot this dependence. This is done for four sources; an explosion and point double-couples at three basic orientations (strike-slip, vertical dip-slip and 45° dip-slip). The explosion source gives an

unrealistic portrayal of Lg amplitude depth-dependence, which is an interesting result, even though explosions are not practical sources below a few kilometers.

The Lg amplitude decreases with depth at the same rate for strike-slip and 45° dip-slip earthquake sources. The decrease is fairly uniform and is a factor of 4 to 5 between 1 and 25 kilometers. The vertical dip-slip source shows the opposite trend, with the amplitude increasing with depth at about the same rate.

II. SEISMOGRAM SYNTHESIS BY MODAL SUPERPOSITION

2.1 INTRODUCTION

Our attention in this report is directed toward the synthesis of Lg and slower phases. Modal superposition is an especially convenient method for synthesizing this portion of the seismogram. We begin with a brief description of the method. We will then compare synthetic seismograms computed with modal superposition with seismograms computed with direct wave-number integration.

Direct wave-number integration leads to a complete solution which, in principle, is "exact." However, direct wave-number integration is computationally very difficult and requires some numerical compromises that inevitably degrade the solution to some degree. This must be considered when evaluating comparisons between the two methods for complex problems.

2.2 DESCRIPTION OF THE METHOD

For a spherical earth the normal modes give the complete ground motion. Knopoff, Schwab and their colleagues (e.g., Knopoff, et al., 1973; Panza and Calcagnile, 1975; Nakanishi, et al, 1977; Montovani, et al, 1977) have used Love wave modal superposition to compute synthetic seismograms in numerous studies of the properties of various observed phases. Modes also give the complete solution for a plane-layered elastic plate over a rigid halfspace. D. V. Harvey and C. B. Archambeau of the University of Colorado have been using this concept to construct "complete" seismograms for regional ground motions from earthquakes (Harvey, 1980).

We have developed a program based on Knopoff's method (Schwab and Knopoff, 1972) that allows rapid and inexpensive computation of all Rayleigh and Love wave modes up to the highest frequencies of interest for seismological problems. The root finding program improves on the basic Schwab and Knopoff algorithm by taking advantage of the frequency independence of many of the computed parameters as the mode search is conducted at a fixed phase velocity.

The published Schwab and Knopoff (1972) algorithm is for calculation of the Love and Rayleigh secular functions only. For seismogram synthesis, excitation parameters and modal eigenfunctions are required. The Laplace's expansion technique used by Schwab and Knopoff has been extended to compute these quantities using the interval elements of the root-finding program. The computed eigenfunctions seem to be relatively insensitive to the instabilities that compromise the accuracy of high frequency calculations with previously available surface wave programs.

2.3 COMPARISON OF MODAL SUPERPOSITION WITH THE COMPLETE SOLUTION FROM PROSE

For a standard earth model, the normal modes represent only a portion of the solution. But the excluded part of the solution may not be very important for many problems of interest. Unfortunately, it is not easy to know what the modal solution is missing without doing the full calculation to see. In this section, we will compare some modal solutions with total solutions obtained with direct wave-number integration.

The layered earth model chosen for our comparison calculations is listed in Table 1. The first 50 Rayleigh wave modes were computed for this structure and the phase and group velocity dispersion are plotted in Figure 1. The cutoff velocity is 4.52 km/sec, the shear velocity of the halfspace. The modal solution can include no energy traveling faster than this velocity.

The comparison calculations were done by Dr. John Orcutt, Scripps Institute of Oceanography, with the PROSE program (Apsel, 1979; Apsel, et al., 1980). This program is much more expensive than the modal superposition program and the cost scales up rapidly with frequency and source-receiver range. The problem parameters were chosen to minimize the expense.

Synthetic seismograms were computed at four ranges (50, 100, 150, 200 km) for a point double-couple representing strike-slip faulting at a depth of 1 km. The azimuth was 45 degrees from the strike and the source time function was a step with a moment of

TABLE 1

EARTH MODEL FOR COMPARING MODE AND DIRECT WAVE-NUMBER INTEGRATED SEISMOGRAMS

Depth (km)	Thickness (km)	α (km/sec)	β (km/sec)	ρ (gm/sec^3)	Q_β
1.5	1.5	3.7	2.16	2.1	35
8.0	6.5	6.1	3.3	2.85	250
34.0	26.0	6.6	3.59	3.05	1800
∞	∞	8.1	4.52	3.35	2000

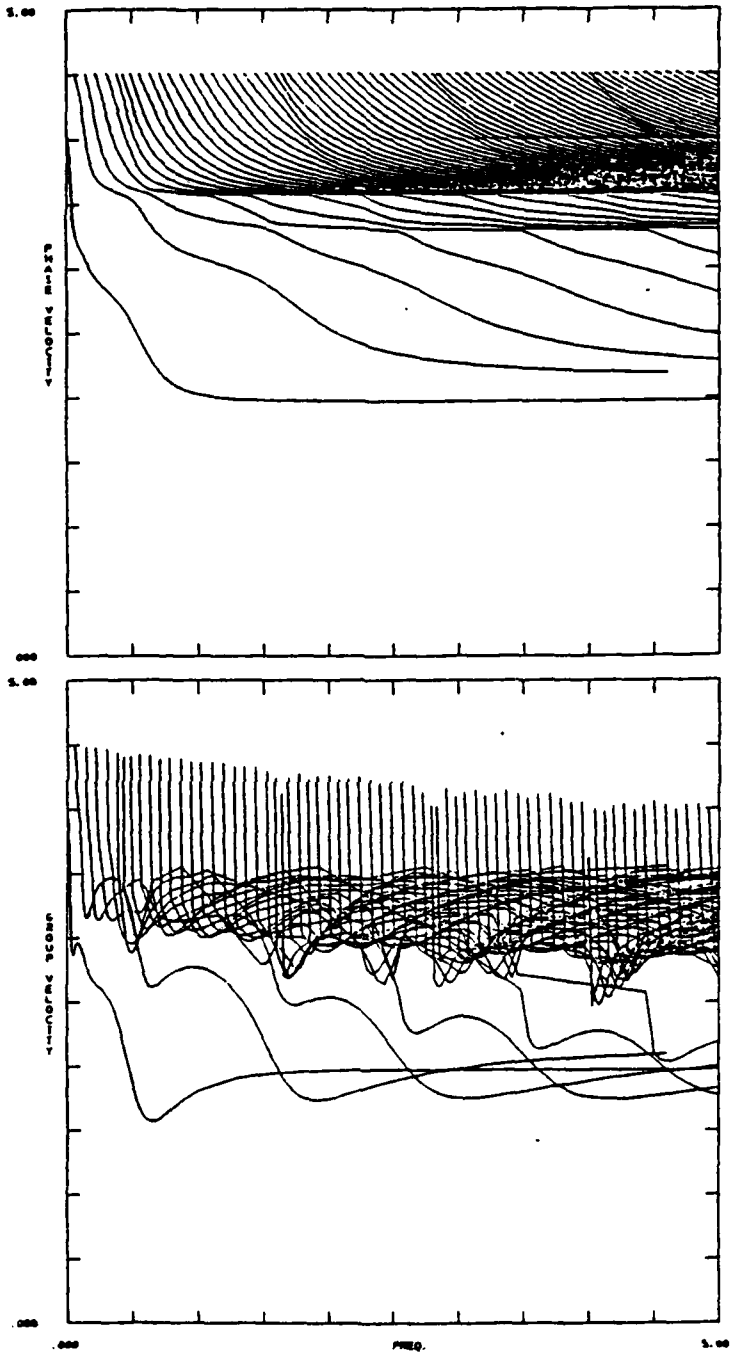

Figure 1. Phase and group velocity dispersion for the model of Table 1.

10^{22} dyne-cm. The WWSSN short period instrument response was applied and the calculations were done with a Nyquist frequency of 5 Hertz after tapering the spectrum to zero between 0.5 and 1.0 Hertz with a cosine-squared filter. (Only thirteen modes contribute to frequencies less than 1 Hertz.) Making appropriate adjustments for the fact that the spectrum is tapered after applying the seismometer response, the tapering filter could be considered part of the source spectrum. It has a strong influence on the solution.

The seismograms are compared in Figure 2 in two ways, on the basis of their waveforms and on the basis of their peak-to-peak amplitudes. The waveform comparisons show that the modes include most of the important features, especially for group arrival times associated with velocities of 3.5 km/sec and slower. Energy arriving with group velocities much faster than 3.5 km/sec is very small for this example.

The amplitude comparison is not very satisfactory. We suspect some minor incompatibility in our specification of the filters used to construct the seismograms, and are attempting to resolve it. We have computed seismograms with both methods in a halfspace where the exact Rayleigh wave solution is easily computed. The methods agree within a few percent when the true ground motion (no filters) is compared.

An irresolvable difference between the PROSE and mode calculations is in the specification of attenuation. In PROSE, attenuation is introduced by computing with complex velocities. The route could be followed for our modal calculations, but only with a large increase in computational effort. We chose to include Q by computing an effective attenuation factor using the theory introduced by Anderson and Archambeau (1964). This first-order perturbation theory is usually used for surface waves. The two methods should give nearly the same results for high Q, but our structure (Table 1) includes low Q in the near surface layers. Our impression is that most of the waveform and amplitude differences between the PROSE and modal seismograms in Figure 2 is due to differences in the way the Q is introduced.

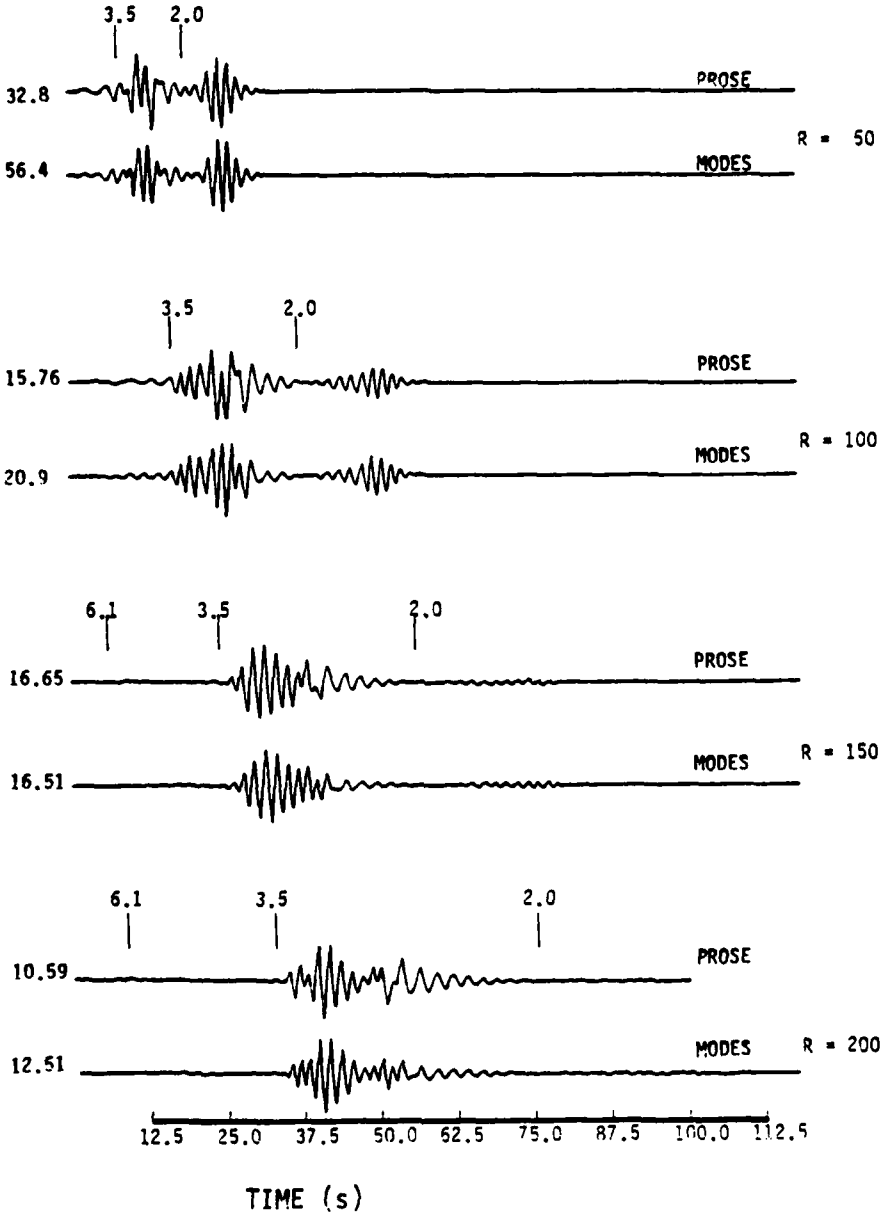

Figure 2. Synthetic seismograms computed with modal superposition are compared with those computed with PROSE. Zero on the time scale of the plots is reduced by R/8.1. The maximum peak-to-peak amplitude in microns is shown at the left and several interesting group velocities are marked in each set.

III. SYNTHESIS OF Lg FOR SHALLOW EXPLOSIONS

3.1 INTRODUCTION

The Lg phase is a high frequency wavetrain which arrives with a group velocity near 3.5 km/sec. It is observed on all three components for both explosions and earthquakes. In this section, we address the following question; using modal superposition for plane-layered earth models, can realistic Lg phases be synthesized for shallow explosions?

To address this question we consider only models that are appropriate for the eastern United States (EUS). The gross characteristics of the crust in this region are fairly well understood, but details vary from place-to-place. We compute seismograms for a number of different models, but they are all meant to be "appropriate for the EUS."

One reason for focussing on EUS crustal models is that this region is representative of stable platform areas that also occur in Eurasia. Also, there was a nuclear explosion experiment, SALMON (5.3 KT) near the southern edge of the region. This event, which was at a depth of 830 meters in Mississippi, was recorded at many stations in the EUS. The Lg phase on these recordings, though not as clear as for many earthquakes, serves as a convenient and useful standard for comparison.

Before continuing, we should say what it means to synthesize Lg seismograms that "match" the data. We will be using the LRSM short period recordings of SALMON (see Figure 20 in Section 3.4) to represent the data, since it is the only large explosion in the eastern U.S. and does have a source function that is rather well known. However, the Lg phase is not very prominent on the LRSM short period seismograms and the onset is not easy to time. Qualitatively, the Lg is a high frequency, extended wavetrain that has a group arrival time near 3.5 km/sec. As we study the phase in more detail, quantitative features that become important are the approximate duration, the spectral asymptotes and the amplitude.

We find that syntnetic seismograms which include Lg phases that are qualitatively similar to the observations can be computed witn earth models that include sufficient detail. However, simple models deduced from observations of the fundamental mode surface waves do not give realistic seismograms. It is necessary to have some low velocity, low Q material at the surface. Gradients in the mid-crust seem to be required if the arrival is to be emergent, as it often is. On the other hand, sharp Lg arrivals can be synthesized with a thick, uniform layer at the base of the crust.

We also conclude that the slow (<2.9 km/sec) high frequency arrivals seen on the observed records are probably impossible to compute with plane-layered models. Some scattering and/or multipathing is probably required to reproduce this portion of the data.

To develop the conclusions listed in the last two paragraphs, we proceed in the following way. We begin with synthetic seismograms for very simple models. They turn out to be unlike the data. By trial-and-error we add required layers of complexity until the synthetics have a realistic appearance, with the SALMON observations serving as a (qualitative) standard for comparison. Parametric studies are then conducted to identify the important controlling parameters. we emphasize that we are not trying to model records in detail, but to reproduce gross features of observed Lg.

An important tool for understanding the controlling features of the models is introduced in Section 3.2. This is a graphical display of the kinetic energy distribution for particular frequencies as a function of layer and mode. With this display we can see where the energy is trapped and which modes are contributing. The display is presented for a model that has most of the required features.

Using the knowledge gained from the models described in Section 3.2, we constructed our preferred EUS crustal model, called S1. This model is introduced at the beginning of Section 3.3. Synthetic seismograms are compared to the SALMON data in that section in both the time and frequency domain. Our conclusions

about this comparison are summarized at the end of Section 3.3. Basically, the synthetics are qualitatitively like the data in the group velocity window from 3.6 to 2.9 km/sec and in the frequency band from 0.5 to 2.5 Hz (where the data have large signal/noise).

The synthetics for the model S1 fail to account for late arriving (slower than 2.9 km/sec) high frequency energy that is prominent on the observed records. Also, frequencies above 2.5 Hz are poorly modeled, especially at the close ($\Delta \approx 240$ km) stations. Also, in Section 3.4 we examine the amplitude attenuation for the model and find that it is much too large compared to eastern United States observations.

In Section 3.5 we describe some parametric studies, primarily of the Q model, carried out to determine whether the model deficiencies can be remedied. Our parametric studies are far from complete, but strongly support the conclusion that plane-layered, constant Q, laterally homogeneous models are not adequate for accounting for those model deficiencies described in the last paragraph. Our conclusions regarding the synthesis of Lg for shallow explosions are summarized in more detail in Section 3.6.

3.2 Lg IN SIMPLE CRUSTAL MODELS

3.2.1 Introduction

This is basically an introductory section in which we describe some of our first synthesis efforts. The results of these calculations lead us to the more realistic and useful parameter studies described in subsequent sections. However, we describe these initial modeling efforts as a reminder of what must be included to synthesize realistic Lg seismograms.

The important points we wish to make in this section may be briefly summarized. Our first synthetics were done for a simple three-layer model (Table 2) which is roughly consistent with the gross charcteristics of the crust in the eastern United States as inferred from fundamental mode dispersion and refraction data. The Q model is based on that of Herrmann and Mitchell (1975).

All of the models discussed in this report are based on the model in Table 1. We add details and make changes when they seem required, but attempt to hold the gross features constant. In particular, the crustal thickness and the velocities in the vicinity of the crust-mantle boundary are not changed.

The initial seismograms are not realistic because they are dominated by a pulse-like fundamental mode. Thus, our first correction is to add lower velocity sedimentary layers at the surface to disperse this mode. We find that the Rayleigh wave is still too large. Hence, we are led to include a very low Q in the top 500 to 1000 meters to damp the unrealistic contribution from this mode. These two ideas, the requirement for low velocity and low Q in the very near surface layers, are held rather consistently throughout this report.

There are some other interesting ideas introduced in this section. It is tempting to think that the main trends can be deduced by computing synthetic seismograms with relatively few modes. We show that this is not the case, but that twenty or more modes are required.

We also introduce the comparison of synthetic Lg seismograms with observations of the SALMON explosion. The LRSM short period recordings of this event are plotted in Figure 20 in Section 3.4. In subsequent sections, we will make extensive use of these data as a standard to judge the realism of our synthetics.

Near the end of this section (sub-section 3.2.7) we introduce an important tool for understanding the controlling features of the crustal models. This is a graphical display of the kinetic energy distribution for particular frequencies as a function of layer and mode. With this display we can see where the energy is trapped and which modes are contributing.

Finally, at the end of this section we list the conclusions drawn from this initial investigation of modal Lg synthetics. The models introduced in our parametric studies in later portions of the report are motivated in large part by these conclusions.

TABLE 2

SIMPLE EASTERN UNITED STATES CRUSTAL MODEL

Depth (km)	Thickness (km)	α (km/sec)	β (km/sec)	ρ (gm/cc)	Q
7	7	6.1	3.3	2.85	250
17	10	6.6	3.59	3.05	250
34	17	6.6	3.59	3.05	2000
∞	∞	8.1	4.52	3.35	2000

3.2.2 Lg in a Simple Model

Fifty modes were computed for the model in Table 2. The dispersion curves are plotted in Figure 3. Synthetic seismograms were computed at several ranges for an explosion (reduced displacement potential) source at several depths. The seismograms at a range of 400 km and 1, 3, 5, 10 km depths are shown in Figure 4. The WWSSN short period instrument response is included.

The seismograms appear reasonable at the deeper depths. However, at shallow depth they are dominated by what is essentially a Rayleigh wave in a halfspace (the surface layer). At the 1 km depth this phase travels at about 3.05 km/sec and has a period near 1 Hz. That is on the flat part of the fundamental mode group velocity curve. It is clearly necessary to disperse this wave if we are to compute realistic seismograms for shallow sources. This can be done by adding some lower velocity material near the surface.

3.2.3 Addition of Surface Sediments to the Model

The same model with some sedimentary layers added at the surface is listed in Table 3. These are like the sedimentary layers inferred for the Cincinnati Arch region by Herrmann (1969) using surface wave observations. The dispersion curves for 50 modes are shown in Figure 5. The group velocity curves are not much different from those in Figure 3 except for the appearance of occasional modes that drop below 3 km/sec.

Seismograms were computed for the same range and depths as for the simpler structure and are shown in Figure 6. A fairly realistic Lg phase now appears. However, the fundamental mode, though no longer dominating, shows up for the shallow sources as a damped sinusoid that is quite unlike real data. To eliminate this unrealistic feature, it is necessary to have very low Q in the near surface region.

3.2.4 Addition of Low Q Near the Surface

In Table 4 we list a new model which is identical to the model of Table 3 below 2.8 km. But we have now added a larger velocity

TABLE 3

EASTERN UNITED STATES CRUSTAL MODEL
WITH SURFACE SEDIMENTS

Depth (km)	Thickness (km)	α (km/sec)	β (km/sec)	ρ (gm/cc)	Q
0.6	0.6	3.7	2.16	2.50	200
4.1	3.5	5.6	3.14	2.67	200
7.0	2.9	6.1	3.3	2.85	250
17.0	10.0	6.6	3.59	3.05	250
34.0	17.0	6.6	3.59	3.05	2000
∞	∞	8.1	4.52	3.35	2000

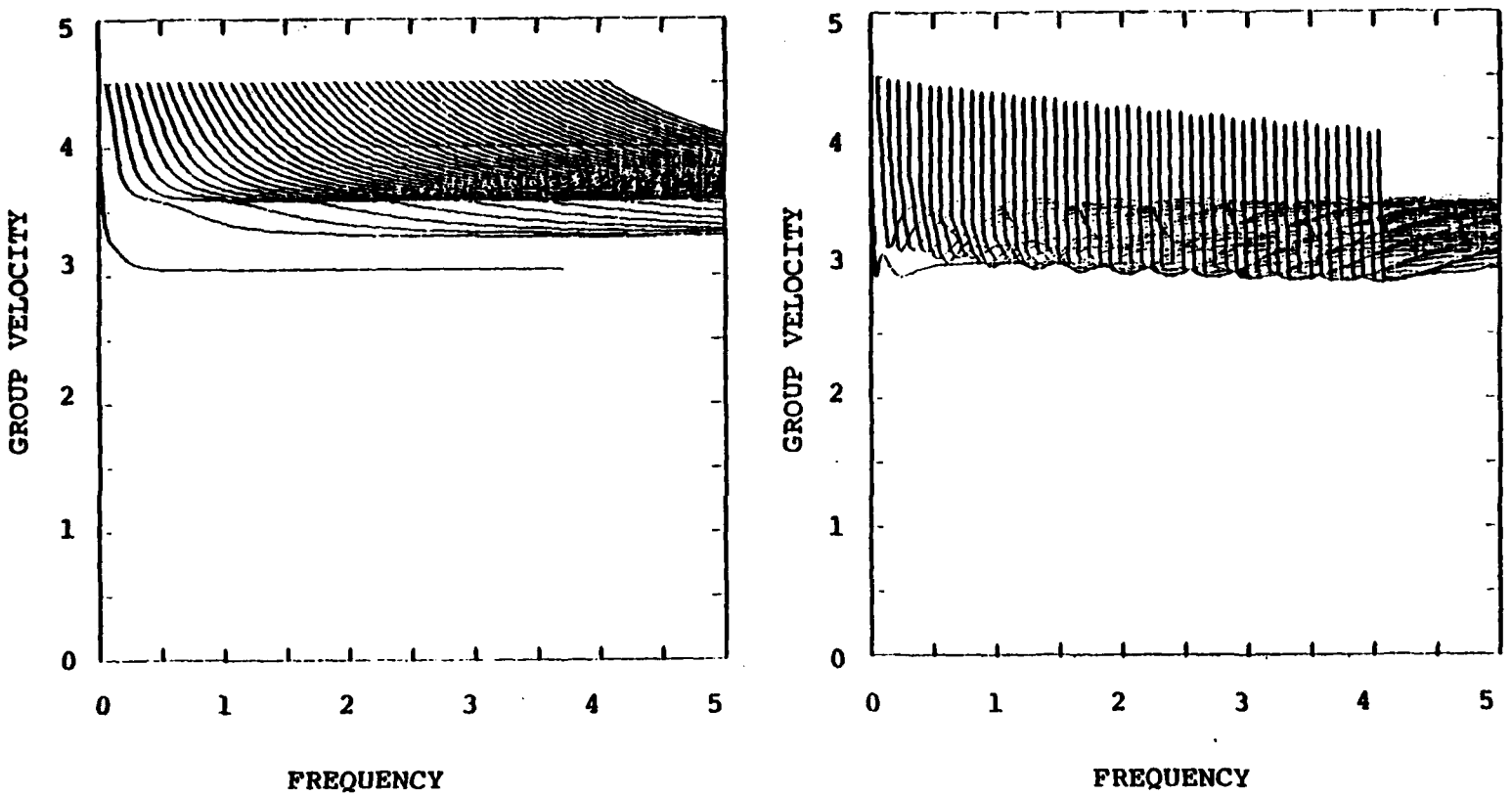

Figure 3. The phase and group velocity dispersion is plotted for the first 50 modes of the four-layer eastern United States crustal model in Table 2.

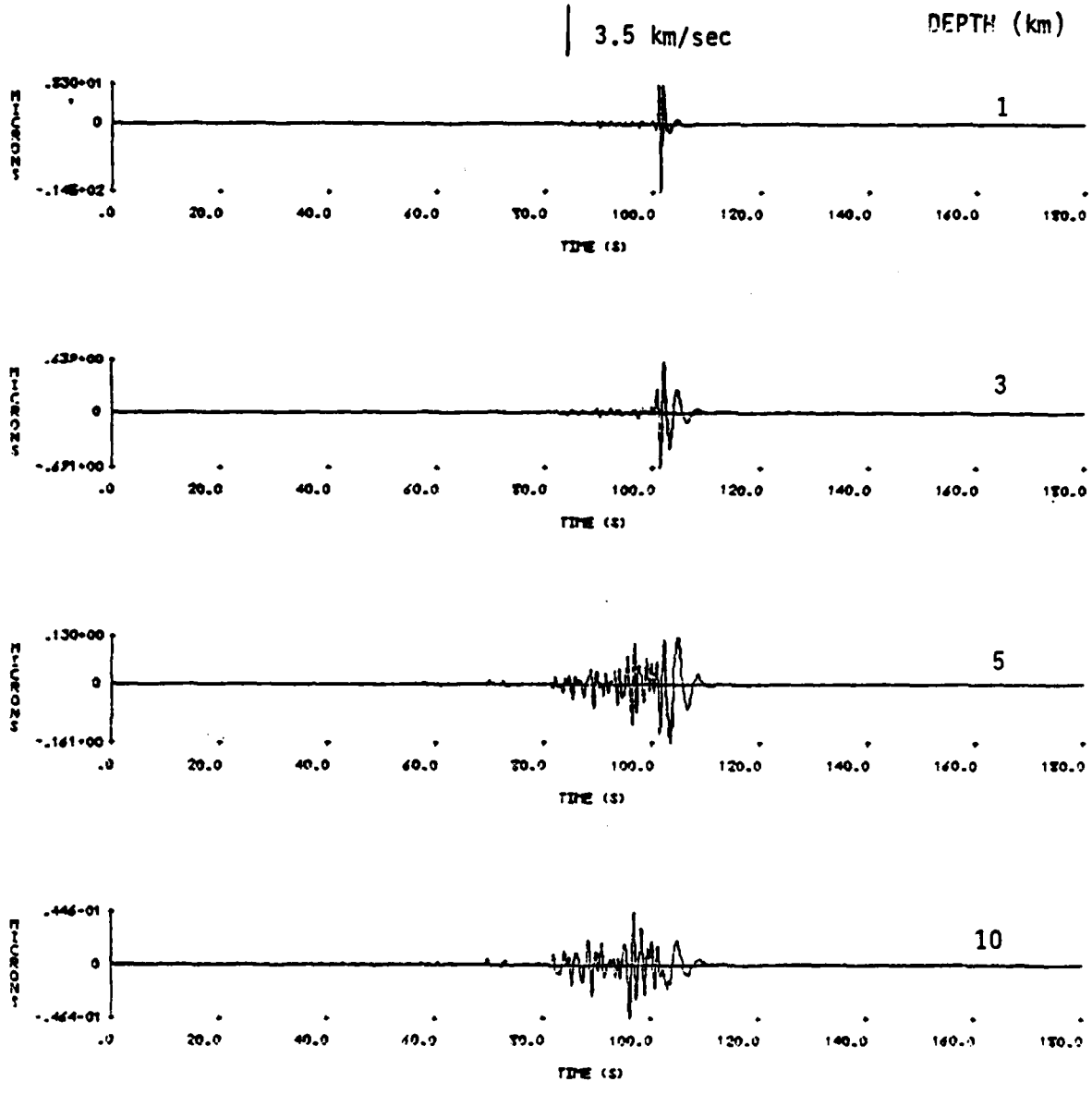

Figure 4. Synthetic seismograms are shown at several depths for the simple eastern United States crustal model of Table 2. The source is a reduced displacement potential with a corner frequency near 1 Hz and the range is 400 km. Fifty modes were summed and the WWSSN short-period instrument response is included. The peak amplitude in microns at 1 Hz is indicated t the left or each record. The time of a 3.5 km/sec arrival is marked. Zero on the time scale is the origin time + 30 seconds.

TABLE 4

EUS CRUSTAL MODEL S3

Depth	Thickness	α	β	ρ	Q_β
0.2	0.2	2.2	1.2	1.8	20
0.6	0.4	3.7	2.16	2.5	20
1.6	1.0	4.23	2.4	2.55	100
2.8	1.2	4.85	2.75	2.6	150
4.1	1.3	5.60	3.14	2.67	200
7.0	2.9	6.1	3.30	2.85	250
17 0	10.0	6.6	3.59	3.05	250
34.0	17.0	6.6	3.59	3.05	2000
∞	∞	8.1	4.52	3.35	2000

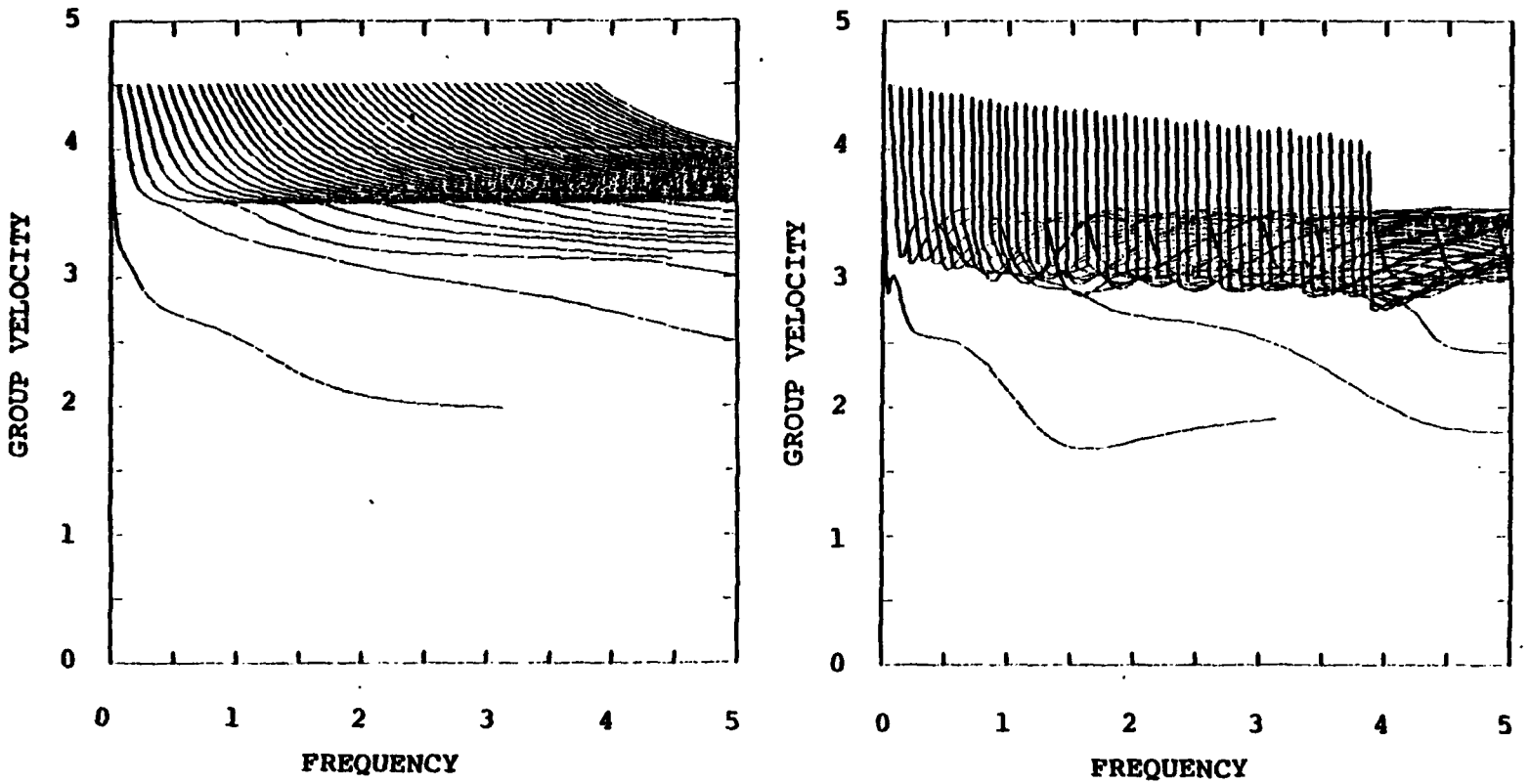

Figure 5. The phase and group velocity dispersion is plotted for the first 50 modes of the simple eastern United States crustal model with sedimentary layers added at the surface. (Table 3)

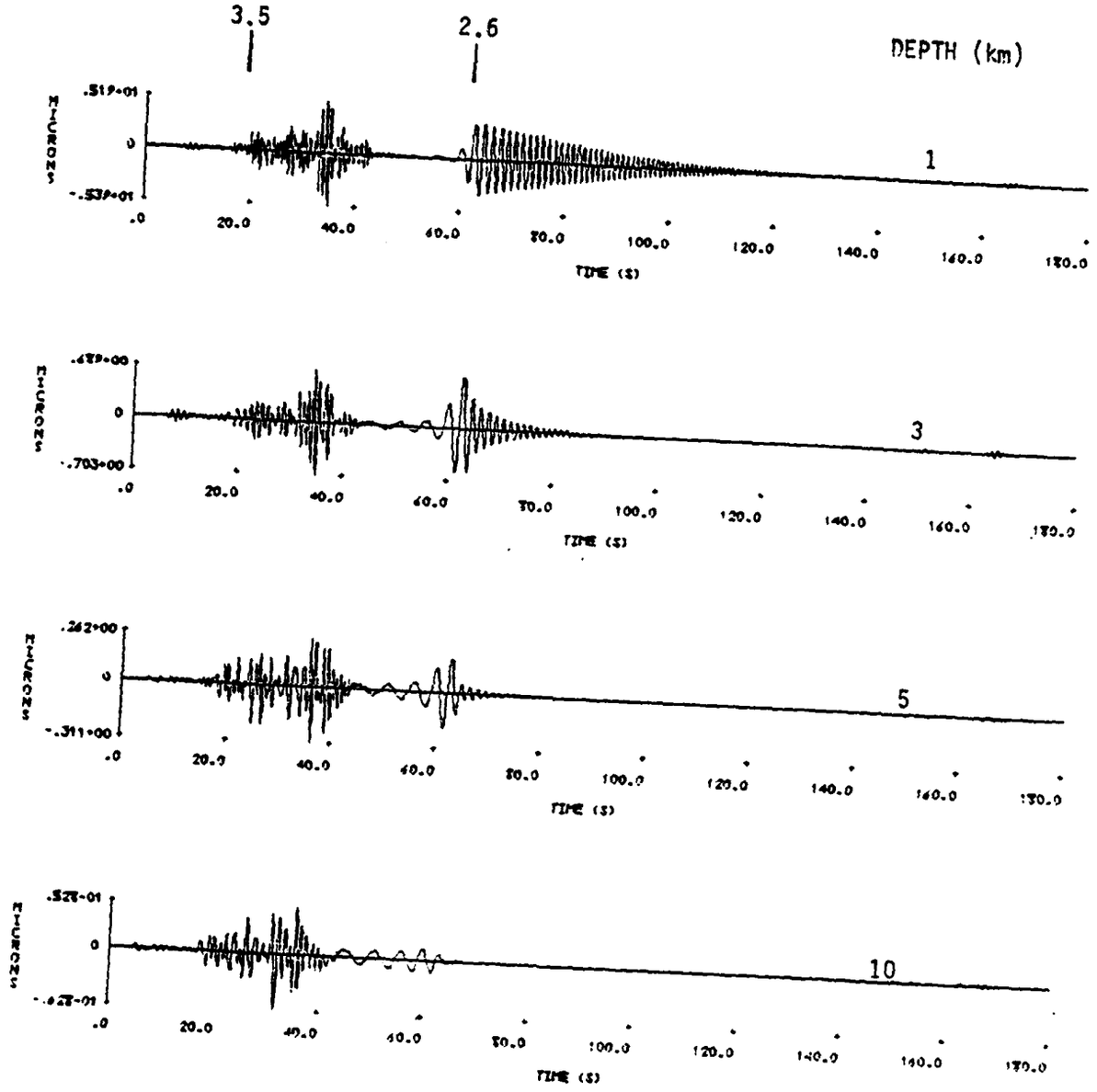

Figure 6. Synthetic seismograms like those in Figure 4 except that the model is that of Table 3 and zero on the time scale is the origin time + 95 seconds.

TABLE 4

EUS CRUSTAL MODEL S3

Depth	Thickness	α	β	ρ	Q_β
0.2	0.2	2.2	1.2	1.8	20
0.6	0.4	3.7	2.16	2.5	20
1.6	1.0	4.23	2.4	2.55	100
2.8	1.2	4.85	2.75	2.6	150
4.1	1.3	5.60	3.14	2.67	200
7.0	2.9	6.1	3.30	2.85	250
17.0	10.0	6.6	3.59	3.05	250
34.0	17.0	6.6	3.59	3.05	2000
∞	∞	8.1	4.52	3.35	2000

gradient in the top 2.8 km and a very low Q in the top 600 meters. The phase and group velocity curves for the first 35 modes are shown in Figure 7.

In Figure 8 we compare a 20 mode synthetic seismogram to recordings of the SALMON event. The range for the synthetic is 244 km compared to 244.6 km (EUAL) and 243.5 km (JELA) for the observations. The amplitude comparison is not meaningful. The explosion depth for the synthetic is 1 km compared to the 0.83 km depth of SALMON. We see that the synthetic is too short in duration and is too long period. The highly dispersed, late arriving long period waves are fundamental mode and simply are not seen in observations, though these observed records are cut off too soon to demonstrate that point.

To be able to change the model to more closely resemble the observations, we need to understand the effects of the controlling parameters. In Figure 9, we compare the synthetic from Figure 8 to synthetics from two modified versions of the earth model. The model for the three synthetics differs only in the depth to which Q_β is assumed to be 20. In the top record this depth is 600 meters (Table 2), in the middle it is 1.6 km and at the bottom it is 2.8 km. The amplitudes of the Lg do scale down with the lower Q_β, but not nearly so much as those of the fundamental mode.

3.2.5 The Effect of Higher Modes

In Figure 10, we compare 5 mode and 20 mode seismograms for two cases. The importance of the higher modes is clearly displayed. The amplitude of the high frequency waves increases by about a factor of four when the higher modes are added. The prominence of the fundamental mode is correspondingly reduced.

3.2.6 A Comparison with SALMON Observations

How well do the synthetic seismograms for this model compare with data at larger ranges? In Figure 11 we compare two SALMON recordings with two synthetic seismograms at nearly the same range. The signal/noise ratio is not very high for the FOTX recording, so it should not be taken too seriously as a standard of comparison.

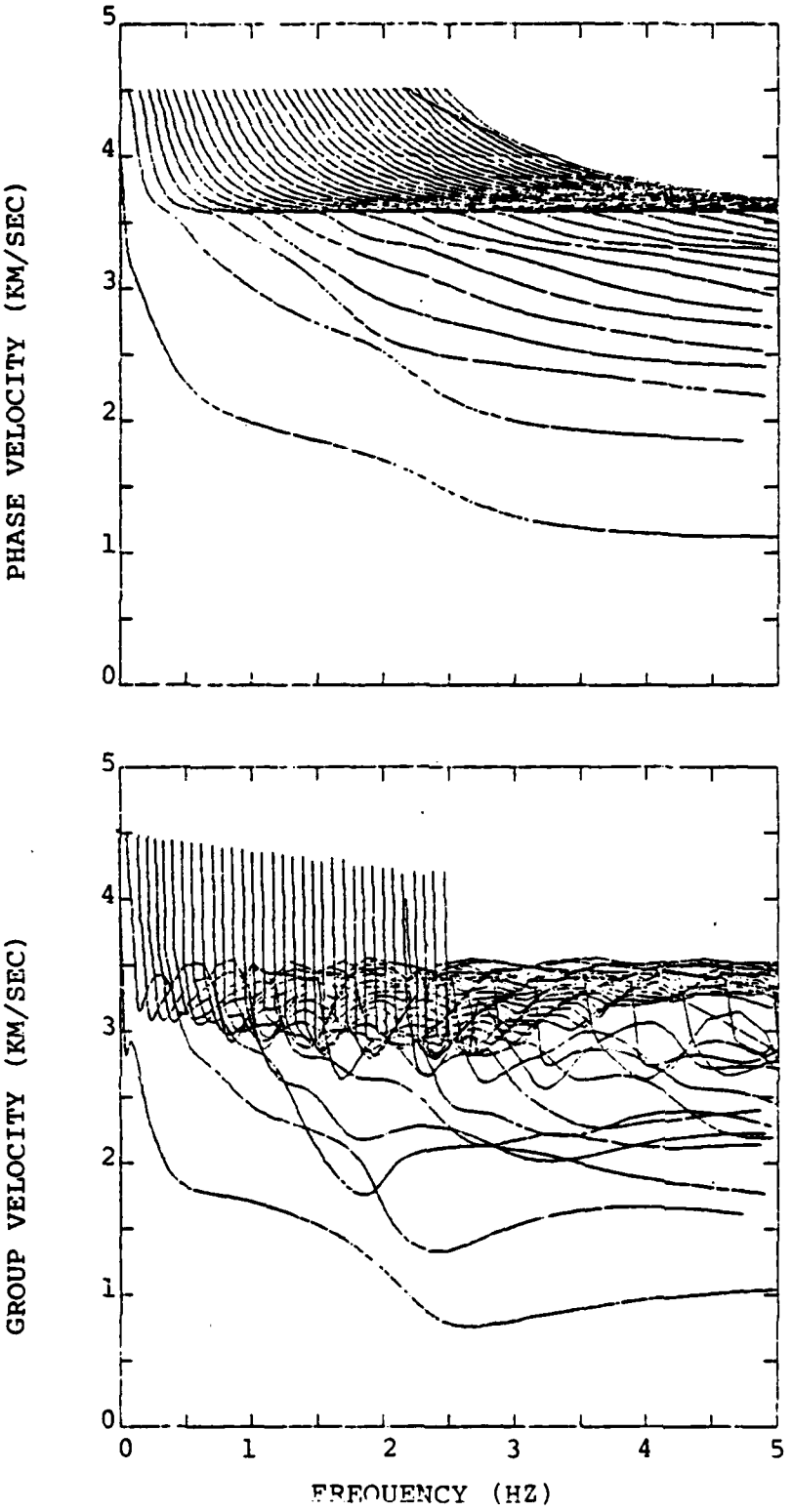

Figure 7. Phase and group velocity dispersion for the first 35 modes of the crustal model S3.

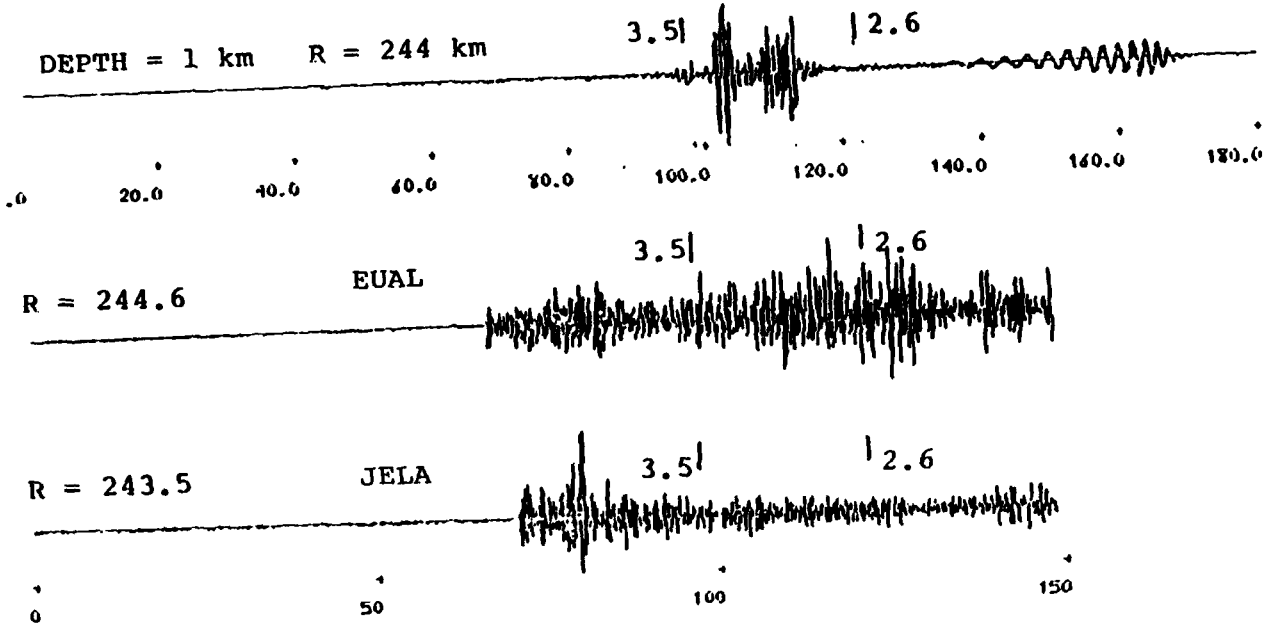

Figure 8. A twenty mode synthetic seismogram for the model of Table 4 is compared to two LRSM short-period recordings of SALMON.

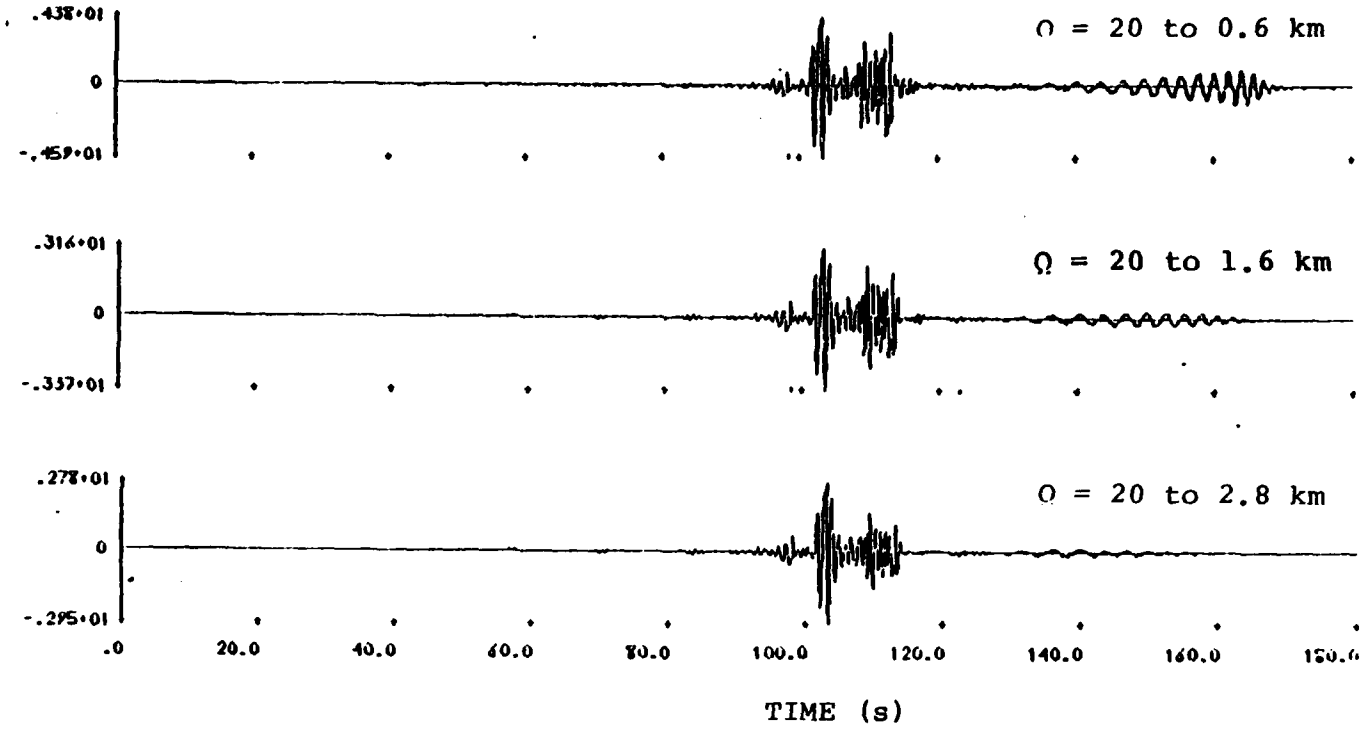

Figure 9. The synthetic seismogram for R = 244 km from Figure 8 is compared to synthetics from two modified versions of the same earth model. The seismograms are computed with 20 modes.

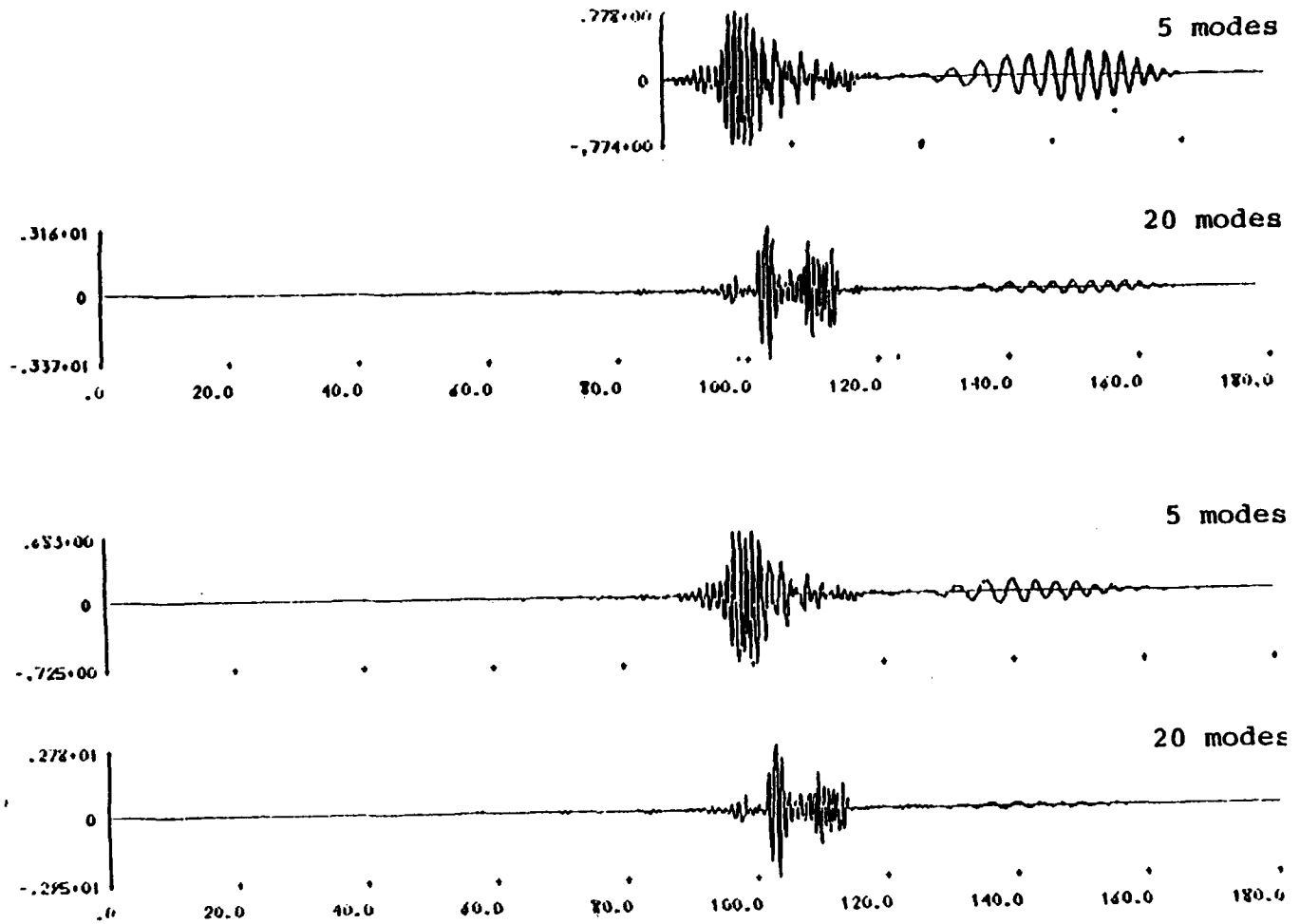

Figure 10. The effect of higher modes is shown for two structures. The model for the top pair has Q = 20 to 1.6 km and that for the bottom pair has Q = 20 to 2.8 km. The 20 mode seismograms are repeated from Figure 9.

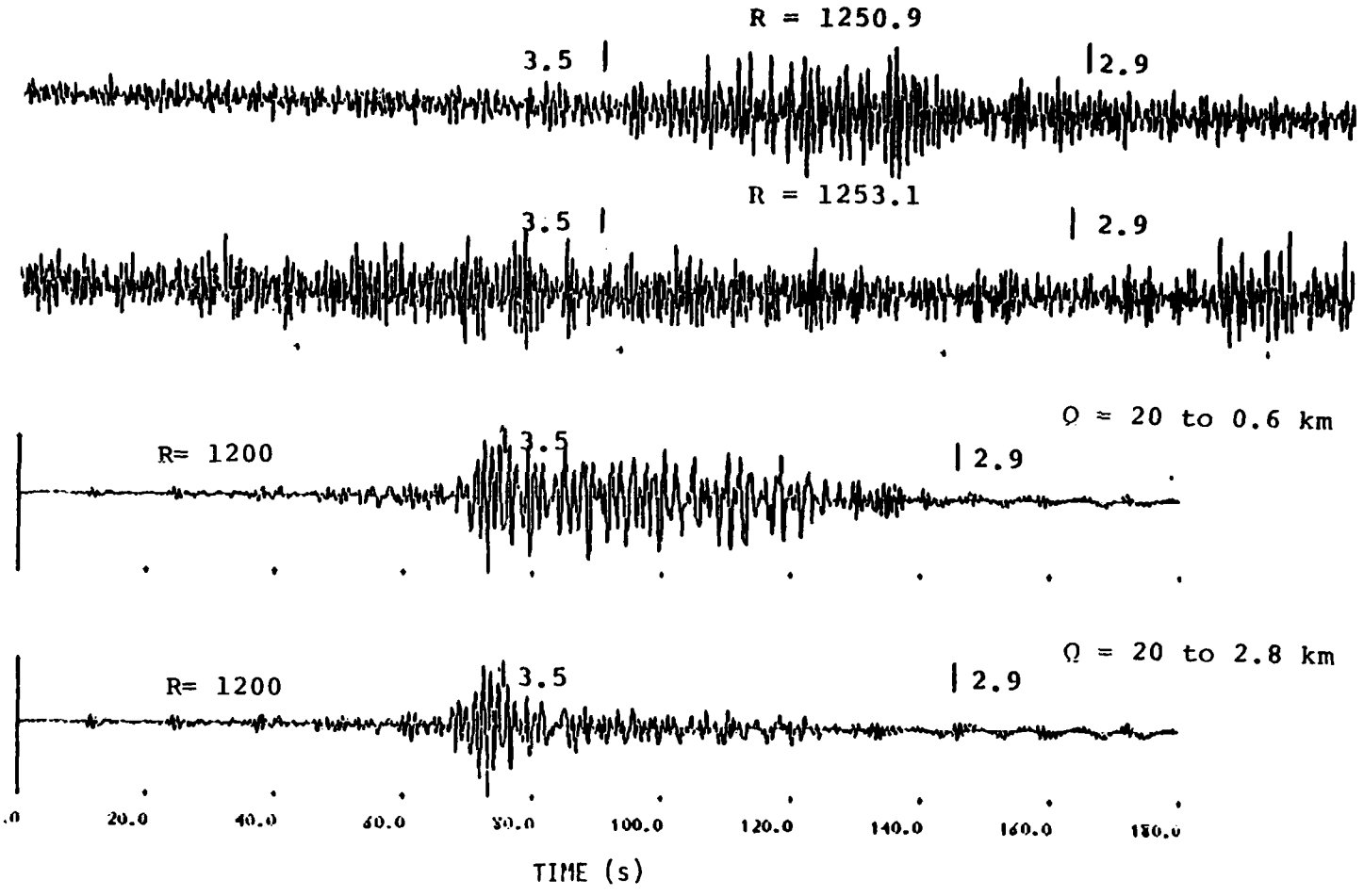

Figure 11. Comparison of observed SALMON recordings to synthetic seismograms for two Q models. Note the range difference. The times corresponding to arrivals at 3.5 and 2.9 km/sec are marked on the seismograms.

The depth of the Q = 20 layer is the only feature distinguishing the synthetics. The model with the smaller low Q zone seems preferable because of its longer duration. It would appear to be qualitatively similar to the VUIU observation if it were shifted to later time. However, even then there is too little high frequency energy in the synthetic.

3.2.7 Kinetic Energy Distribution Plots

The group velocity curves in Figure 7 are some help in understanding what features of the model are controlling the synthetic seismograms. But what is really needed is an indication of where the important energy is being trapped. An excellent way to obtain this is to look at the kinetic energy for particular frequencies as a function of layer and mode number.

A tabular portrayal of the kinetic energy characteristics of the model is presented in Table 5. In this table we list the quantities K_{ij}, E_{ij} and Γ_i for three frequencies, 1, 2, and 3 Hz. The β, Q_β and depth to the bottom of each layer are also shown with each quantity. The K_{ij}, E_{ij} and Γ_i are computed the following way:

1. A target frequency (f) is chosen, in this case 1, 2, and 3 Hz.
2. The root finding algorithm varies f for fixed phase velocity (c). The closest f to the target frequency is found. For each mode this frequency and the associated phase and group (U) velocities are printed. These are the values plotted in Figure 7.
3. For each selected f we compute

$$K_{ij} = \frac{I_{ij}}{\sum_{i=1}^{n} I_{ij}}$$

where I_{ij} denotes the kinetic energy in the ith layer for the jth mode.

4. Also computed is

$$E_{ij} = \frac{\hat{E}_{ij}}{\max_{\substack{i=1,n \\ j=1,m}} E_{ij}} \times 100 \quad ,$$

$$\hat{E}_{ij} = K_{ij} \frac{A_R^{(j)} e^{-\gamma_j r}}{(\omega/c_j)^{1/2}}$$

where $A_R^{(j)}$ is the modal amplification and

$$\gamma_j = \frac{\pi f}{U_j Q_j^{(e)}} \quad ,$$

where $Q_j^{(e)}$ is the effective Q_β for the jth mode.

5. Finally, we compute

$$\hat{\Gamma}_i = \sum_{j=1}^{m} E_{ij} \quad \text{and} \quad \Gamma_i = \frac{\hat{\Gamma}_i}{\max_{i=1,n} \hat{\Gamma}_i} \times 100 \quad .$$

Thus, for each selected frequency we print three tables. The first displays the distribution of kinetic energy for each mode. For the second table the energies are weighted by the factors used to compute synthetic seismograms (excluding the source depth dependent eigenfunctions). These weighted energies are normalized to allow comparison from mode-to-mode. Finally, the weighted energy in each layer is summed.

A graphical display makes it easier to absorb the information contained in tables like those in Table 5. In Figure 12 we show plots of the K_{ij} and E_{ij} distribution for four cases. The mode number versus depth tables are displayed by shading the appropriate positions in a two-dimensional grid, with the degree of shading

TABLE 5. KINETIC ENERGY DISTRIBUTION FOR MODEL S3.

K_{ij}

M	F	C	U	1	2	3	4	5	6	7	8	9
1	1.0-1	2.0-	1.7-	47.0	42.0	27.0	.0	.0	.0	.0	.0	.0
2	1.0-1	2.0-	2.4-	2.0	7.1	21.0	47.1	22.3	4.1	.0	.0	.0
3	1.0-0	2.0-	2.8-	4.0	12.1	12.0	8.2	12.2	44.7	6.0	.0	.0
4	1.0-0	2.0-	2.1-	0.0	12.4	5.1	2.7	4.9	12.2	46.2	2.7	.0
5	1.0-1	2.0-	1.7-	1.7	1.5	.6	.4	.0	1.7	12.4	80.6	.0
6	1.0-0	2.0-	2.8-	2.0	2.0	1.2	1.2	1.2	7.7	31.0	55.1	.1
7	1.0-0	2.0-	2.7-	2.6	3.0	1.2	1.7	1.2	4.4	28.3	55.4	.1
8	1.0-1	2.0-	2.2-	4.7	4.6	1.2	2.0	1.0	6.0	28.9	49.8	.2
9	1.0-1	2.0-	2.1-	4.0	3.9	1.2	2.6	2.3	6.7	29.7	47.8	.3
10	.99	2.0-	2.1-	3.0	3.7	1.2	2.7	2.5	6.7	28.4	50.5	.6
11	1.0-0	2.0-	2.0-	2.3	1.7	.9	2.7	2.7	6.0	30.5	52.0	1.2
12	.99	4.1-	2.0-	1.0	1.2	.9	2.2	2.4	6.0	27.8	53.9	3.0
13	1.0-0	4.0-	2.0-	1.0	1.0	1.1	2.6	2.7	6.4	26.8	49.1	7.5
14	1.0-0	4.4-	2.0-	1.7	1.7	1.3	4.1	2.9	6.4	22.0	41.2	19.3

M	F	C	U	1	2	3	4	5	6	7	8	9
1	1.0-0	1.7-	1.2-	66.7	31.5	1.7	.0	.0	.0	.0	.0	.0
2	1.0-0	2.0-	1.7-	49.5	15.7	33.7	4.1	.0	.0	.0	.0	.0
3	2.0-1	2.0-	1.0-	55.6	3.3	20.3	10.9	.1	.0	.0	.0	.0
4	2.0-0	2.0-	2.2-	11.0	5.7	27.3	49.8	7.1	.1	.0	.0	.0
5	2.0-1	2.0-	2.0-	4.7	2.9	12.2	32.2	46.8	12.7	.0	.0	.0
6	2.0-1	2.0-	2.0-	1.6	1.2	5.0	9.3	9.2	72.1	2.7	.0	.0
7	2.0-1	2.0-	2.0-	1.7	1.3	5.1	9.1	17.8	47.2	25.8	.0	.0
8	2.0-0	2.0-	2.0-	1.2	1.1	3.4	7.6	7.6	7.8	59.7	20.1	.0
9	1.0-0	2.0-	2.0-	.1	.0	.2	.2	.2	1.3	39.6	58.3	.0
10	1.0-0	2.0-	2.0-	.1	.0	.2	.2	.4	1.6	32.6	64.8	.0
11	2.0-0	2.0-	2.0-	.1	.1	.4	.6	.8	2.2	36.2	59.4	.0
12	2.0-0	2.0-	2.0-	.2	.1	.5	.8	1.1	3.2	37.2	56.9	.0
13	2.0-1	2.0-	2.0-	.3	.2	.9	1.2	1.6	4.5	32.3	58.9	.0
14	1.0-0	2.0-	2.0-	.3	.3	1.2	1.4	2.0	5.6	35.3	54.1	.1
15	1.0-0	2.0-	2.0-	.4	.3	1.2	1.8	2.3	6.4	32.2	55.2	.1
16	2.0-0	2.0-	2.0-	.5	.4	1.6	2.1	2.4	5.8	32.9	54.1	.1
17	2.0-1	2.0-	2.0-	.5	.4	1.6	2.1	2.4	5.7	31.8	55.4	.2
18	2.0-0	2.0-	2.0-	.6	.5	1.9	2.3	2.4	5.5	30.8	55.7	.2
19	1.0-0	2.0-	2.0-	.6	.5	1.9	2.3	2.5	5.8	31.8	54.2	.4
20	2.0-0	2.0-	2.0-	1.1	.9	3.3	3.7	3.4	7.0	28.3	51.9	.4
21	2.0-1	2.0-	2.0-	1.0	1.2	4.4	4.9	4.3	8.3	27.8	47.0	.6
22	2.0-1	4.0-	2.0-	1.0	1.0	5.3	5.7	4.3	8.8	25.8	45.6	.8
23	2.0-1	4.1-	2.0-	1.6	1.3	4.7	4.8	3.8	7.6	27.9	47.2	1.2
24	2.0-0	4.1-	2.0-	1.2	1.0	3.8	3.7	3.2	6.5	28.2	50.4	2.2
25	2.0-1	4.2-	2.0-	1.0	.8	3.2	2.9	2.4	5.3	29.7	51.0	4.0
26	2.0-0	4.2-	2.0-	1.0	.7	3.3	2.8	2.3	6.1	27.2	48.7	8.0
27	2.0-1	4.4-	2.0-	1.0	.6	3.9	2.9	2.4	7.0	25.3	45.0	12.2

M	F	C	U	1	2	3	4	5	6	7	8	9
1	2.0-0	1.7-	.8-	97.9	2.1	.0	.0	.0	.0	.0	.0	.0
2	2.0-0	2.0-	1.3-	72.3	27.6	2.1	.0	.0	.0	.0	.0	.0
3	2.0-0	2.0-	2.1-	22.6	19.9	56.7	.9	.0	.0	.0	.0	.0
4	3.0-2	2.0-	2.0-	.6	16.2	48.5	19.1	.2	.0	.0	.0	.0
5	2.0-0	2.0-	2.1-	11.7	22.1	24.4	52.7	2.6	.0	.0	.0	.0
6	3.0-2	2.0-	2.0-	.2	9.6	19.7	39.2	24.4	.2	.0	.0	.0
7	2.0-0	2.0-	2.0-	4.2	5.3	11.6	16.7	39.1	23.4	.0	.0	.0
8	3.0-2	2.0-	2.0-	2.4	3.2	5.8	4.7	10.4	64.7	.9	.0	.0
9	2.0-0	2.0-	2.0-	3.2	4.3	9.0	17.7	14.6	53.9	.4	.0	.0
10	3.0-1	2.0-	2.0-	2.6	2.6	7.1	8.7	13.3	47.9	24.5	.0	.0
11	3.0-1	2.0-	2.0-	2.2	1.3	3.2	3.2	2.9	7.9	59.8	20.2	.0
12	2.0-0	2.0-	2.0-	.1	.1	.2	.0	.3	.8	32.9	65.0	.0
13	2.0-1	2.0-	2.0-	.2	.2	.4	.5	.7	2.4	32.9	62.6	.0
14	3.0-1	2.0-	2.0-	.6	1.4	2.4	2.4	2.2	5.7	35.4	49.9	.0
15	3.0-1	2.0-	2.0-	.7	.6	1.0	1.0	1.3	3.6	37.0	56.3	.0
16	3.0-1	2.0-	2.0-	.7	.5	1.0	1.0	1.3	2.9	32.9	60.0	.0
17	3.0-1	2.0-	2.0-	.8	.7	1.6	1.4	2.0	4.2	35.9	51.2	.0
18	2.0-0	2.0-	2.0-	.2	.4	.8	.9	1.4	3.5	34.7	57.9	.0
19	3.0-1	2.0-	2.0-	.8	.7	1.7	1.7	2.4	5.2	32.6	54.6	.0
20	2.0-0	2.0-	2.0-	.8	.7	1.6	1.4	2.0	5.7	33.0	52.9	.0
21	3.0-2	2.0-	2.0-	.8	1.0	2.2	2.2	2.4	5.8	30.8	54.8	.0
22	2.0-0	2.0-	2.0-	.7	1.0	1.9	2.1	2.0	5.7	32.5	52.4	.1
23	2.0-0	2.0-	2.0-	.7	1.0	1.9	2.1	2.0	5.8	30.9	54.7	.1
24	2.0-0	2.0-	2.0-	.8	1.0	2.0	2.0	2.0	5.4	31.7	54.6	.1
25	3.0-1	2.0-	2.0-	1.0	1.0	2.5	2.4	2.2	6.1	30.2	53.8	.1
26	3.0-1	2.0-	2.0-	1.0	1.0	2.7	2.6	2.7	7.5	28.7	50.0	.1
27	3.0-2	2.0-	2.0-	1.0	1.2	2.4	2.3	2.1	7.0	29.3	46.1	.2
28	3.0-1	2.0-	2.0-	1.0	1.0	2.7	2.6	2.2	7.6	28.2	48.9	.2
29	3.0-1	2.0-	2.0-	1.0	1.0	2.7	2.7	2.6	7.2	30.0	49.9	.2
30	2.0-0	2.0-	2.0-	1.0	1.0	2.7	2.4	2.2	6.4	29.7	52.2	.3
31	2.0-0	2.0-	2.0-	1.0	1.0	2.7	2.3	2.1	6.7	27.8	52.4	.4
32	3.0-1	4.0-	2.0-	1.0	1.0	3.0	2.6	2.2	6.6	29.1	51.7	.5
33	2.0-0	4.0-	2.0-	1.0	1.0	3.0	2.6	2.1	7.1	28.2	46.3	.6
34	3.0-0	4.1-	2.0-	1.0	1.0	3.0	2.6	2.1	6.5	28.2	43.7	.6
35	2.0-0	4.1-	2.0-	1.0	1.0	3.0	2.6	2.1	6.7	27.9	41.1	.8

TABLE 5. (Continued)

E_{ij}

TABLE 5 (continued)

I	R = 1200 H	BE	Γ_i Q	1 Hz Energy	2 Hz Energy	3 Hz Energy
1	0.20	1.20	20	2.72	0.88	0.53
2	0.60	2.16	20	3.02	0.67	0.76
3	1.60	2.40	100	1.10	2.78	1.43
4	2.80	2.75	150	1.39	3.12	1.56
5	4.10	3.14	200	1.26	3.38	1.95
6	7.00	3.30	150	3.89	8.79	4.71
7	17.00	3.59	250	26.55	58.67	55.40
8	34.00	3.59	2000	100.00	100.00	100.00
9	∞	4.52	2000	1.35	2.66	0.04

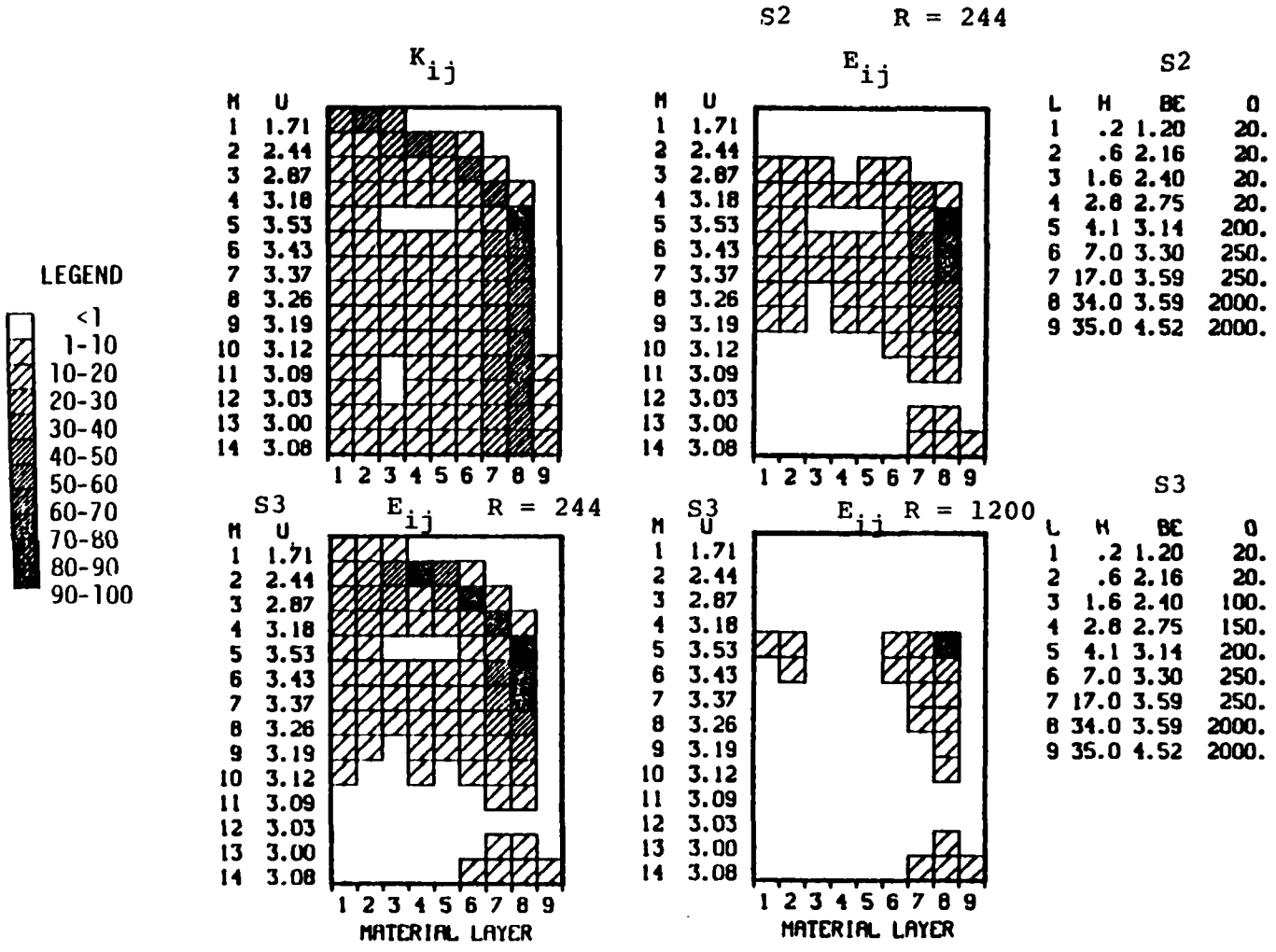

Figure 12. The kinetic energy energy distribution at 1 Hz is plotted for the models S2 and S3. The K_{ij} is the same for both models. The legend for the shading is shown at the left. A table with the depth to interfaces and the layer shear velocity (BE) and Q is printed at the right for each model. At the left side of each graph we list the mode number and the group velocity for that mode at the selected frequency (1 Hz in this case).

determined by the amplitude of the number in that position. All the graphs in the figure are for 1 Hertz. We display the K_{ij} for the model S3 in Table 4 and show the E_{ij} at R = 244 km for this model and the model we call S2, which has Q = 20 to a depth of 2.8 km. We also show the E_{ij} at 1200 km for S3. The first and last plots correspond to tabular data given in Table 5.

Some interesting features of the K_{ij} data in the table and figure are:

- Only 14 modes contribute to 1 Hz. For 2 Hz, 27 modes contribute and at least 35 modes (the number computed) may contribute to 3 Hz.
- The energy in the fundamental mode is almost entirely in the top 600 meters of the model.
- The energy in the higher modes is almost entirely in the β = 3.59 km/sec layers at the base of the crust.
- Energy in the intermediate crust is restricted to low modes. At 1 Hz it is modes 2 and 3 while at 3 Hz, it is modes 2 to 10.

The E_{ij} table is the important one for understanding the energy paths for the synthetic seismograms. This quantity depends on the Q model and the range. Our observations about the E_{ij} in the table and figure include the following:

- Only 20 modes were used to construct the synthetics. This is enough to compute 1 Hz and, apparently, 3 Hz at 1200 km. However, a significant amount of 2 Hz energy (and probably other frequencies) is lost by truncating after 20 modes.
- The Q has a dramatic effect. At 1 Hz the dominant energy is in the 5th mode and is trapped at the base of the crust. The group velocity of this mode is 3.53 km/sec.

- At 2 Hz, the modes 9 to 20 dominate with group velocities of 3.08 to 3.56 km/sec. At 3 Hz it is modes 12 to 18.

- The effect of lowering the Q in the top 2.8 km (compare models S2 and S3) is to sharply attenuate the energy in the low number modes which have low group velocities. This is what we saw in Figures 3 and 5.

- Nearly all the high frequency energy is in the layer at the base of the crust. This is easily seen in the tabulated values of Γ_i as well as in the figure.

3.2.8 Conclusions

These data and the comparison of synthetic and observed seismograms suggest how the model needs to be changed to more closely agree with the observations. The low Q and gradient at the surface were introduced to damp the unrealistic long period fundamental mode ringing that occurs with simple crustal models. Apparently, only a thin low Q layer (thought of as a laterally heterogeneous weathered layer) is needed.

For Lg propagation, the base of the crust is most important. A thick layer at the base is likely to give a sharp Lg onset at the shear velocity of this layer, as we see in Figure 11. A more emergent Lg, as seems to be seen in the SALMON data, probably requires the presence of some gradients in the mid- and lower-crust. Late arriving high frequency waves, say at 2.9 km/sec or slower, can be associated with low number modes trapped near the surface where the shear velocities are low. However, high number modes with energy at the base of the crust can also have low group velocities. In the next section we describe a new model that gives better agreement with the data.

3.3 Lg FOR AN EASTERN UNITED STATES CRUSTAL MODEL

The parametric variations described in the previous section allow us to construct a model that does give synthetic Lg waveforms

that are qualitatively like the data. The new EUS model (called S1) is listed in Table 6. It is compared with the simple EUS crust (Table 2) with which we began in Figure 13. We see that the velocity model is much the same below 4.1 km, except that a gradient has been introduced in the mid-crust. The Q_β is low near the surface, but increases to fairly high values for depths below 6.2 km.

The phase and group velocity dispersion for the first 35 modes of model S1 are shown in Figure 14. Comparing to the dispersion for Model S3 in Figure 7, we observe several interesting features including:

- There are no longer modes with group velocities below 2 km/sec. This is due to the absence of the very low velocity surface layer.
- The higher mode Airy phases nearly all occur in the 2.75 to 3.5 km/sec group velocity window.
- The band where the group velocity curves form a dense pattern is somewhat narrower than it was for S3.
- There is an indication of a weaker set of Airy phases at about 2.5 km/sec.

Seismograms were computed for this model for specific comparison to the SALMON data. The source function of Mueller and Murphy (1971) was used with the parameters for salt given by Murphy (1969). This source function provides a fairly good fit to the measured near-field ground motion data when the SALMON yield (5.3 KT) and depth (0.83 km) are used. The data were recorded by LRSN short period seismometers and the appropriate filter is applied to the synthetics.

Synthetic seismograms are compared to the observations at two ranges in Figure 15. In the group velocity window from 3.5 to 2.9 km/sec, the synthetics are like the observations in a qualitative sense, particularly at the larger range. Thus, we are encouraged to think that we have done a reasonable job of synthesizing Lg. Our

TABLE 6

EUS CRUSTAL MODEL - S1

Depth	Thickness	α	β	ρ	Q_β
0.6	0.6	3.7	2.16	2.10	20
2.6	2.0	4.55	2.54	2.20	50
4.1	1.5	5.60	3.14	2.65	250
6.2	2.1	6.1	3.30	2.85	400
13.2	7.0	6.3	3.41	2.94	1200
19.0	5.8	6.4	3.46	3.00	1500
34.0	15.0	6.6	3.59	3.05	2000
∞	∞	8.1	4.52	3.35	2000

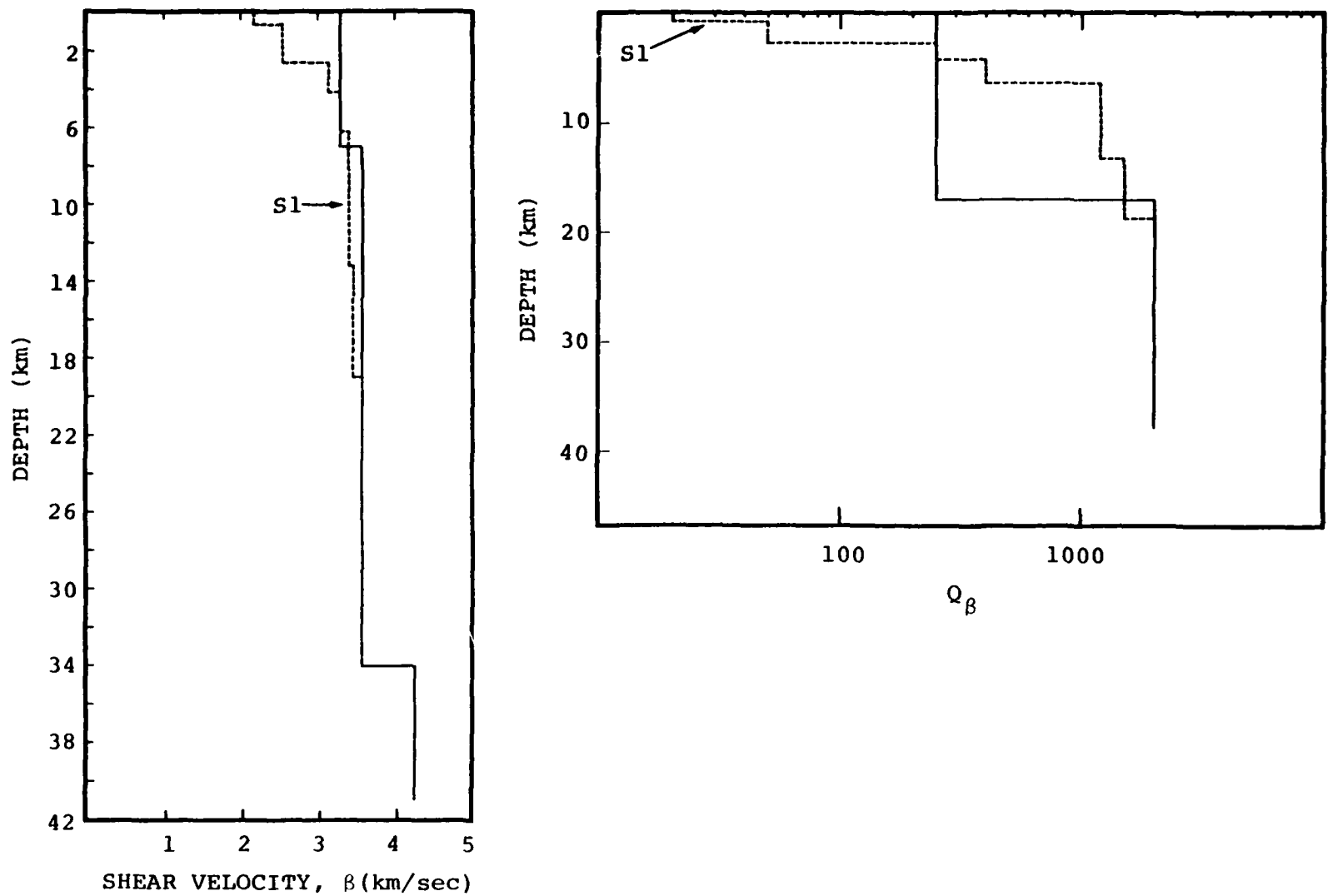

Figure 13. The model S1 is compared to the shear velocity and Q models of Table 2.

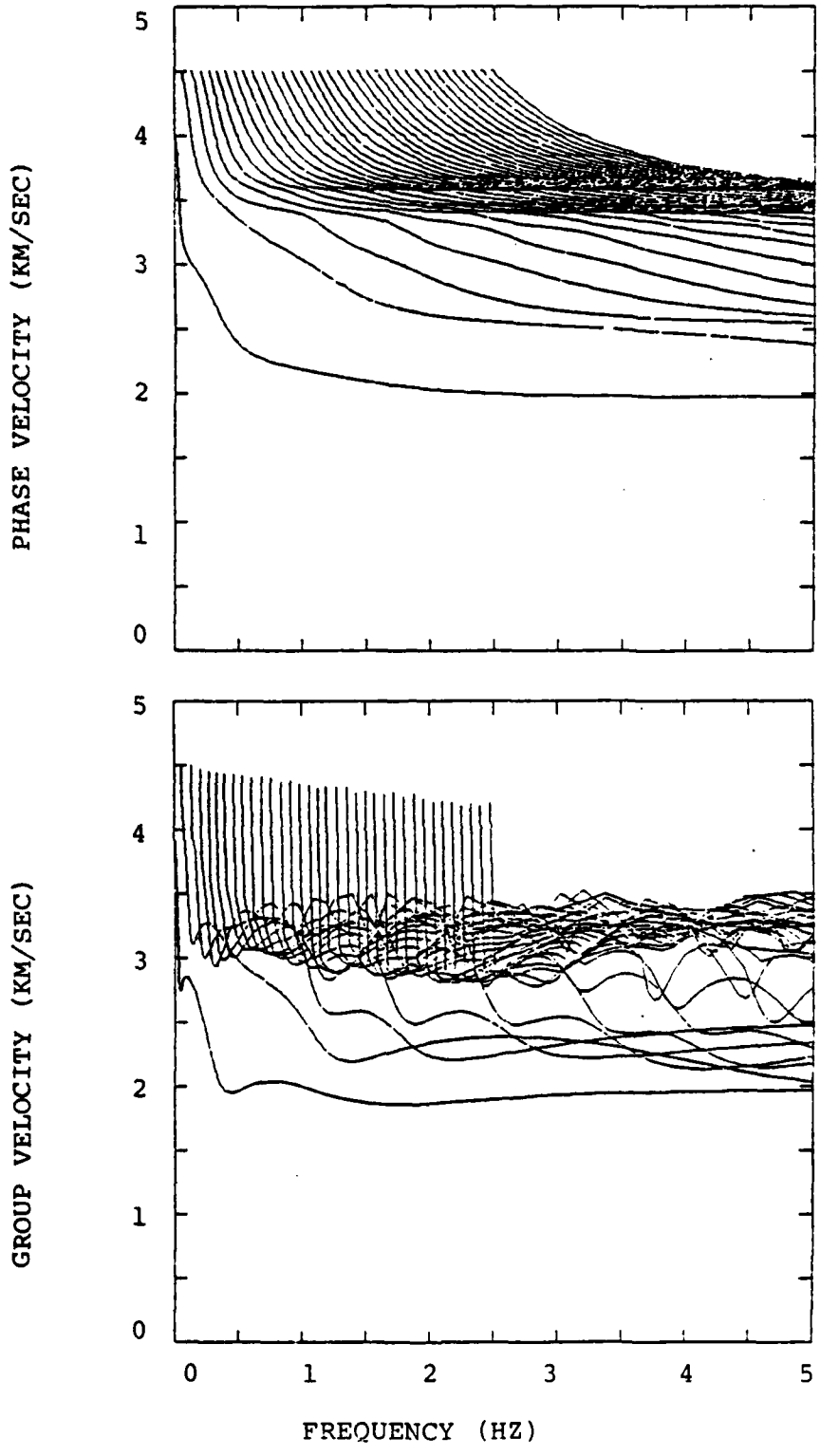

Figure 14. Phase and group velocity for the first 35 modes of the crustal structure S1.

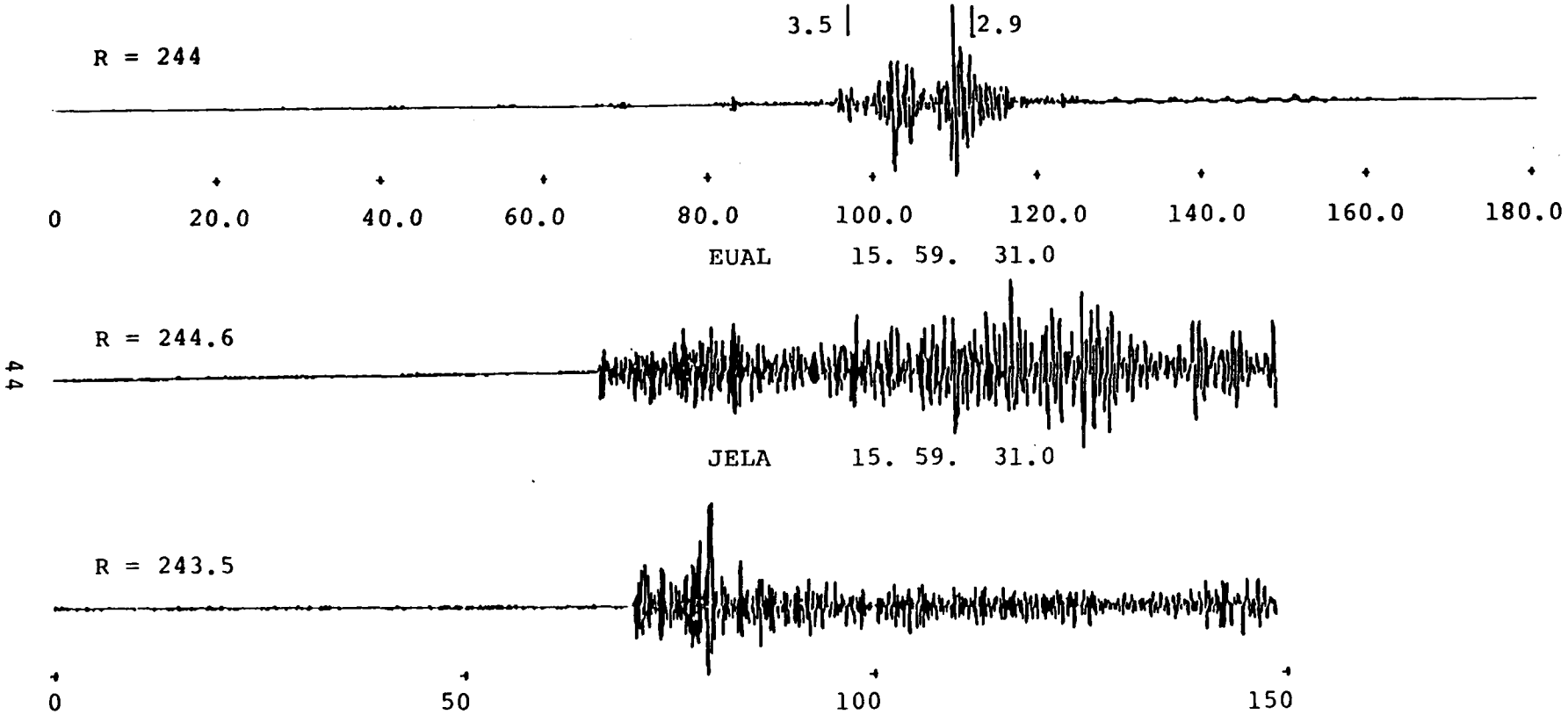

Figure 15. Synthetic seismograms are compared with SALMON observations from four stations. The synthetics were computed with LRSM short-period seismometer response. The times are aligned at the 3.5 km/sec group velocity arrival time. 35 modes in the model S1 and a SALMON source function are included.

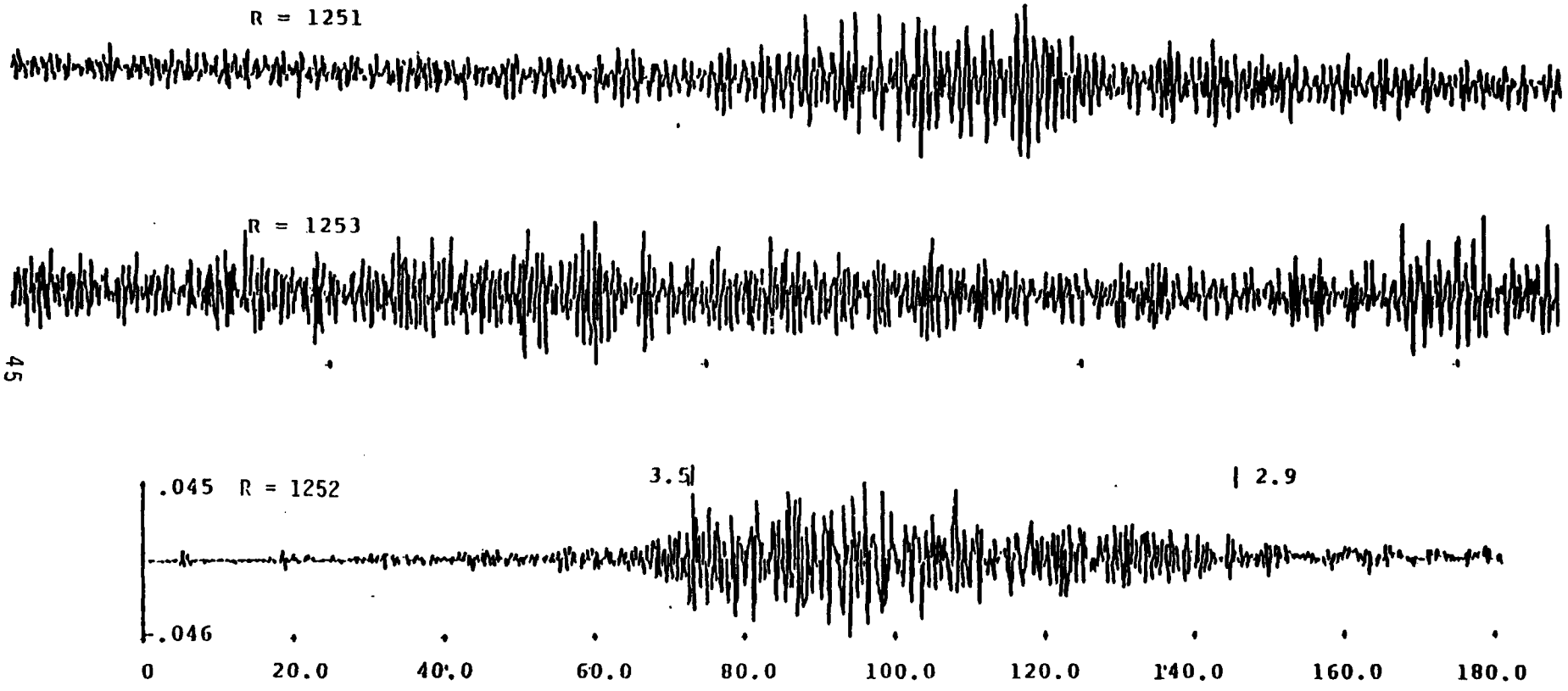

Figure 15. (continued)

The K_{ij} and E_{ij} for the model S1 are plotted in Figure 16, while the Γ_i are tabulated in Table 7. The E_{ij} and Γ_i were computed for both 244 km and 1252 km. From the examination of the data in the figure and table, we deduce the following:

- The truncation at 35 modes appears to be reasonable. Most of the energy is in modes that are near the middle of the band computed.
- At 1252 km the high frequency energy is nearly all in the high Q layers at the bottom of the crust. That is, between 6.2 km and 34 km where the shear velocities are 3.41 to 3.59 km/sec.
- At 244 km the energy is more evenly distributed throughout the crust.
- The energy is much more evenly distributed over modes at closer ranges. At high frequencies and larger ranges, very few modes contribute.

The tables indicate that the low (< 2.8 km/sec) group velocities are associated with low number modes, which is expected from the plot in Figure 14. From the K_{ij} plots we see that the energy in these modes is trapped near the surface. Since the Q is quite low in the near surface layers of our model, this energy does not propagate. This is seen in the E_{ij} plots and Γ_j table.

Another way to compare the observed and synthetic Lg phases is in the spectral domain. In Figure 17, we plot the spectrum of the group velocity window from 3.6 to 2.9 km/sec for the four vertical component SALMON observations in Figure 12 and for four other stations. The spectra from the larger range (> 1000 km) stations generally peak near 1 Hz and fall off at a rate between ω^{-2} and ω^{-3}. At the two closer stations, the spectral peak occurs at higher frequency and the rate of falloff is about ω^{-3}. The signal/noise is generally quite good in the frequency band from 0.7 to 2.0 Hz. Outside this band the signal/noise is often too small to allow much confidence in conclusions about the spectral behavior.

synthetics have very little energy arriving before 3.5 km/sec. As long as the mantle is represented by a halfspace (β = 4.52 km/sec), this will be the case. Adding some layering in the mantle would allow computation of higher velocity energy.

A more serious shortcoming of the model is that there is too little late-arriving high frequency energy. This is especially true at 244 km. How can this energy be included? The group velocity curves in Figure 14 show modes with stationary group velocities between 2.6 and 3.0 km/sec. The kinetic energy distribution can be used to determine the portion of the model that controls these modes.

The K_{ij} and E_{ij} for the model S1 are plotted in Figure 16, while the Γ_i are tabulated in Table 7. The E_{ij} and Γ_i were computed for both 244 km and 1252 km. From the examination of the data in the figure and table, we deduce the following:

- The truncation at 35 modes appears to be reasonable. Most of the energy is in modes that are near the middle of the band computed.
- At 1252 km the high frequency energy is nearly all in the high Q layers at the bottom of the crust. That is, between 6.2 km and 34 km where the shear velocities are 3.41 to 3.59 km/sec.
- At 244 km the energy is more evenly distributed throughout the crust.
- The energy is much more evenly distributed over modes at closer ranges. At high frequencies and larger ranges, very few modes contribute.

The tables indicate that the low (< 2.8 km/sec) group velocities are associated with low number modes, which is expected from the plot in Figure 14. From the K_{ij} plots we see that the energy in these modes is trapped near the surface. Since the Q is

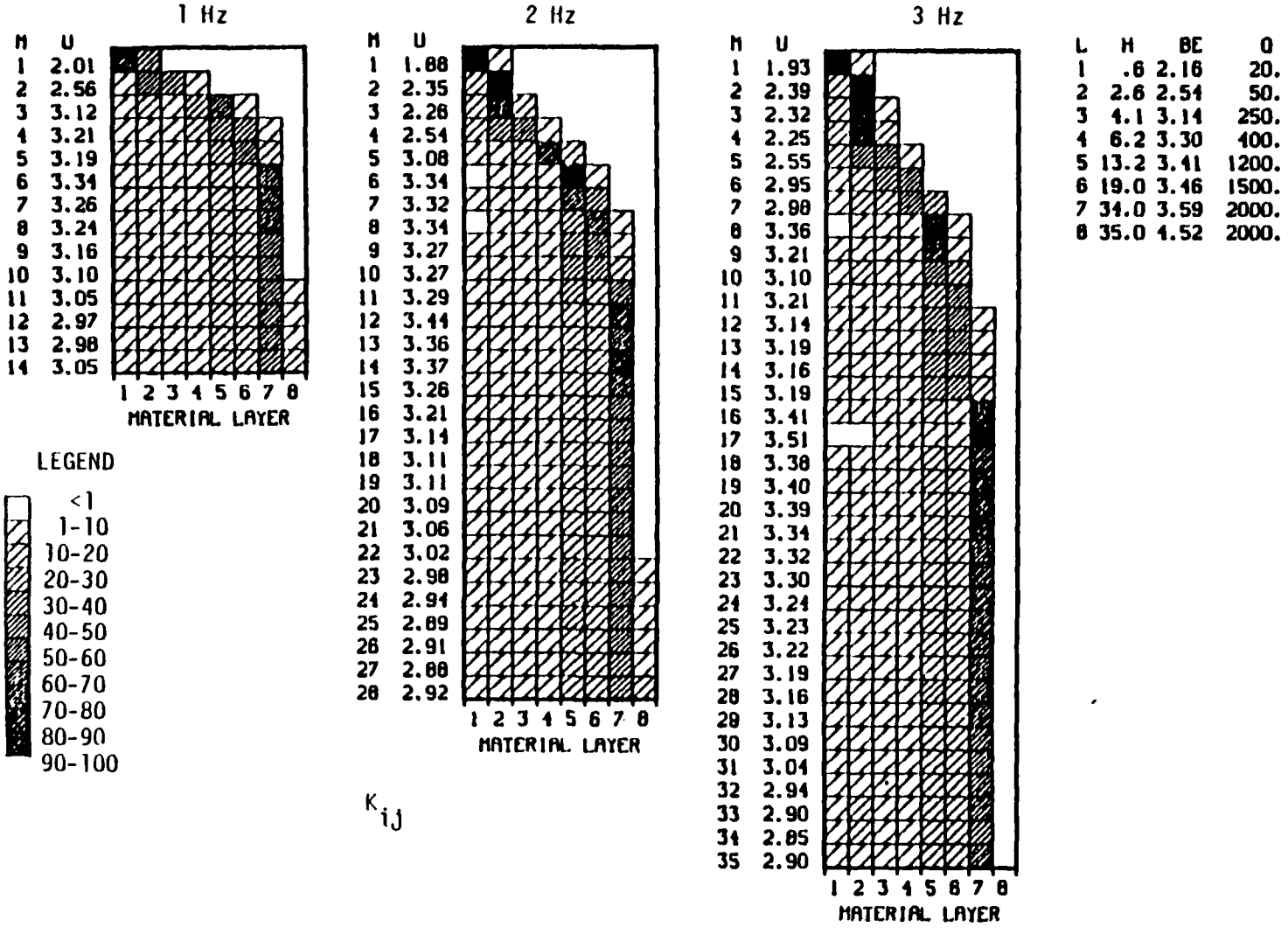

Figure 16a. The kinetic energy distribution, K_{ij}, for three frequencies is portrayed graphically for the Model S1. For each mode the percentage of energy in each layer is indicated by shading according to the legend. The mode number and its group velocity at the selected frequency is listed at the left of each graph. A table showing the interface depths, shear velocity (BE) and Q_β for the model is also printed.

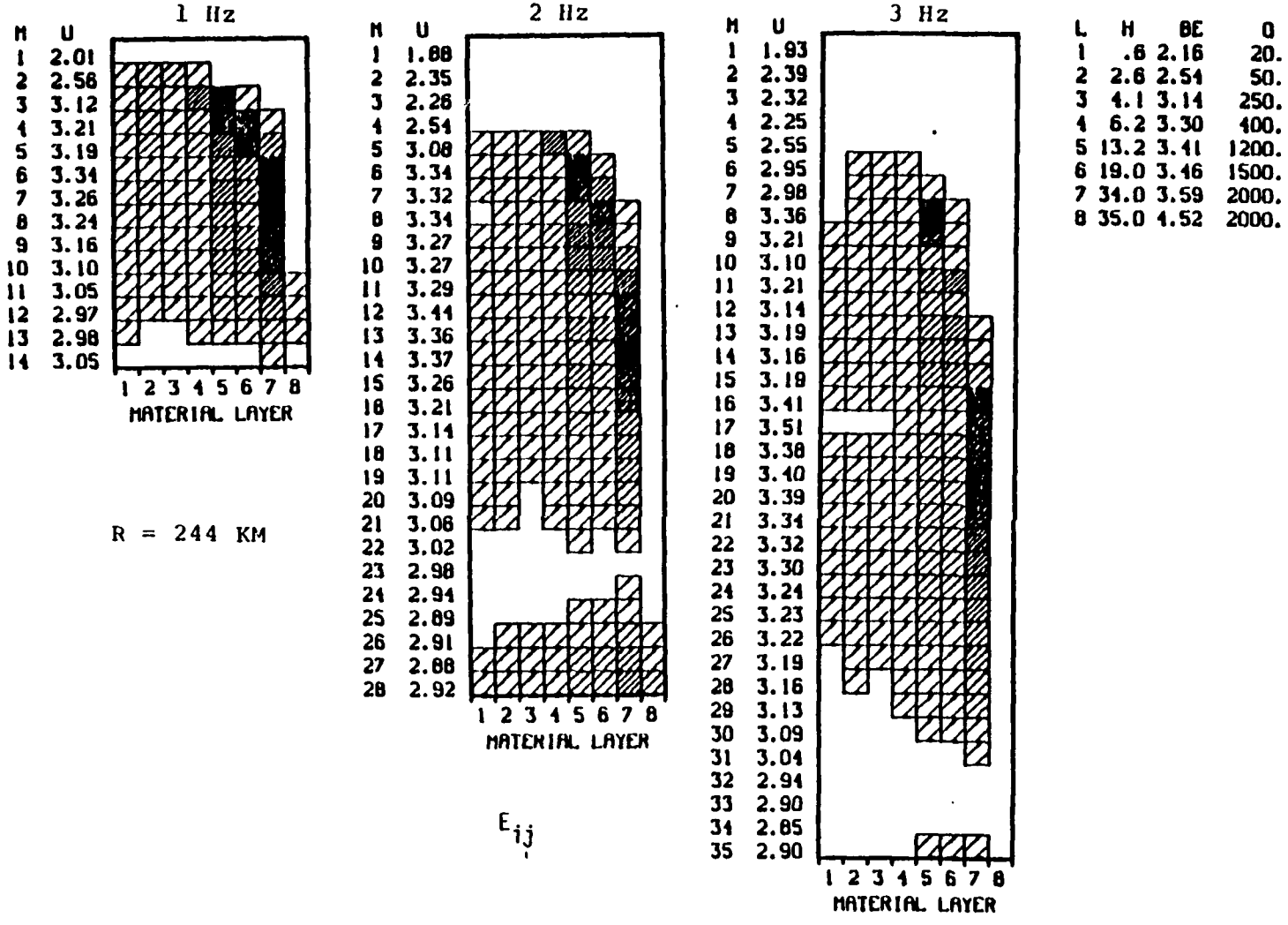

Figure 16b. The E_{ij} for structure S1 are displayed for three frequencies at two ranges. The maximum E_{ij} is scaled to have the value 100. The plots are then made with the shading indicated in the legend.

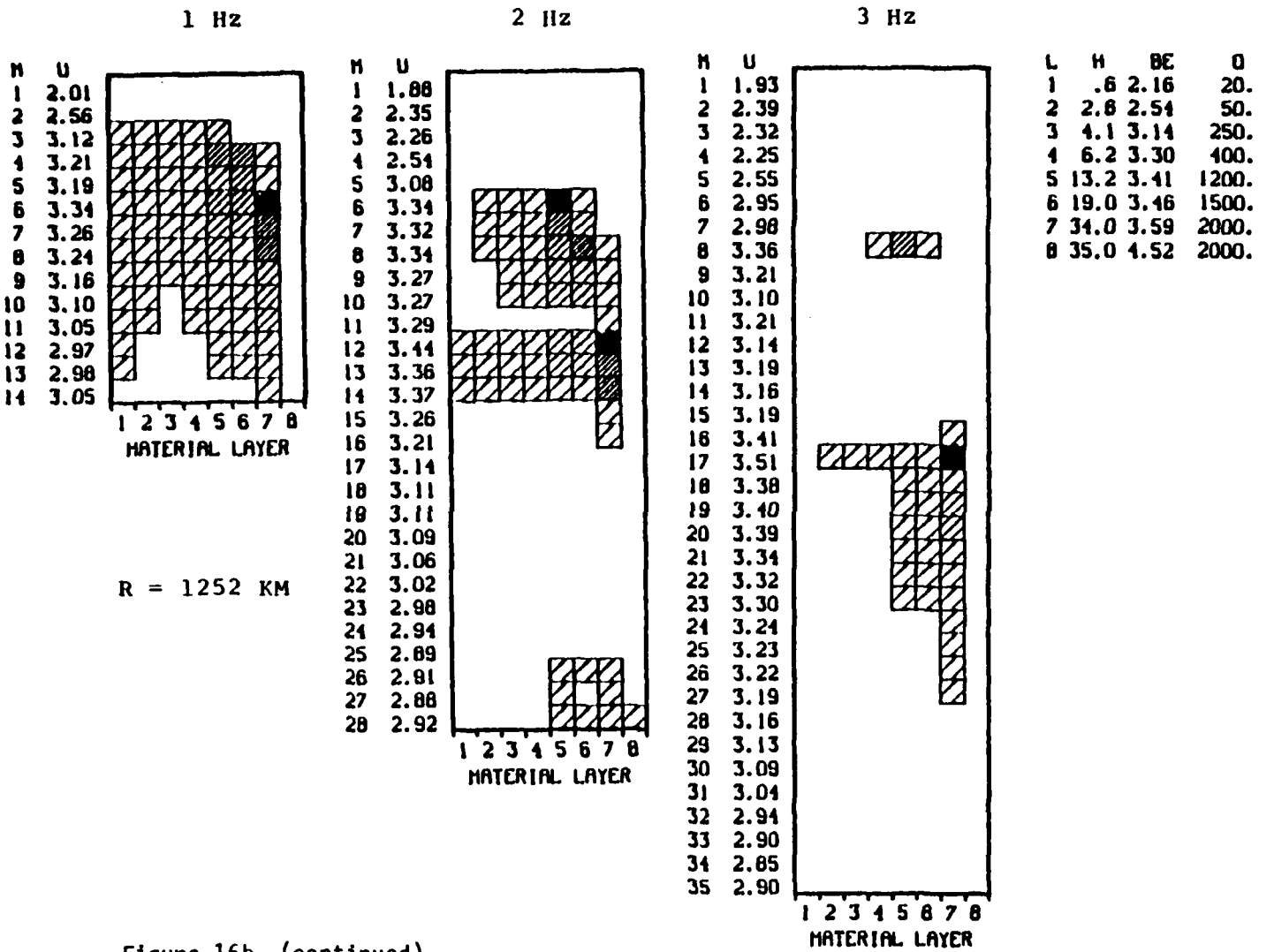

Figure 16b. (continued)

TABLE 7

WEIGHTED KINETIC ENERGY DISTRIBUTION (Γ_i)
BY LAYER FOR THE MODEL S1

R = 244 KM

I	H	BE	Q	1 Hz Energy	2 Hz Energy	3 Hz Energy
1	.6	2.16	20	15.33	8.49	6.04
2	2.6	2.54	50	21.15	11.12	8.58
3	4.1	3.14	250	11.92	9.86	7.08
4	6.2	3.30	400	21.64	22.22	11.98
5	13.2	3.41	1200	73.20	79.01	59.62
6	19.0	3.46	1500	55.09	60.96	41.86
7	34.0	3.59	2000	100.00	100.00	100.00
8	∞	4.52	2000	1.20	4.09	0.09

R = 1252

I	H	BE	Q	1 Hz Energy	2 Hz Energy	3 Hz Energy
1	0.6	2.16	20	11.45	3.94	1.77
2	2.6	2.54	50	14.18	5.82	2.34
3	4.1	3.14	250	7.45	7.02	2.62
4	65.2	3.30	400	13.04	14.81	4.21
5	13.2	3.41	1200	54.51	100.00	36.57
6	19.0	3.46	1500	47.72	70.62	13.28
7	34.0	3.59	2000	100.00	98.79	100.00
8	∞	4.52	2000	1.04	1.06	0.03

quite low in the near surface layers of our model, this energy does not propagate. This is seen in the E_{ij} plots and Γ_j table.

Another way to compare the observed and synthetic Lg phases is in the spectral domain. In Figure 17, we plot the spectrum of the group velocity window from 3.6 to 2.9 km/sec for the four vertical component SALMON observations in Figure 12 and for four other stations. The spectra from the larger range (> 1000 km) stations generally peak near 1 Hz and fall off at a rate between ω^{-2} and ω^{-3}. At the two closer stations, the spectral peak occurs at higher frequency and the rate of falloff is about ω^{-3}. The signal/noise is generally quite good in the frequency band from 0.7 to 2.0 Hz. Outside this band the signal/noise is often too small to allow much confidence in conclusions about the spectral behavior.

In Figure 18 we compare the synthetic and observed Lg spectra (windowed between 3.6 and 2.9 km/sec) from the seismograms plotted in Figure 15. It is not easy to draw conclusions from these comparisons. We do see that at 244 km the synthetic spectra fall off much more rapidly than the observed for frequencies above 2.5 Hz or so. The same is true at the larger distance, but the observations are contaminated with noise.

In summary, the comparisons of Figures 15 and 18 lead to the following conclusions:

- The Lg time signal is qualitatively similar to the observed Lg. The onset of synthetic Lg may be a bit more abrupt than is observed.
- Energy arriving with velocities greater than about 3.6 km/sec is not modeled.
- The model fails to account for the late arriving (slower than 2.9 km/sec) high frequency energy. This is associated with low order modes trapped in the top few kilometers where Q is low.

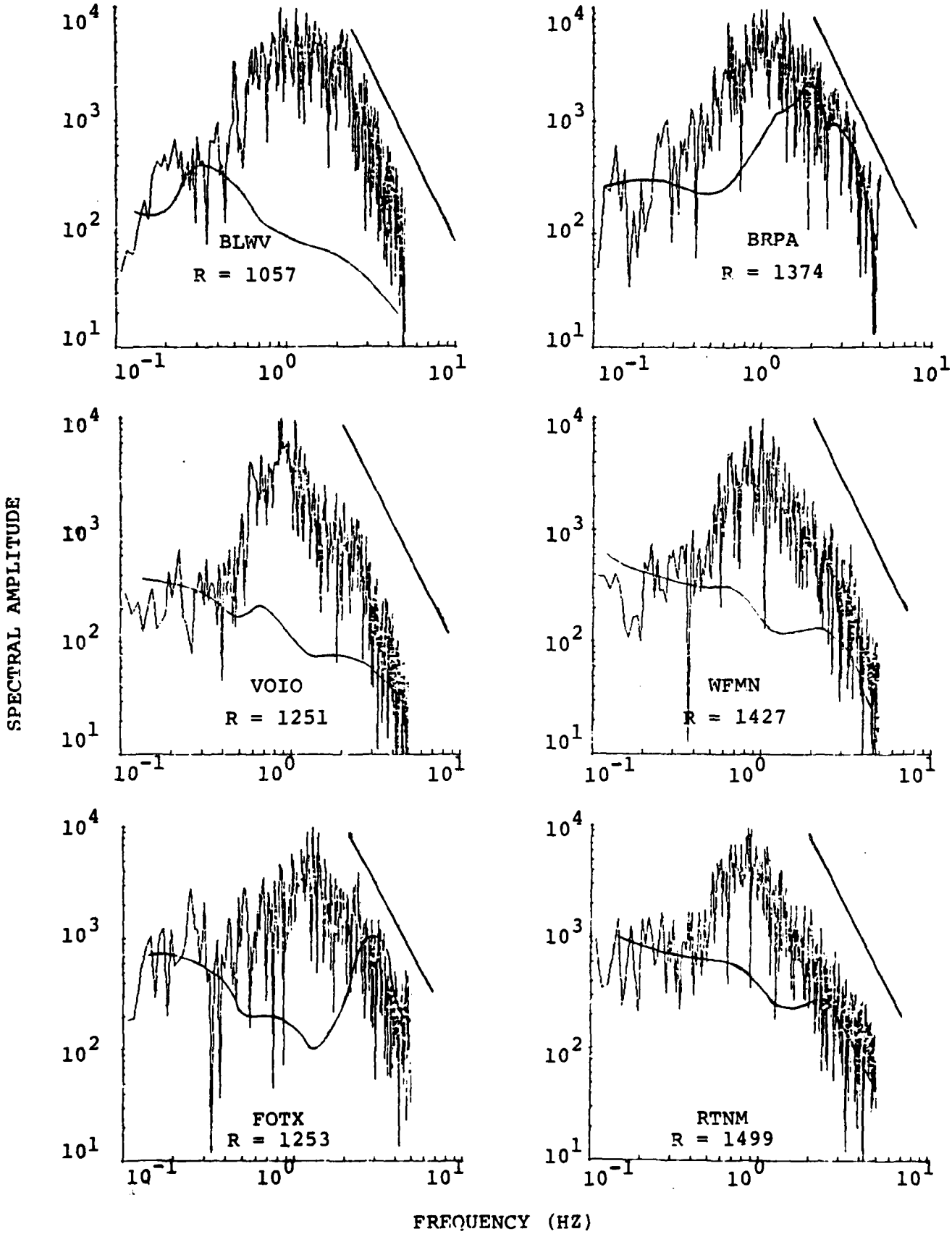

Figure 17. (Caption on next page)

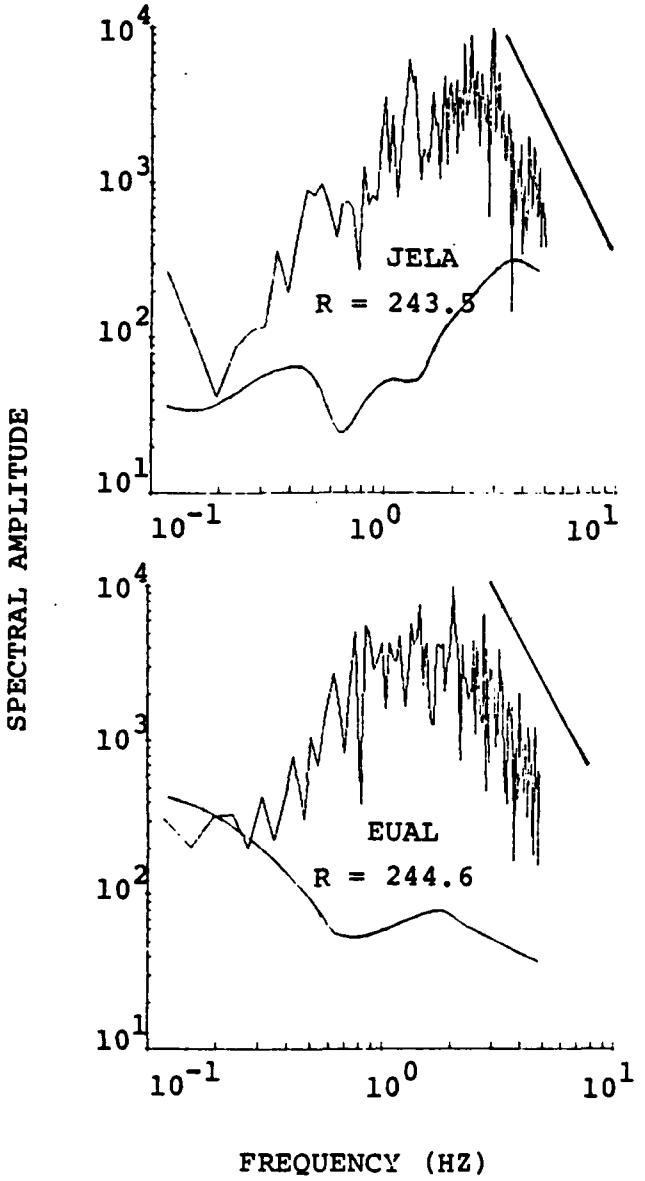

Figure 17. (continued) The Lg spectra (3.6 to 2.9 km/sec) are shown for observations of SALMON at eight LRSM stations. The spectral amplitudes have been normalized and lines of slope ω^{-3} are drawn on each plot. On each of the observed spectra, we plot a line drawn through the center of the spectrum of a noise sample taken before the P_n arrival time. The amplitude of the oscillations about this line is similar to the oscillations in the spectra from stations with R > 1000 km.

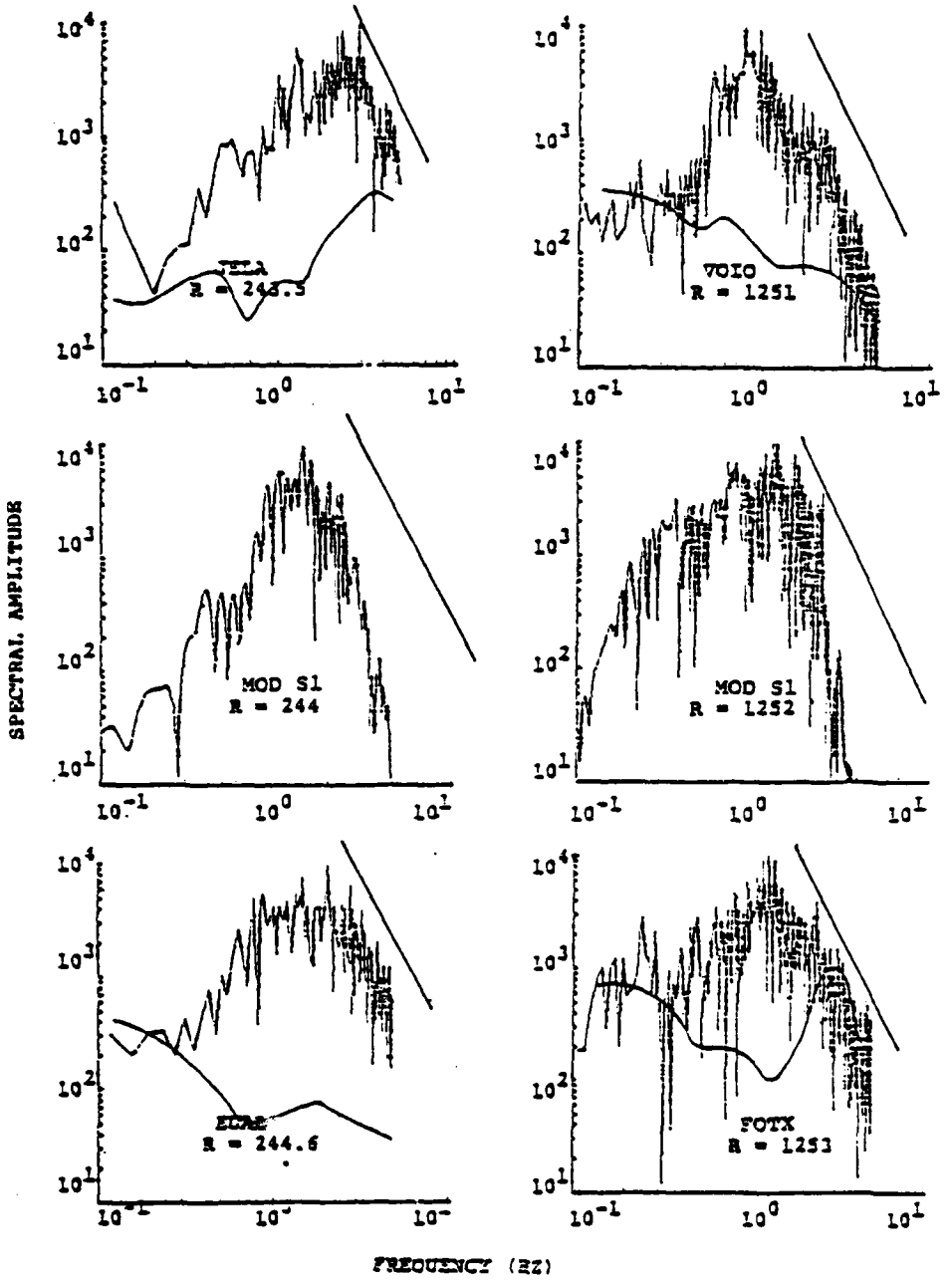

Figure 18. The Lg spectra (within the 3.6 to 2.9 km/sec group velocity window) for the synthetic seismograms in Figure 15 are compared to observed spectra at the same range. The observed spectra are truncated by a cosine filter above 4 Hz.

3.4 COMPARISON OF OBSERVED AND THEORETICAL AMPLITUDES

Thus far we have been entirely concerned with the waveform and spectral shape of the Lg synthetic seismograms. A satisfactory model must also give Lg phases that are in reasonable agreement with observed amplitude data.

There have been numerous studies of the attenuation of the 1 Hz Lg phase (vertical component) in the eastern United States (e.g., Nuttli, 1973; Bollinger, 1973, 1979; Street, 1976; Jones, et al., 1977). These studies employ a common method to describe the attenuation rate, which was suggested by Nuttli (1973). The amplitude is assumed to attenuate with distance as an Airy phase. That is,

$$A = K_1 \Delta^{-1/3} (\sin\Delta)^{-1/2} \exp(-\gamma\Delta), \qquad (1)$$

where K_1 is some constant and Δ is the range. The attenuation is then described by the γ which gives the best-fitting curve through the observations.

Nuttli (1973) gives $\gamma = 0.07$ deg^{-1} as the value that best characterizes the attenuation of 1 second vertical component Lg in North America, east of the Rocky Mountains. Bollinger (1979) found the 0.07 deg^{-1} attenuation rate to be appropriate for epicentral distances from 100 to 700 km in the southeastern United States. At longer distances, the rate is somewhat greater (0.10 deg^{-1}) for some events. A slightly greater attenuation rate (0.11 deg^{-1}) was found by Street (1976) for ranges of 4° to 30° in the northeastern United States.

In Figure 19 we plot the distance attenuation curves for several γ together with Lg amplitudes measured from recordings of SALMON at six stations. These recordings are displayed in Figure 20. To determine the Lg amplitude measurement, our convention was to measure the largest sustained amplitude (several cycles) within 10 seconds of the group arrival time associated with 3.5 km/sec group velocity.

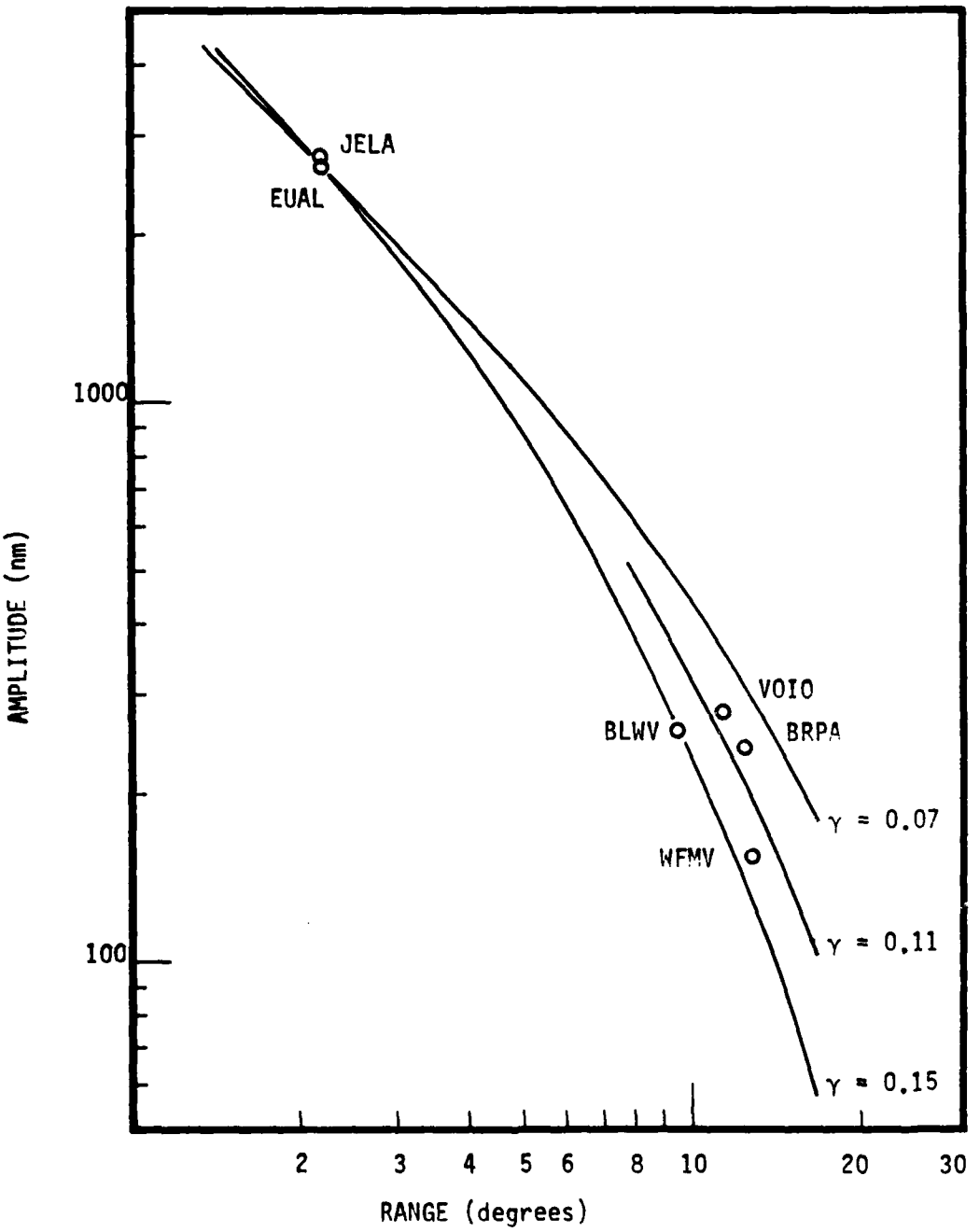

Figure 19. The Lg amplitudes from LRSM recordings of SALMON are plotted versus range. Curves are plotted for several apparent attenuation rates.

THIS PAGE LEFT BLANK

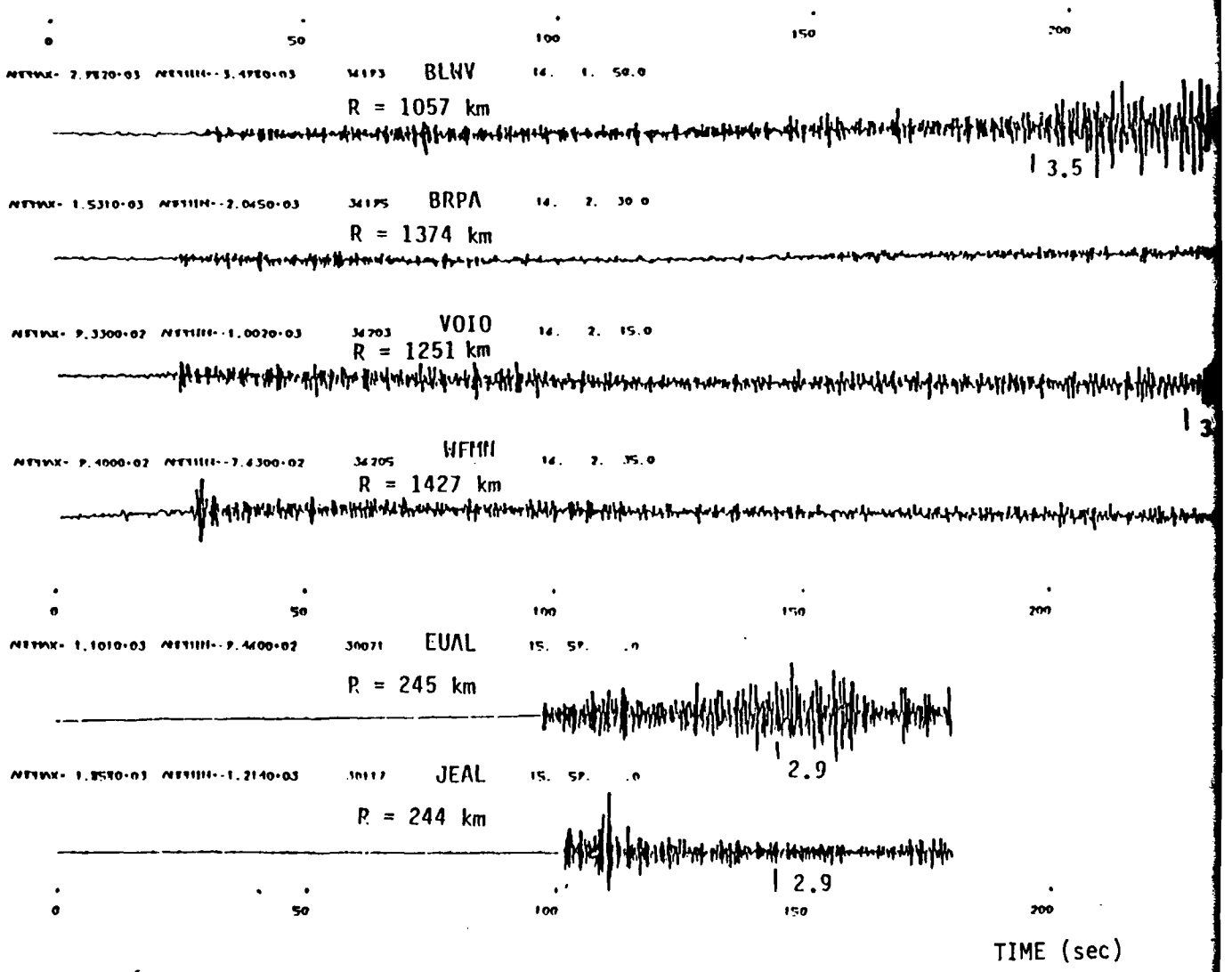

Figure 20. Observed short period recordings of SALMON a
minimum amplitudes are indicated along with
origin time was 16:00). The times for sever
record.

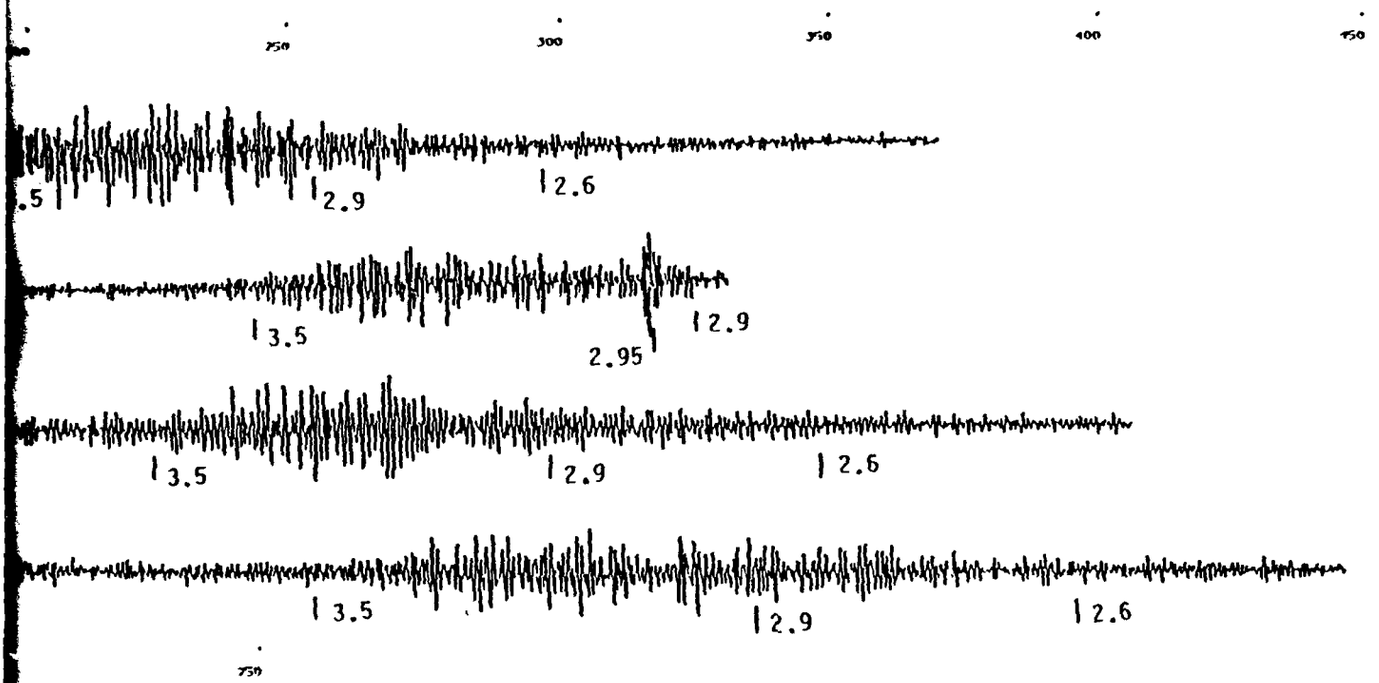

sec)

f SALMON are shown from six LRSM stations. The maximum and
long with the time of zero on the time scale (the event
s for several apparent group velocities are indicated on each

THIS PAGE LEFT BLANK

The attenuation curves in Figure 19 are forced to pass through the Lg amplitude at EUAL. The SALMON data appear to be consistent with an attenuation rate of about 0.10 to 0.15 deg^{-1}. However, the data points are restricted to two narrow distance bands (1.2 to 2.2 degrees and 9.5 to 12.9 degrees) so we cannot fit a γ curve very confidently. Further, the Lg attenuation for several of the southeastern United States events studied by Bollinger (1979) changed from 0.07 deg^{-1} for ranges less than 6 degrees to 0.10° deg^{-1} for greater ranges. Since the SALMON data are in clusters on either side of this division, we are again cautioned about the reliability of a γ determination from them.

In Figure 21 we again plot the SALMON Lg amplitudes along with analogous amplitudes measured on synthetic seismograms for our model S1. These synthetics are plotted in Figure 22 where we indicate the Lg amplitude measurement.

The obvious conclusion from Figure 21 is that the S1 model predicts greater Lg attenuation than is observed in the eastern United States. The synthetic data are consistent with a γ of about 0.34 deg^{-1}. The γ is related to the effective Q_β for the crust by

$$Q = \frac{\pi f}{U\gamma} \quad , \qquad (2)$$

where f is the frequency and U is group velocity. For 1 Hz energy at 3.5 km/sec group velocity, the effective Q is 294.

The kinetic energy distribution for S1 in Figure 16 and Table 7 indicates that most of the energy in the synthetic seismograms is in the layers in the lower crust where Q is 1200 to 2000. However, there appears to be enough energy in the low Q upper layers to substantially reduce the effective Q. The effective Q can be estimated by computing the mean Q^{-1} weighted by the Γ_i in Table 7. That is,

$$Q_{eff}^{-1} = \frac{1}{W} \sum_{i=1}^{n} \frac{\Gamma_i}{Q_i} \quad ,$$

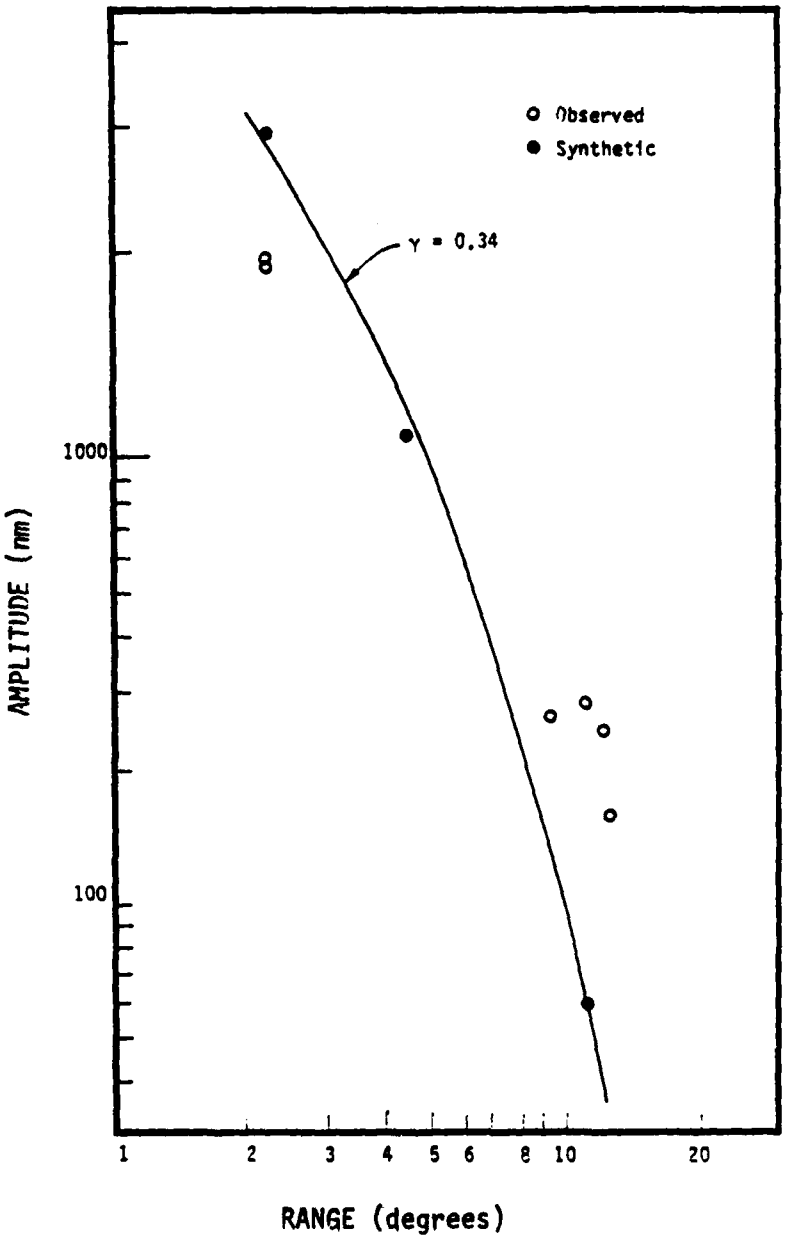

Figure 21. The synthetic Lg amplitudes from the S1 synthetic seismograms are plotted with the SALMON data.

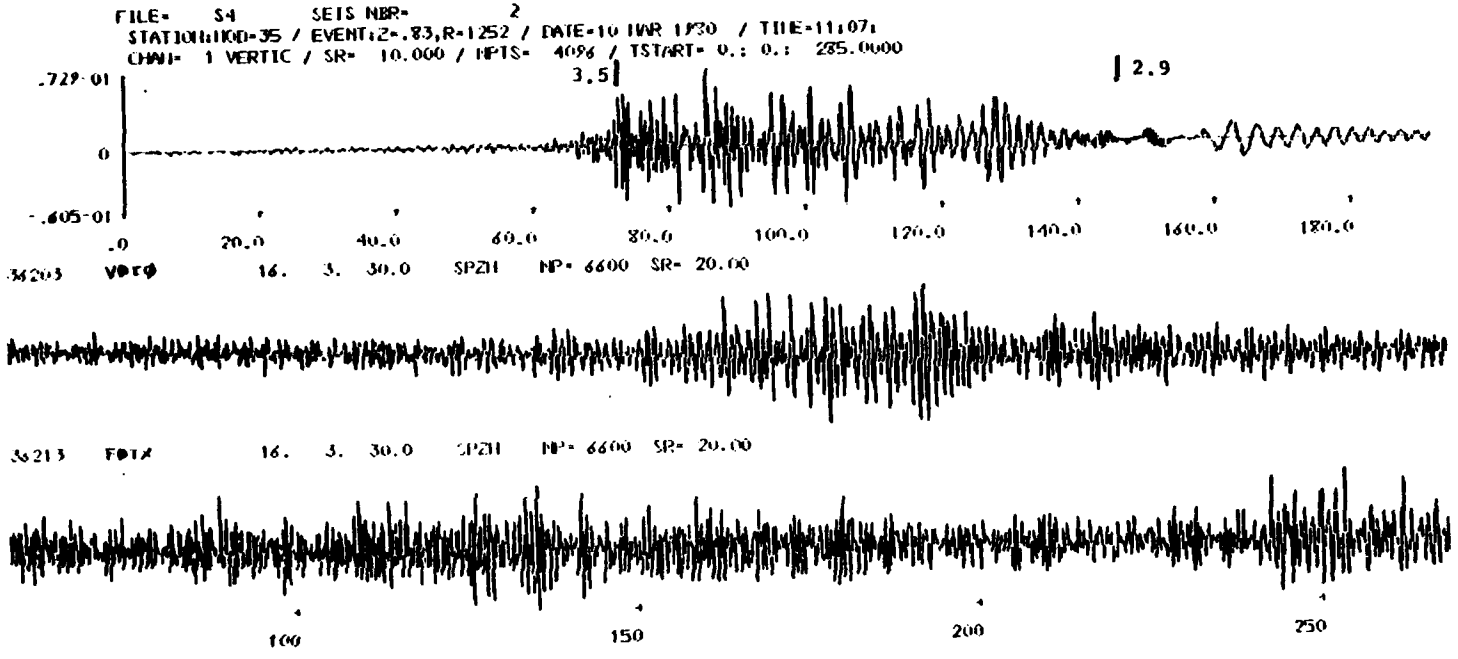

Figure 22. Synthetic seismograms are compared to SALMON observations for the model S4.

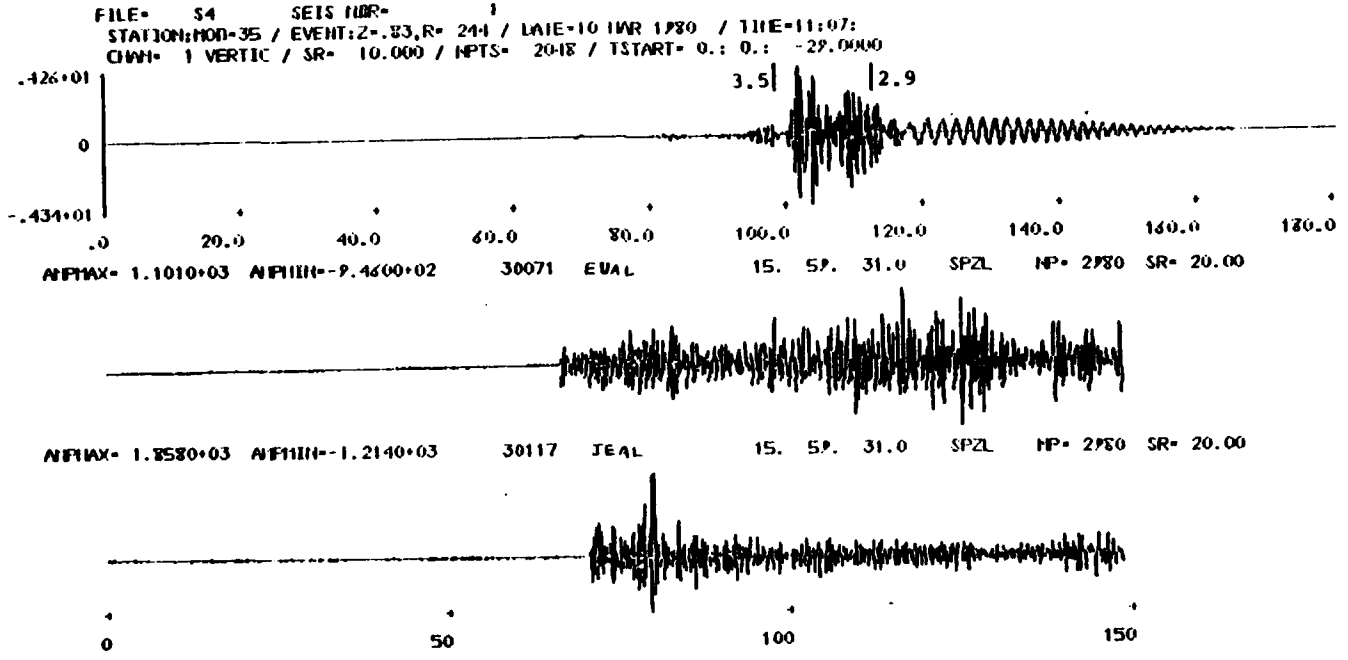

Figure 22. (continued)

where (3)

$$W = \frac{1}{n} \sum_{i=1}^{n} \Gamma_i \quad .$$

This effective Q should not be confused with the Rayleigh Q of a particular mode, but it is an estimate of the total Q for all modes which contribute to the seismograms at a particular frequency. The Q_{eff} values computed from the Γ_i for S1 in Table 7 are listed below:

	R = 244 km	R = 1252 km
1 Hz	208	238
2 Hz	328	540
3 Hz	356	655

The effective Q associated with the γ fit in Figure 21 is 294, which falls between the 1 and 2 Hertz values in the above listing. The dominant frequency where the Lg amplitudes are measured in the seismograms in Figure 22 is in this range.

The good agreement between the effective Q determined by Nuttli's (1973) method in Figure 21 and the Q_{eff} determined from the mean Q^{-1} weighted by the amount of kinetic energy in each layer is quite an interesting result. Note that the Q_{eff} increases with range. This means that the path for the dominant energy is deeper for larger ranges, which is in accordance with our expectation. The Q_{eff} also increases with frequency. This is because the higher frequency energy at shallow depths is severaly attenuated and contributes very little energy to the seismogram.

The increase in Q_{eff} with range suggests that the γ should decrease with range. In fact, the amplitude data in Figure 21 show this trend. The two smallest range plots are fit with $\gamma = 0.42$, which implies a 1 Hz effective Q of 238, while the two larger range points are fit with $\gamma = 0.32$, which implies an effective Q of 312.

3.5 PARAMETRIC VARIATIONS OF THE MODEL S1

3.5.1 Introduction

The model S1 leads to synthetic Lg that resemble observed Lg in the group velocity window from 3.5 to 2.9 km/sec. The associated spectra are also in reasonable qualitative agreement with the data. But there are several data features that are not modeled very well by the synthetic seismograms. These are:

- The synthetics include too little late arriving high frequency energy.
- The synthetic Lg spectra fall off too rapidly at high frequencies, especially at the closer range.
- The synthetic Lg amplitude attenuation is much greater than observed in the eastern United States.

In this section we show the results from several models in which we attempted to improve the synthetic seismogram match to the data characteristics mentioned above. Most of our attention is on changing the Q model to reduce the attenuation, since the listed model deficiencies all seem to indicate that S1 has too much attenuation. However, we are constrained by the requirement for low Q near the surface to reduce the amplitude of the fundamental mode, as was discussed in Section 3.2. Also, we saw in Figure 21 that the agreement of observed and synthetic Lg amplitudes is really not too bad as far as absolute values are concerned. Simply raising the Q to match the observed amplitude-distance attenuation will not be satisfactory because it will give synthetic seismogram amplitudes that are huge compared to the observed SALMON amplitudes.

In this section we will first describe more carefully the source functions and instrument response used in in constructing the synthetic seismograms. While there may be some errors in these factors, especially the source specification, they are not likely to influence the gross features we are looking for in our comparison with data.

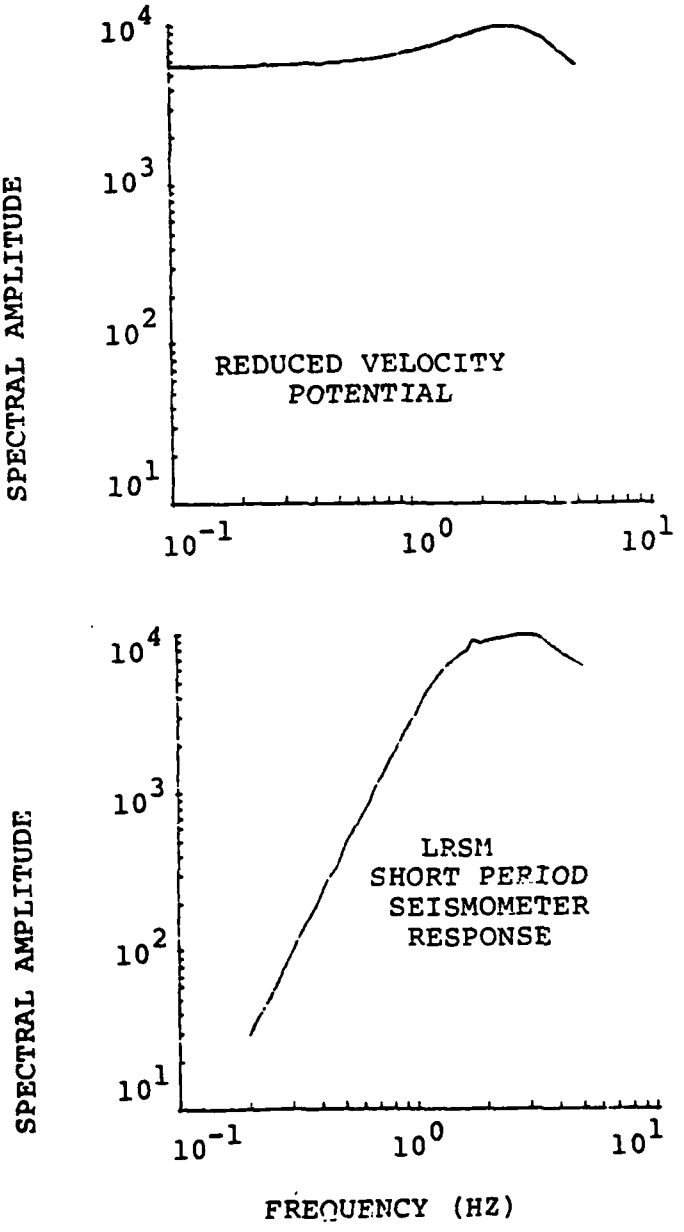

Figure 23. Spectral amplitude of the instrument response and source function used to construct the synthetic seismograms. There appears to be an anomalous point in the instrument response near 1.6 Hz, but this should have little effect.

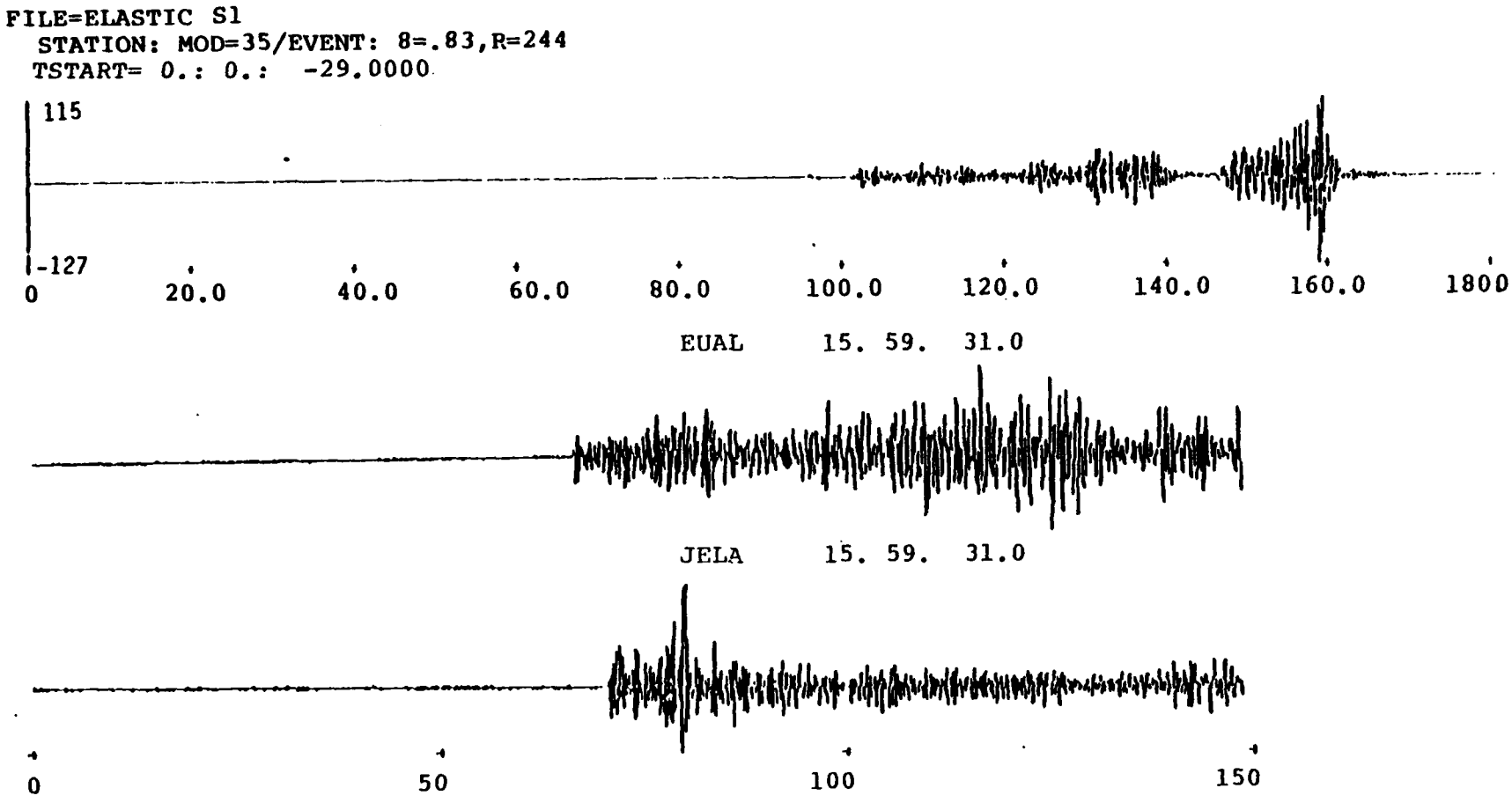

Figure 24. Synthetic seismograms for the crustal model S1 with infinite Q are compared to observations of SALMON. Zero time on the synthetics is correctly aligned with the observations.

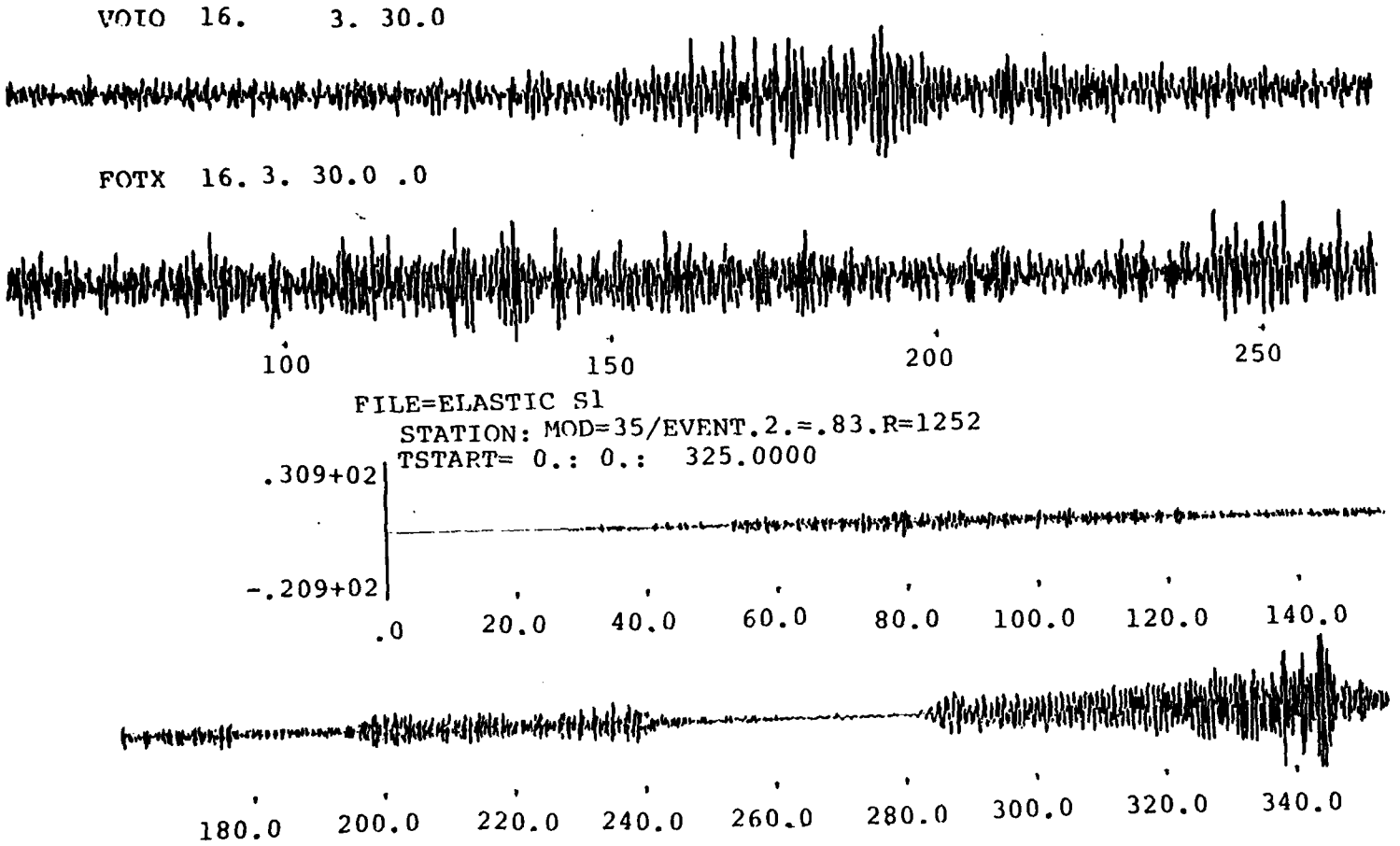

Figure 24. (continued. Note that the synthetic is plotted in two sections, broken at the time corresponding to the end of the observed records).

TABLE 8

WEIGHTED KINETIC ENERGY DISTRIBUTION (Γ_i) BY LAYER FOR S1 WITH INFINITE Q

R = 1252

I	H	BE	Q	1 Hz Energy	2 Hz Energy	3 Hz Energy
1	0.60	2.16	∞	100.00	100.00	100.00
2	2.60	2.65	∞	61.50	18.21	12.92
3	4.10	3.14	∞	7.20	3.71	2.59
4	6.20	3.30	∞	4.06	1.11	1.52
5	13.20	3.41	∞	9.44	1.35	2.68
6	19.0	3.46	∞	6.64	1.00	2.02
7	34.00	3.59	∞	11.84	2.13	1.37
8	35.00	4.52	∞	0.15	0.07	0.00

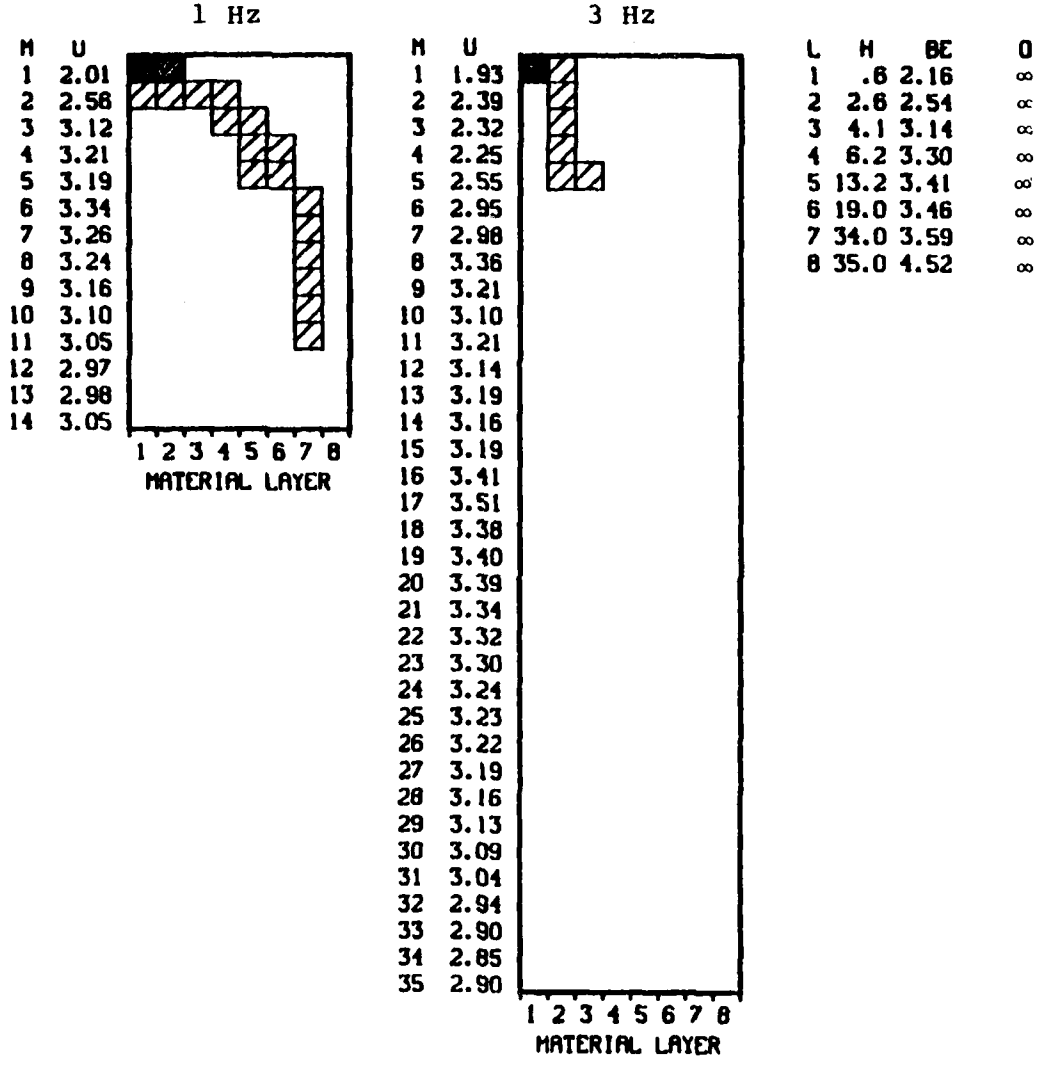

Figure 25. The E_{ij} is plotted at R = 244 km for the model S1 with infinite Q.

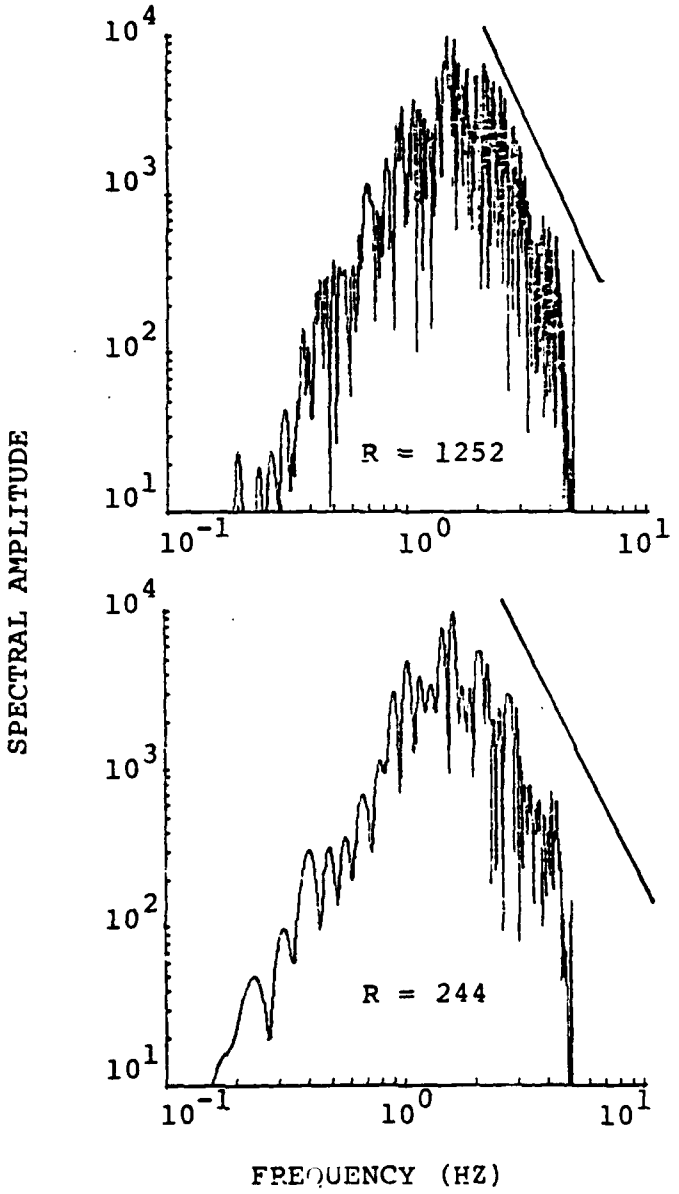

Figure 26. The Lg spectra are plotted at two ranges for the model S1 with infinite Q. These spectra are truncated with a cosine filter above 4 Hz.

Since the Q model is the main issue, we look at the synthetics for infinite Q as a bound. We then compute seismograms for several Q models that might be thought to improve agreement with the data. We also look at one model in which the velocity-depth profile is somewhat different from S1, though the crustal thickness is held fixed. Our conclusions based on these parameter variations are listed in Section 3.6.

3.5.2 Source and Seismometer Contributions

In Figure 23 we plot the spectrum of the source function and seismometer response used for the synthetic seismogram calculations. The source is presented in terms of the spectral amplitude of the reduced velocity potential. This is the SALMON source function proposed by Murphy (1969) which gives good fit to the observed near-field ground motions.

The source spectrum is nearly that of a delta function over the relevant frequency band. The actual source function would have to be very strongly peaked at frequencies greater than 2.5 Hz to bring the observed and theoretical spectra into closer agreement. The near-field data (Springer, et al., 1968) give no indication that this is the case.

3.5.3 An Elastic Model

What is the effect of the Q model we have assumed? In Figure 24 we show the seismograms for the structure S1 with infinite Q. That is, the model is elastic. Later arriving high frequency energy is present, but the seismogram is dominated by the sinusoidal fundamental mode waveform. This can be clearly seen in the E_{ij} plots in Figure 25 and Γ_i listing in Table 8. Nearly all the energy at high frequencies is in the fundamental mode and is trapped in the top 600 meters. Even at 1 Hz only the top two layers, extending to a depth of 2.6 km, are important.

The Lg spectra for the elastic model seismograms are plotted in Figure 26. Comparing to the observed spectra in Figure 17, we

see that the elastic model does lead to spectra with about the right high frequency falloff, though, the high frequencies are actually too dominant in these spectra. An elastic model is by no means thought to be realistic, but does indicate that higher Q will bring the high frequency part of the synthetic spectra in closer agreement with observations.

3.5.4 The Effect of Variations in the Q Model

In Table 9 we list four Q models for which seismograms will be compared. The first is S1 from Table 6 and all the models have this velocity profile. The next model, S5, has higher Q in the mid-crust and much higher Q in the near-surface layers. The Model S6 has a very low Q in the top 600 meters and is essentially elastic at the base of the crust. In the mid-crust it is a high Q model. An extreme example of a high Q model is S7, for which only low Q values are in the top 2.6 km. Synthetic seismograms are compared for these four models in Figure 27.

The Lg amplitudes of these seismograms are listed in Table 10 along with the observed SALMON amplitudes from stations at the same range. Models S5 and S7 have amplitudes very close to those observed at the large distance, and S6 is not too much different. However, the higher Q models all have amplitudes much larger than those observed at the 244 km range. This is because the attenuation parameter γ remains too large.

To quantify the attenuation we again look at the energy distribution in these models in Figure 28 and Table 11. The γ for these models can be computed from the Γ_i in Table 11 using (2) with the Q_{eff} computed from (3) in Section 3.4. This gives a γ for a specific range. We know that γ decreases with range because the proportion of energy in the higher Q deep layers is greater.

We compute the γ for S5, S6 and S7 at R = 1242 km and for f = 1.5 Hz. The Q_{eff} at 1.5 Hz is taken to be the mean of the Q_{eff} values for 1 and 2 Hz, computed from (3) using the Γ_i in Table

TABLE 9

Q MODELS FOR THE STRUCTURE OF TABLE 3 MODEL

Depth	β	S1	S2	S6	S7
0.6	2.16	20	50	20	20
2.6	2.54	50	350	200	200
4.1	3.14	250	400	400	2000
6.2	3.30	400	500	500	5000
13.2	3.41	1200	2000	3000	10000
19.0	3.46	1500	2000	4000	10000
34.0	3.59	2000	2000	5000	10000
∞	4.52	2000	2000	5000	10000

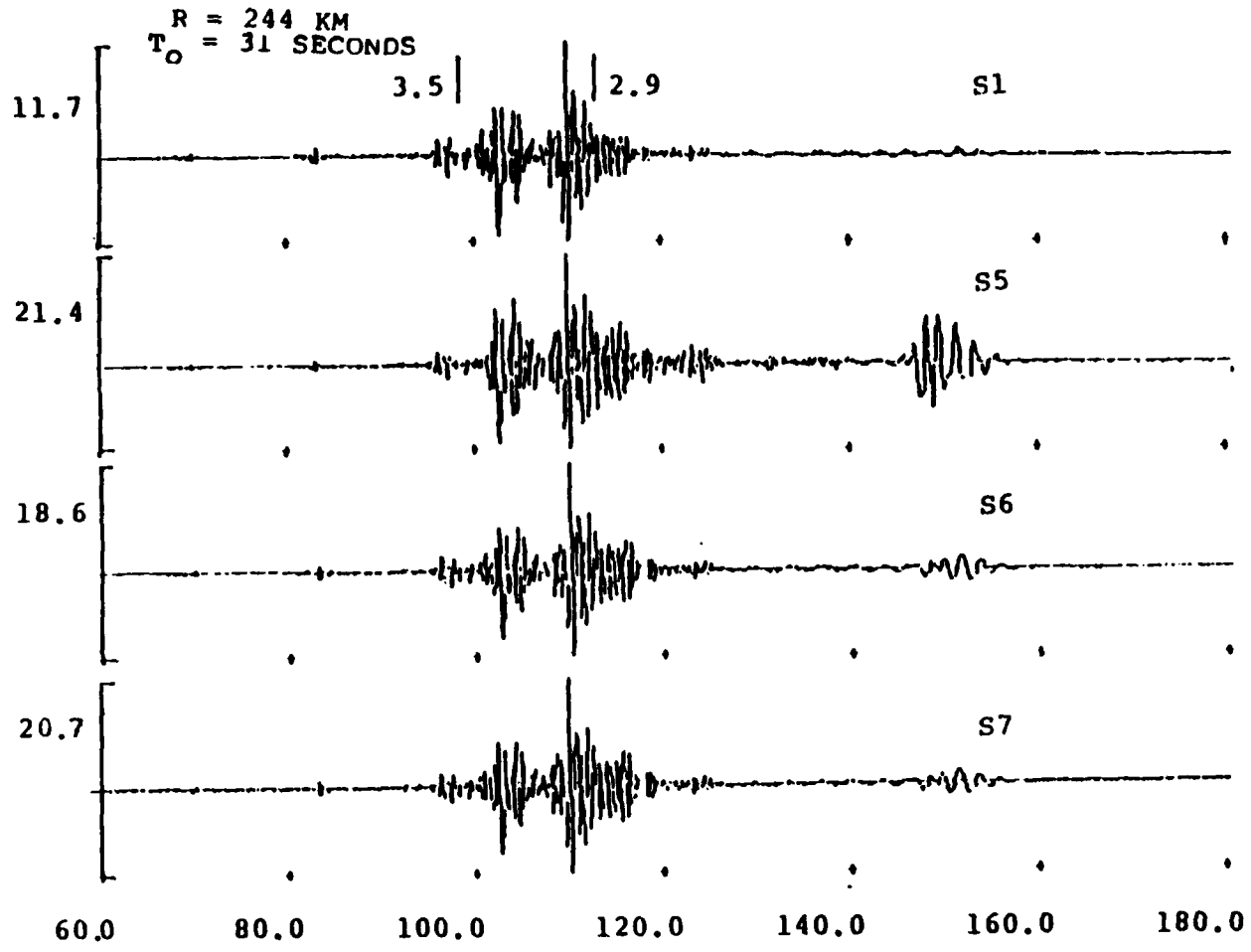

Figure 27. Synthetic seismograms (35 modes) are compared for five Q models used with the structure S1. The Mueller/Murphy SALMON source and LPSM instrument were used in the calculation. The peak-to-peak amplitude in microns is listed with each seismogram.

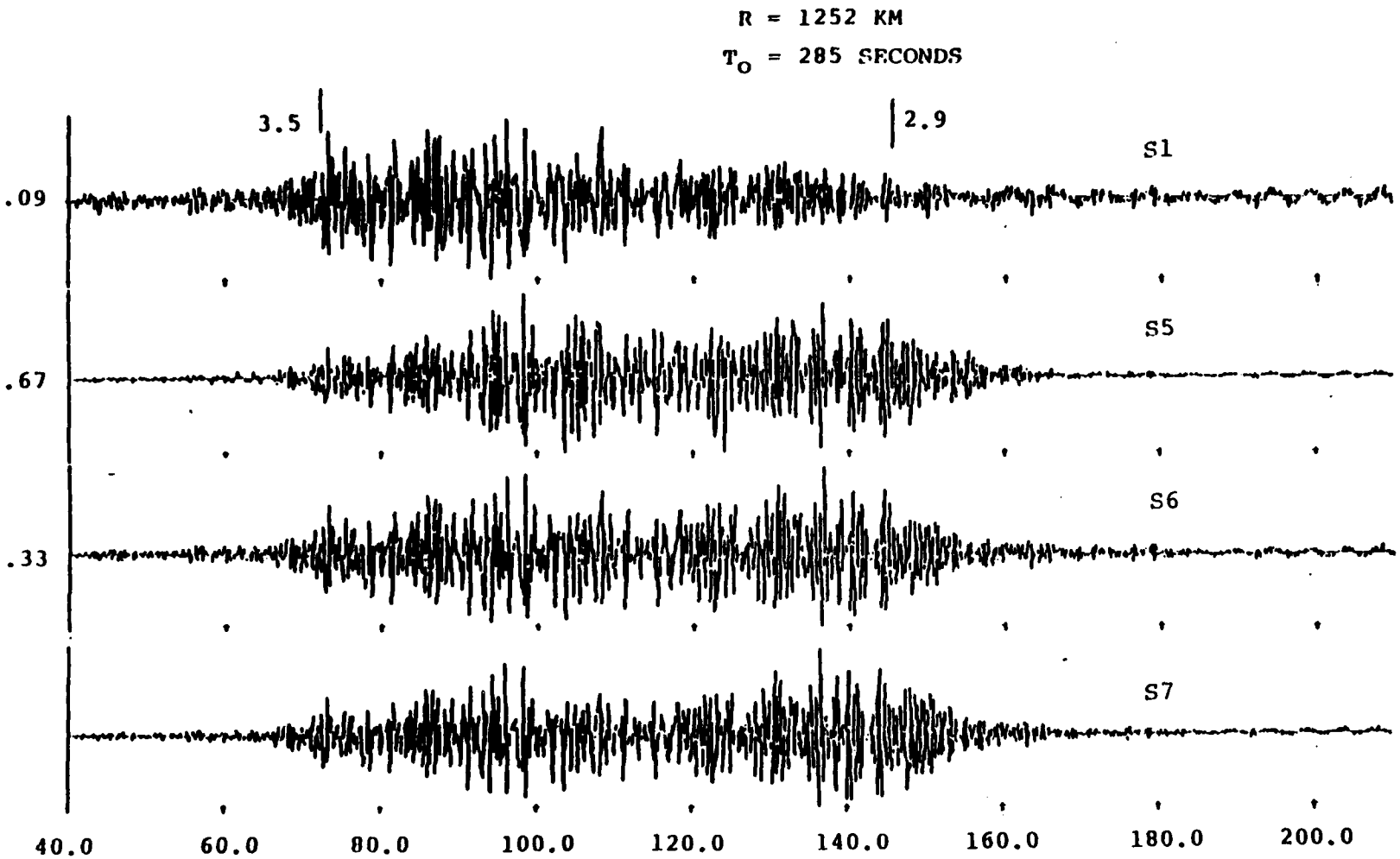

Figure 27. (continued)

TABLE 10

Lg AMPLITUDES FOR THE SEISMOGRAMS IN FIGURE 27

Model	Lg Amplitude (nm) R = 244 km	R = 1252 km
S1	5250	58
S5	11140	266
S6	8930	167
S7	11590	265
	Observed Amplitude	
JEAL	2746	
EUAL	2649	
VOIO		279

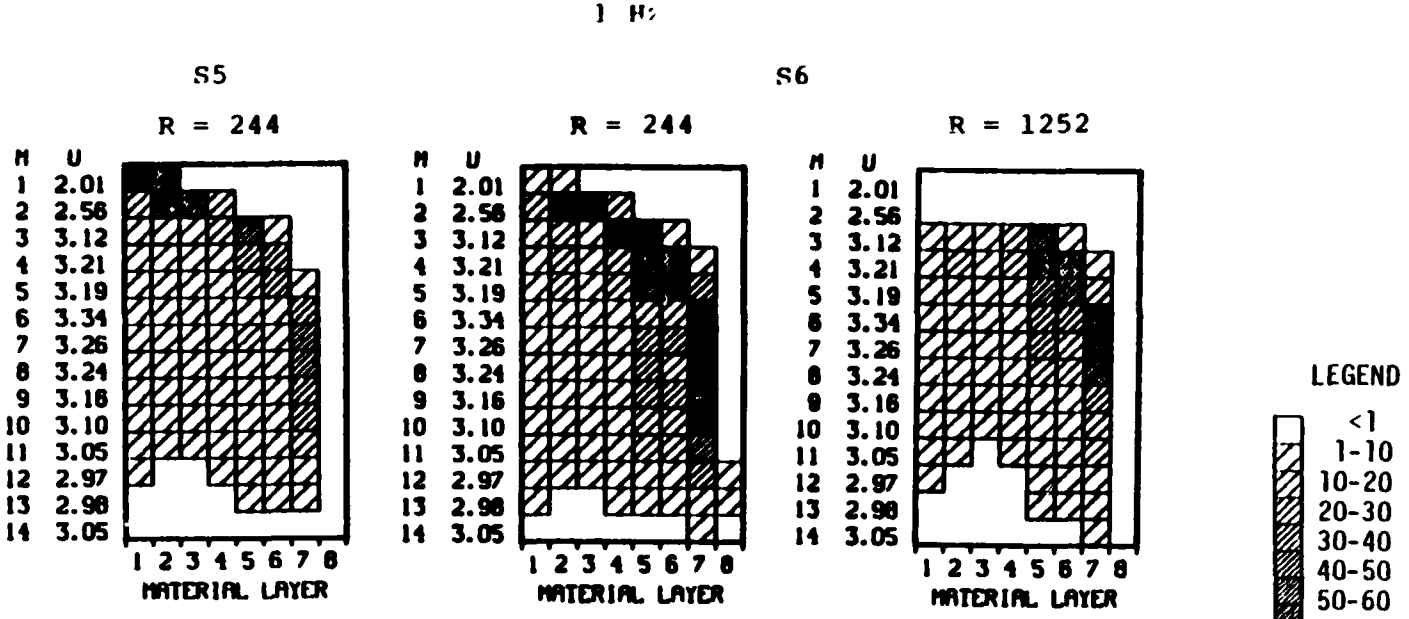

L	H	BE	Q
1	.6	2.16	50.
2	2.6	2.54	350.
3	4.1	3.14	400.
4	6.2	3.30	500.
5	13.2	3.41	2000.
6	19.0	3.46	2000.
7	34.0	3.59	2000.
8	35.0	4.52	2000.

L	H	BE	Q
1	.6	2.16	20.
2	2.6	2.54	200.
3	4.1	3.14	400.
4	6.2	3.30	500.
5	13.2	3.41	3000.
6	19.0	3.46	4000.
7	34.0	3.59	5000.
8	35.0	4.52	5000.

Figure 28. The K_{ij} distributions are plotted for the models S5 and S6 at two frequencies. The plots for S7 are nearly the same as those for S6.

3 Hz

S5

R = 244

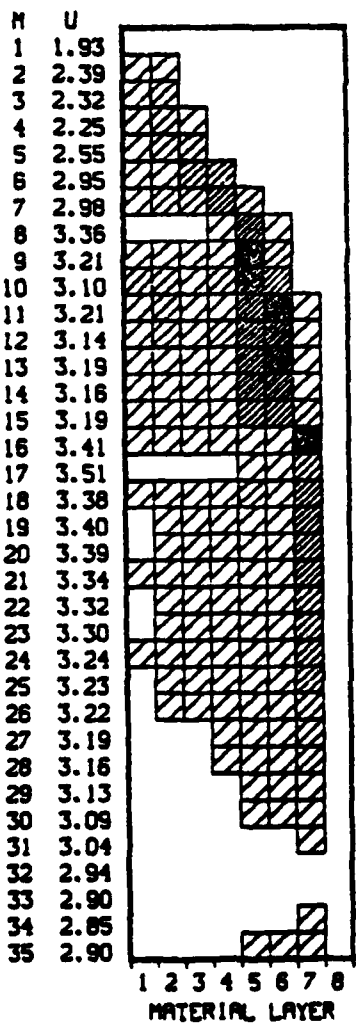

L	H	BE	Q
1	.6	2.16	50.
2	2.6	2.54	350.
3	4.1	3.14	400.
4	6.2	3.30	500.
5	13.2	3.41	2000.
6	19.0	3.46	2000.
7	34.0	3.59	2000.
8	35.0	4.52	2000.

S6

R = 244

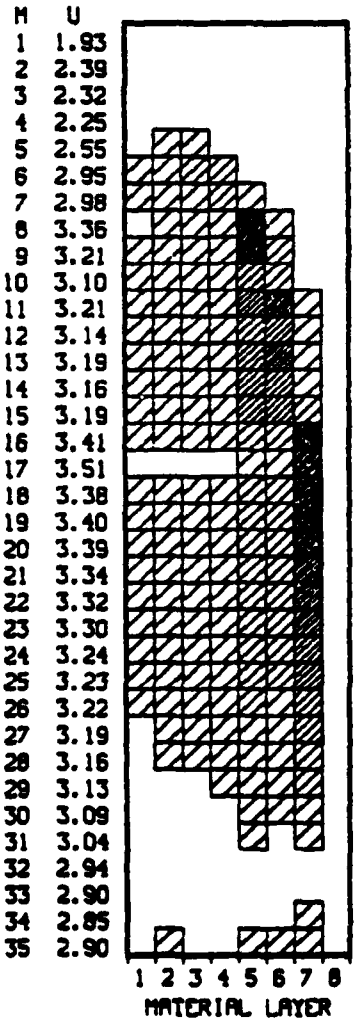

L	H	BE	Q
1	.6	2.16	20.
2	2.6	2.54	200.
3	4.1	3.14	400.
4	6.2	3.30	500.
5	13.2	3.41	3000.
6	19.0	3.46	4000.
7	34.0	3.59	5000.
8	35.0	4.52	5000.

Figure 28. (continued)

TABLE 11

WEIGHTED KINETIC ENERGY DISTRIBUTION (Γ_1) IN THREE Q MODELS

S5 — k = 244

I	H	BE	Q	1 Hz Energy	2 Hz Energy	3 Hz Energy
1	0.60	2.16	50	76.24	17.44	14.87
2	2.60	2.54	350	80.68	43.68	28.93
3	4.10	3.14	400	36.68	21.96	21.04
4	6.20	3.30	500	28.58	29.34	31.60
5	13.20	3.41	2000	77.84	67.74	100.00
6	19.00	3.46	2000	56.25	51.85	77.35
7	34.00	3.59	2000	100.00	100.00	81.77
8	35.00	4.52	2000	1.20	3.78	0.09

S6

I	H	Q	Energy	Energy	Energy
1	0.60	20	20.28	9.49	9.02
2	2.60	200	40.71	13.18	13.72
3	4.10	400	27.27	11.31	11.45
4	6.20	500	26.82	26.47	19.69
5	13.20	3000	78.76	76.83	79.64
6	19.00	4000	57.21	58.72	58.01
7	34.00	5000	100.00	100.00	100.00
8	35.00	5000	1.15	4.78	0.11

S7

I	H	Q	Energy	Energy	Energy
1	0.60	20	21.48	10.13	10.50
2	2.60	200	46.44	13.68	16.91
3	4.10	2000	31.80	13.21	16.37
4	6.20	5000	29.09	34.95	27.96
5	13.20	10000	82.18	80.68	86.40
6	19.00	10000	58.10	60.02	61.66
7	34.00	10000	100.00	100.00	100.00
8	35.00	10000	1.16	4.90	0.11

S5 — R = 1252

I	H	Q	1 Hz Energy	2 Hz Energy	3 Hz Energy
1	0.60	50	14.62	6.66	4.10
2	2.60	350	20.15	9.60	5.61
3	4.10	400	11.11	9.05	4.95
4	6.20	500	20.17	17.28	8.18
5	13.20	2000	71.25	93.88	52.47
6	19.00	2000	56.36	68.96	28.73
7	34.00	2000	100.00	100.00	100.00
8	35.00	2000	1.02	4.65	0.08

S6

I	H	Q	Energy	Energy	Energy
1	0.60	20	13.45	4.21	2.40
2	2.60	200	18.26	7.20	3.23
3	4.10	400	9.19	7.74	3.49
4	6.20	500	19.46	15.44	5.74
5	13.20	3000	72.71	100.00	51.64
6	19.00	4000	58.96	70.28	17.34
7	34.00	5000	100.00	85.14	100.00
8	35.00	5000	0.80	3.98	0.05

S7

I	H	Q	Energy	Energy	Energy
1	0.60	20	15.07	4.03	2.71
2	2.60	200	21.92	7.12	3.73
3	4.10	2000	10.88	7.78	4.03
4	6.20	5000	25.95	16.16	6.74
5	13.20	10000	89.07	100.00	66.74
6	19.00	10000	64.20	69.87	19.39
7	34.00	10000	100.00	70.81	100.00
8	35.00	10000	0.85	4.00	0.06

11. The γ computed this way are 0.21 deg^{-1} for S5 and S7 and 0.26 deg^{-1} for S6. These should be compared to γ = 0.34 deg^{-1} for S1 which we found in Section 3.4. Our confidence that these are the correct γ characterizing these four structures is enhanced by the fact that they almost perfectly predict the relative Lg amplitudes at R = 1252 km listed in Table 10.

The final comparison is that for the Lg spectra and is shown in Figure 29. These spectra are remarkably similar. Since all the seismograms were computed with the same velocity model, and the Lg is mostly associated with propagation near the base of the crust where the Q is high in every model, this should not be too surprising. The lowest Q model is S1, and this is evidenced in the high frequency part of the spectrum, especially at 1252 km.

3.5.5 Lg Synthetic Seismograms for an Altered Velocity Model

Before listing our conclusions from comparing the Q models listed in Table 9, we examine the seismograms from a model with a somewhat different velocity-depth profile. This is the model S4 listed in Table 12. The β and Q for this model are compared to those for S1 in Figure 30. We see that the two models have the same crustal thickness. The high velocity crustal granites are closer to the surface in S4 and a small gradient has been added at the base of the crust. The S4 has higher Q in the top 4 km and lower Q in the mid-crust between 4 and 12 km.

The phase and group velocity curves for S4 are shown in Figure 31. Comparing to those for S1 in Figure 12, we see that there are relatively few modes with group velocities less than 3 km/sec, due to there being less gradient near the surface.

The seismograms for this model are shown in Figure 32, where they are compared to the SALMON data and to the seismograms from S1. The Lg has a more abrupt onset for S4. It is also longer period. This can be seen in Figure 33 where we compare Lg spectra for the two models. The lower Q in the mid-crust is apparently the cause for this frequency shift. Also, as we have seen before, the

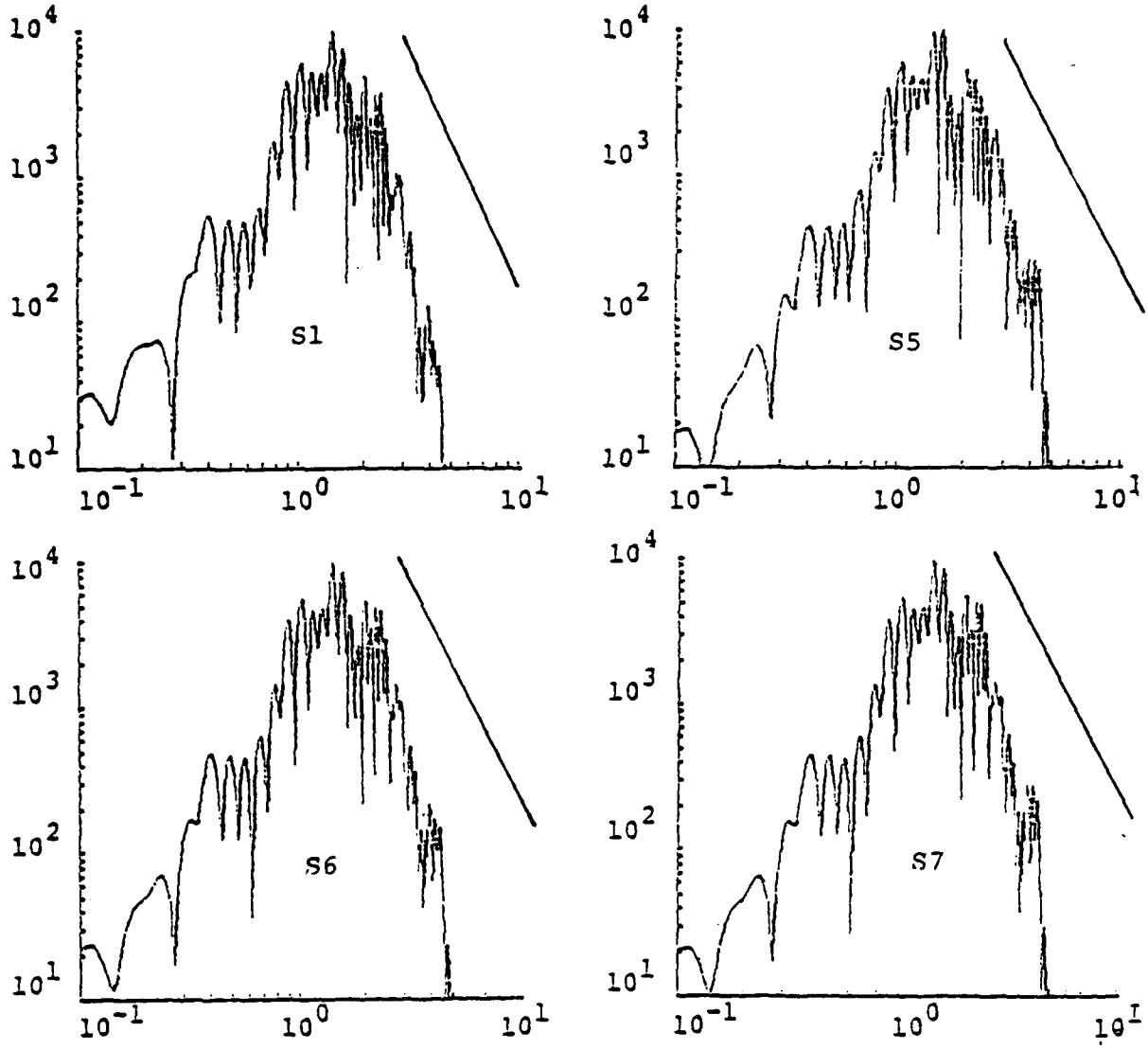

Figure 29. Lg spectra for the synthetic seismograms of Figure 27. These spectra are cosine tapered to zero between 4 and 5 Hz. The lines are drawn with a slope of ω^{-3}.

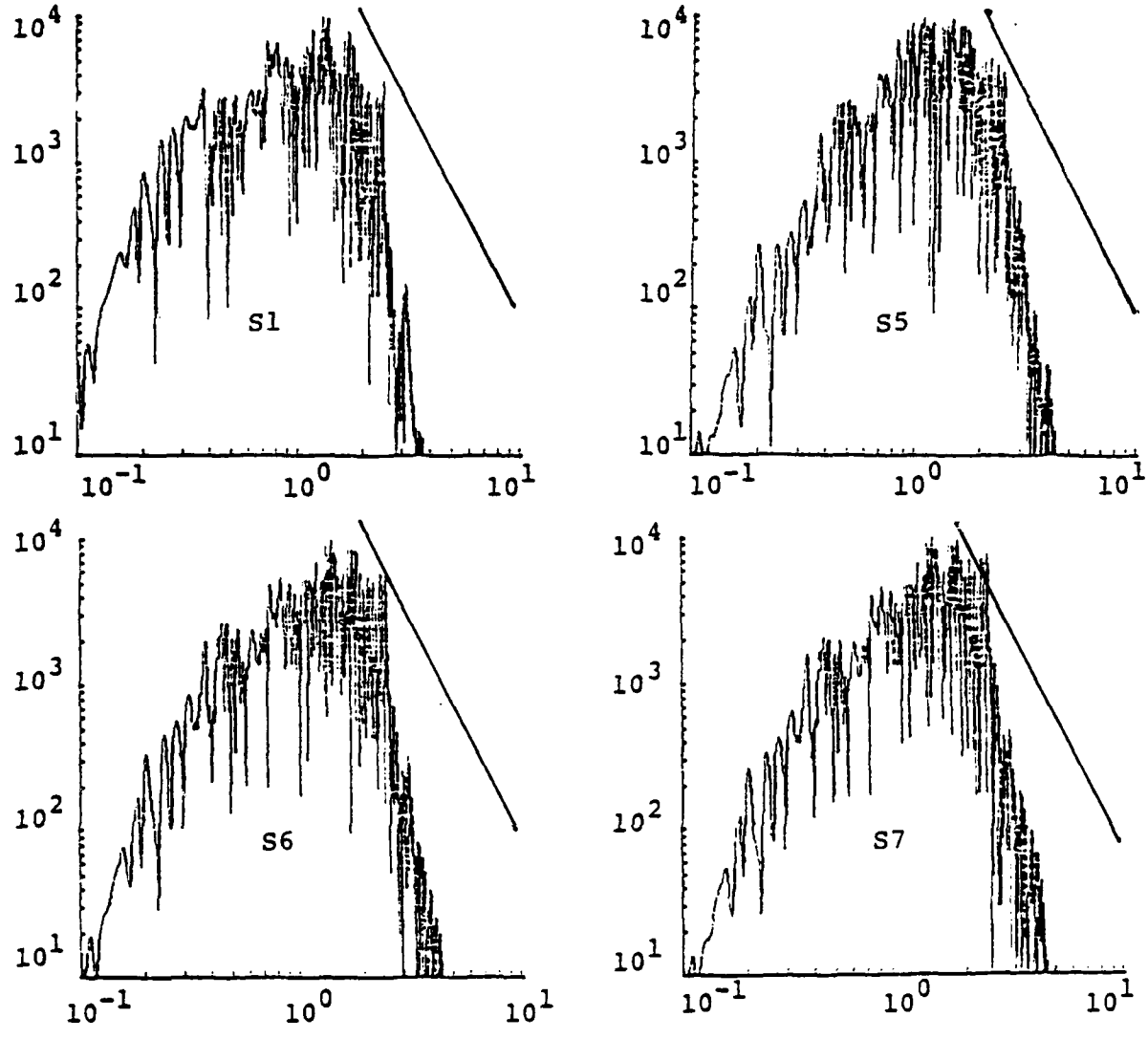

R = 1252 KM

Figure 29. (continued)

TABLE 12

CRUSTAL MODEL S4

Depth	Thickness	α	β	ρ	Q_β
0.6	0.6	3.70	2.16	2.1	20
1.3	0.7	4.55	2.54	2.2	70
7.0	5.7	6.10	3.30	2.85	350
12.0	5.0	6.20	3.35	2.90	500
18.0	6.0	6.40	3.46	3.00	1500
31.0	13.0	6.60	3.59	3.05	2000
34.0	3.0	6.90	3.75	3.10	2000
∞	∞	8.10	4.52	3.35	2000

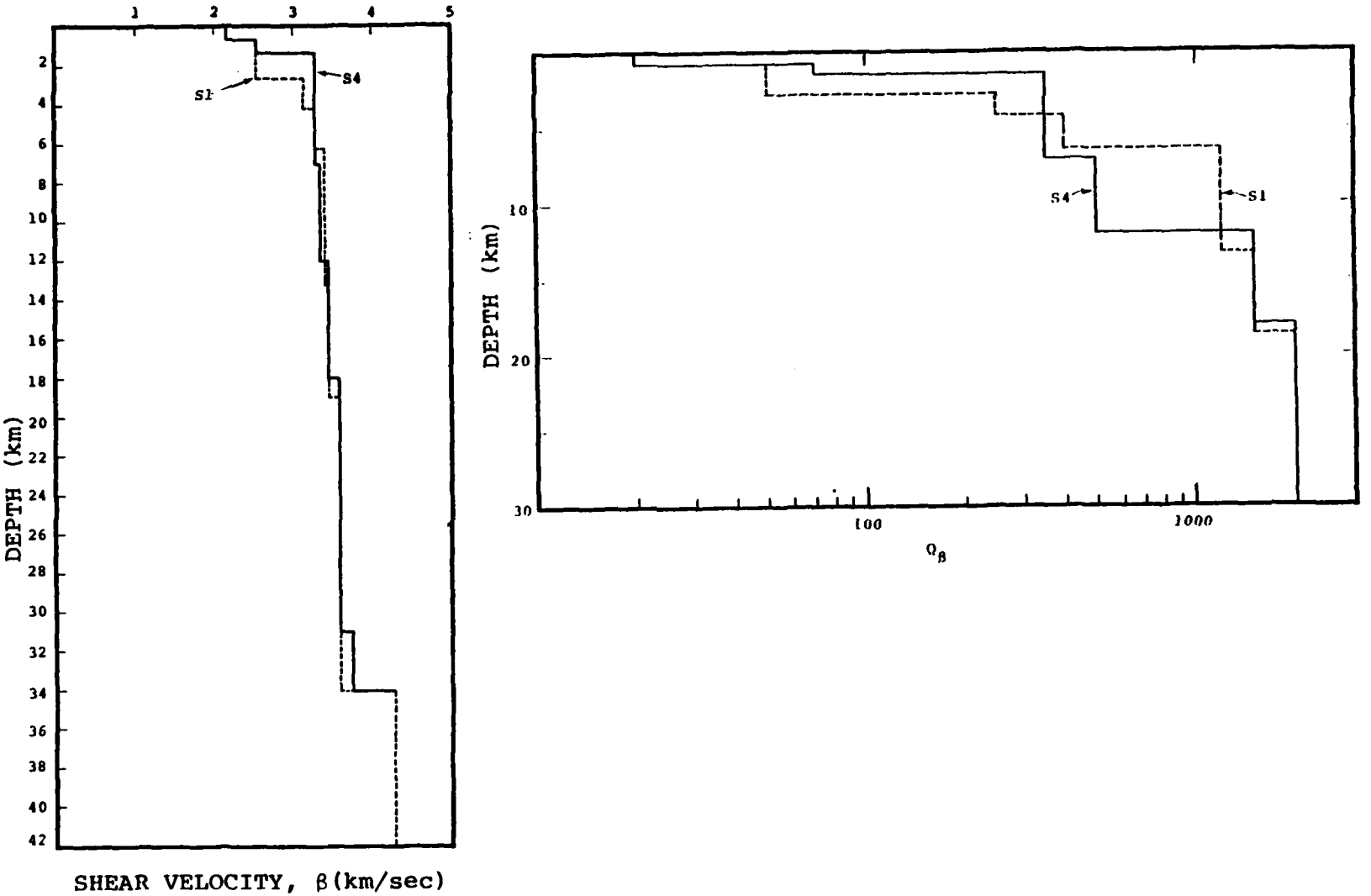

Figure 30. Comparison of models S1 and S4.

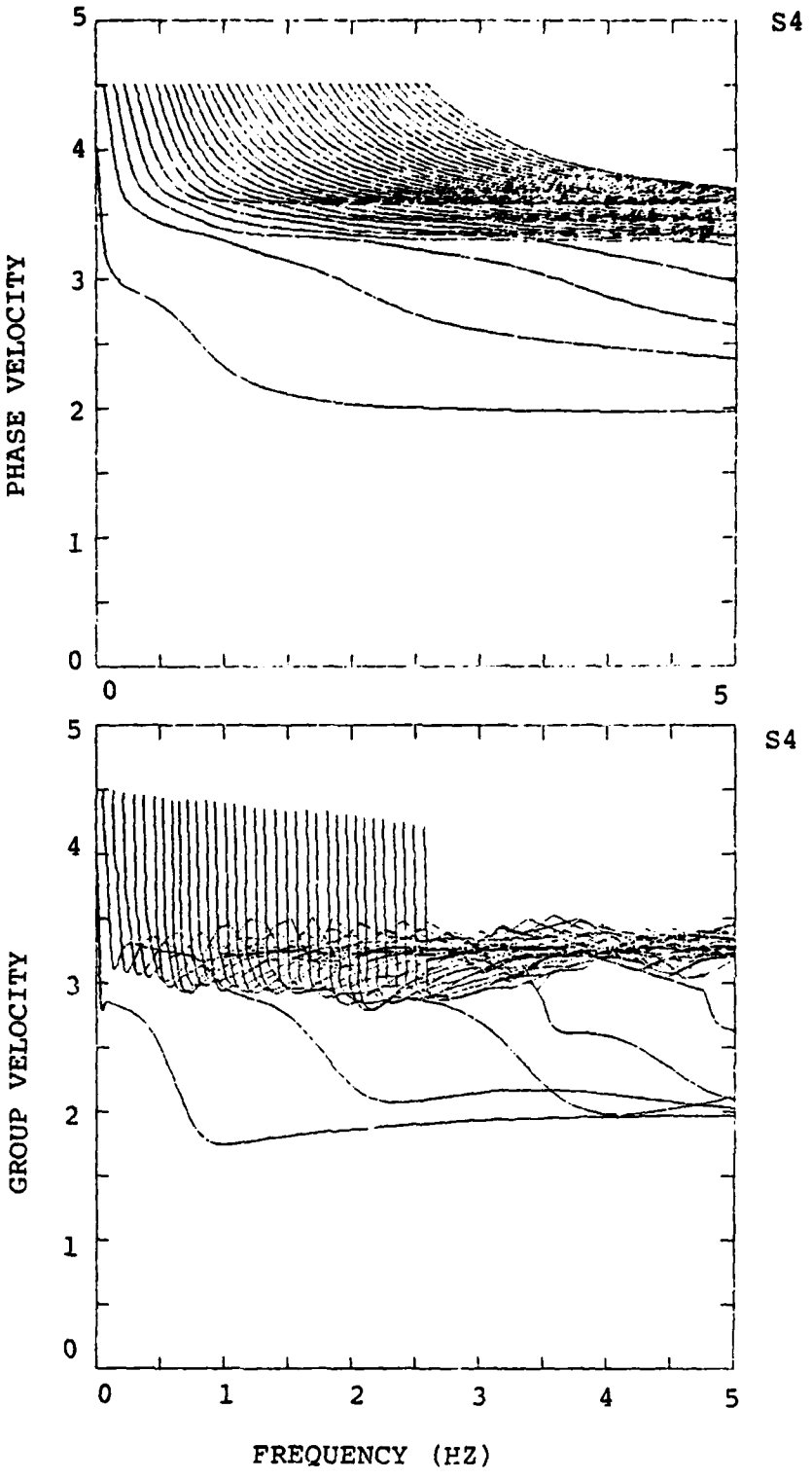

Figure 31. The first 35 modes for the model S4.

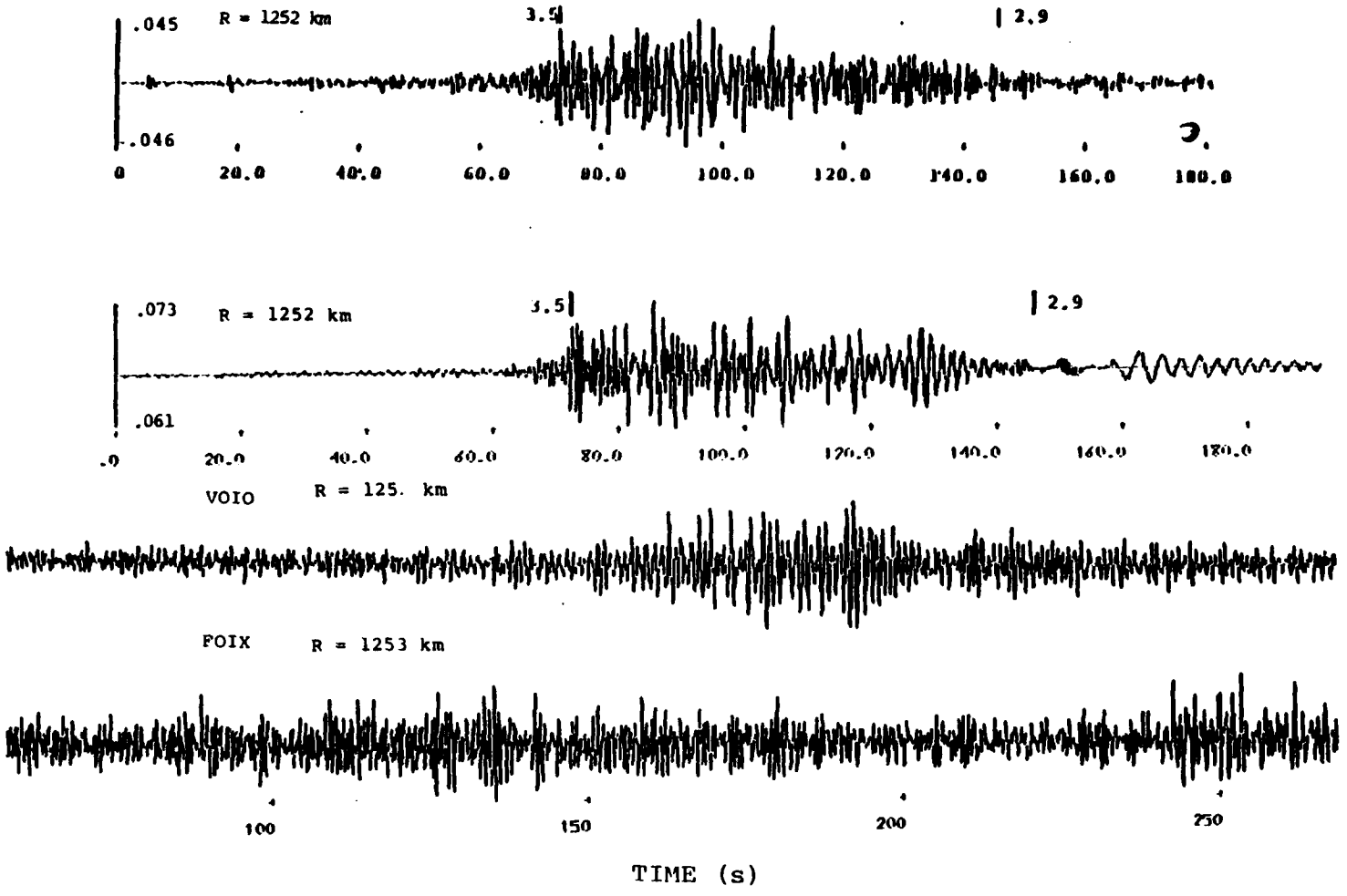

Figure 32. Thirty-five synthetic seismograms for the models S1 (Figure 15) and S4 are compared to SALMON observations from two stations. The peak amplitude in microns is listed at the left of each synthetic. The time scales are aligned at 3.5 km/sec.

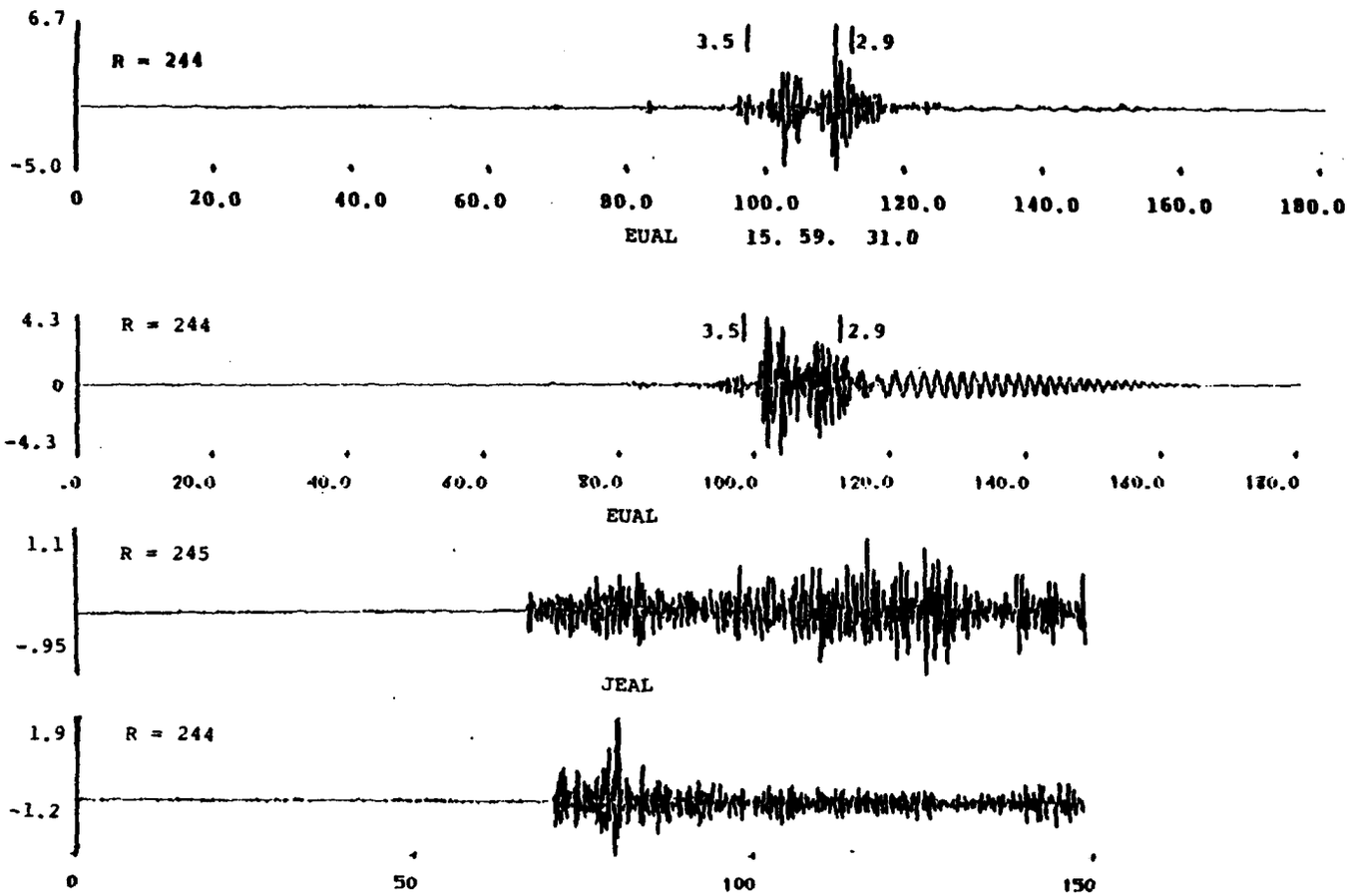

Figure 32. (continued)

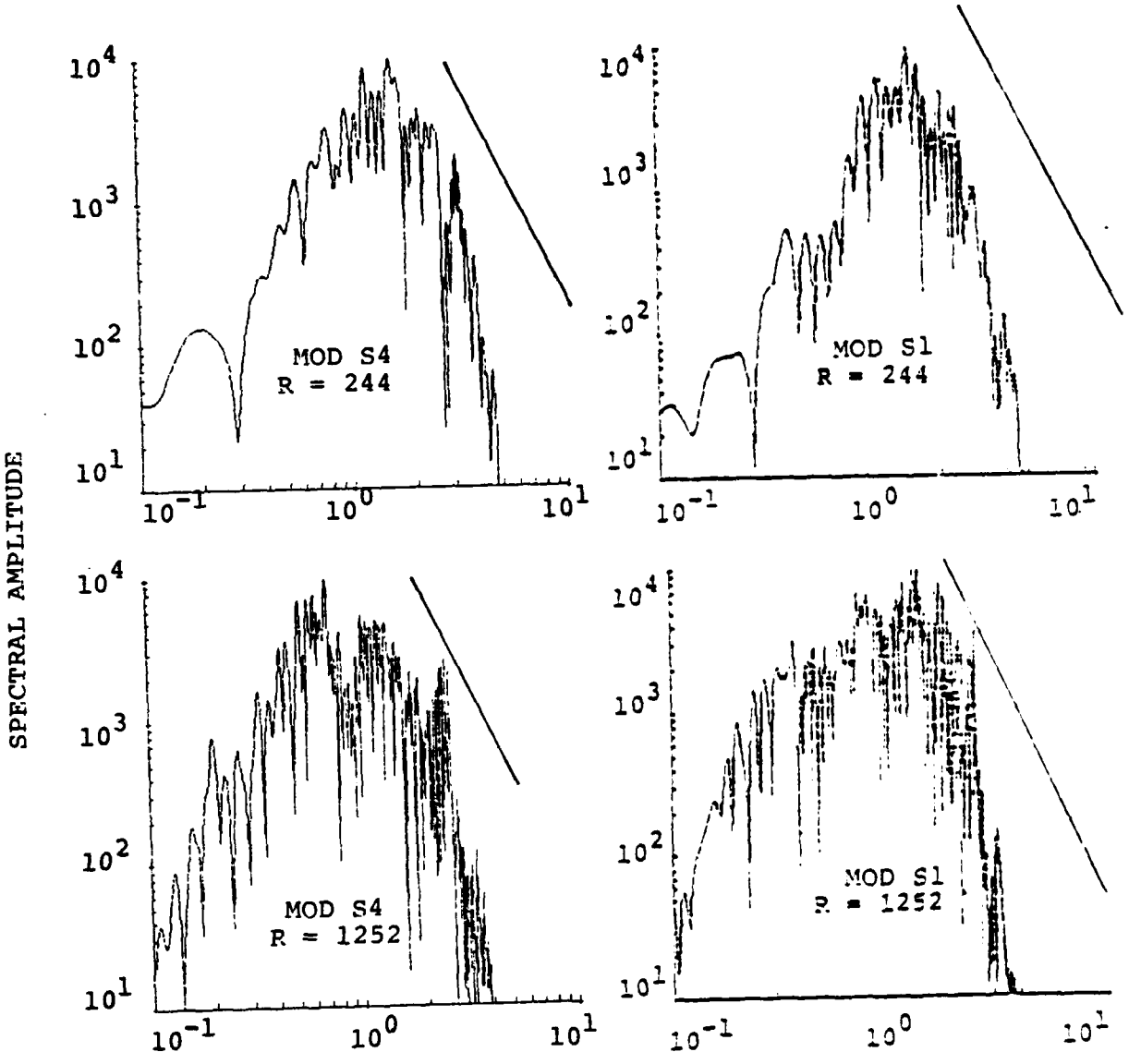

Figure 33. Comparison of Lg spectral for model S1 and S4. The lines are drawn with a slope of ω^{-3}

relatively high Q near the surface in S4 admits a large fundamental mode contribution with a sinusoidal waveform not seen in the data.

In Figure 34 we show the K_{ij} and E_{ij} distributions for this model. The Γ_i are tabulated in Table 13. From the K_{ij} we see immediately that the added layer at the base of the crust will not have a strong effect. The β = 3.59 km/sec layer still dominates the kinetic energy distribution for the higher modes.

The Lg amplitudes for the seismograms in Figure 32 are 6550 nm at R = 244 and 92 nm for R = 1252 km. These are between the amplitudes for S1 and S6 in Table 10. That is, like those from all the other models, they fall off much too rapidly between these two ranges. The γ computed using (2) and (3) and the Γ_i at R = 1252 km in Table 13 is 0.34 deg^{-1}. This is the 1.5 Hz γ computed the same way we determined the γ for models S5, S6 and S7. This value is quite close to the γ we derived for the model S1 in Section 3.3.

3.6 CONCLUSIONS

In Section 3.2 we found that some low velocity, low Q material is needed in the near surface (< 1 km) region to prevent domination by an unrealistic fundamental mode harmonic wavetrain. As we varied the Q models in the last section, we saw that in several cases, especially S4 and S5, the near surface Q was about as high as it could be and not have the fundamental mode become too large to be realistic. Yet none of the models include the high frequency energy arriving after 2.9 km/sec that is seen on the observed SALMON recordings. The higher Q models do have larger amplitudes at lower velocities; for example, compare S1 and S7 at R = 1252 km in Figure 27, but still do not have much energy after 2.9 km/sec.

The spectral comparisons are in Figures 29 and 33. Recall from Figure 17 that the data have a high frequency slope near ω^{-3} at the closest stations and seem to fall off at a rate between ω^{-2} and ω^{-3} at the larger ranges (some uncertainty is introduced at the larger ranges by the influence of seismic noise). The high

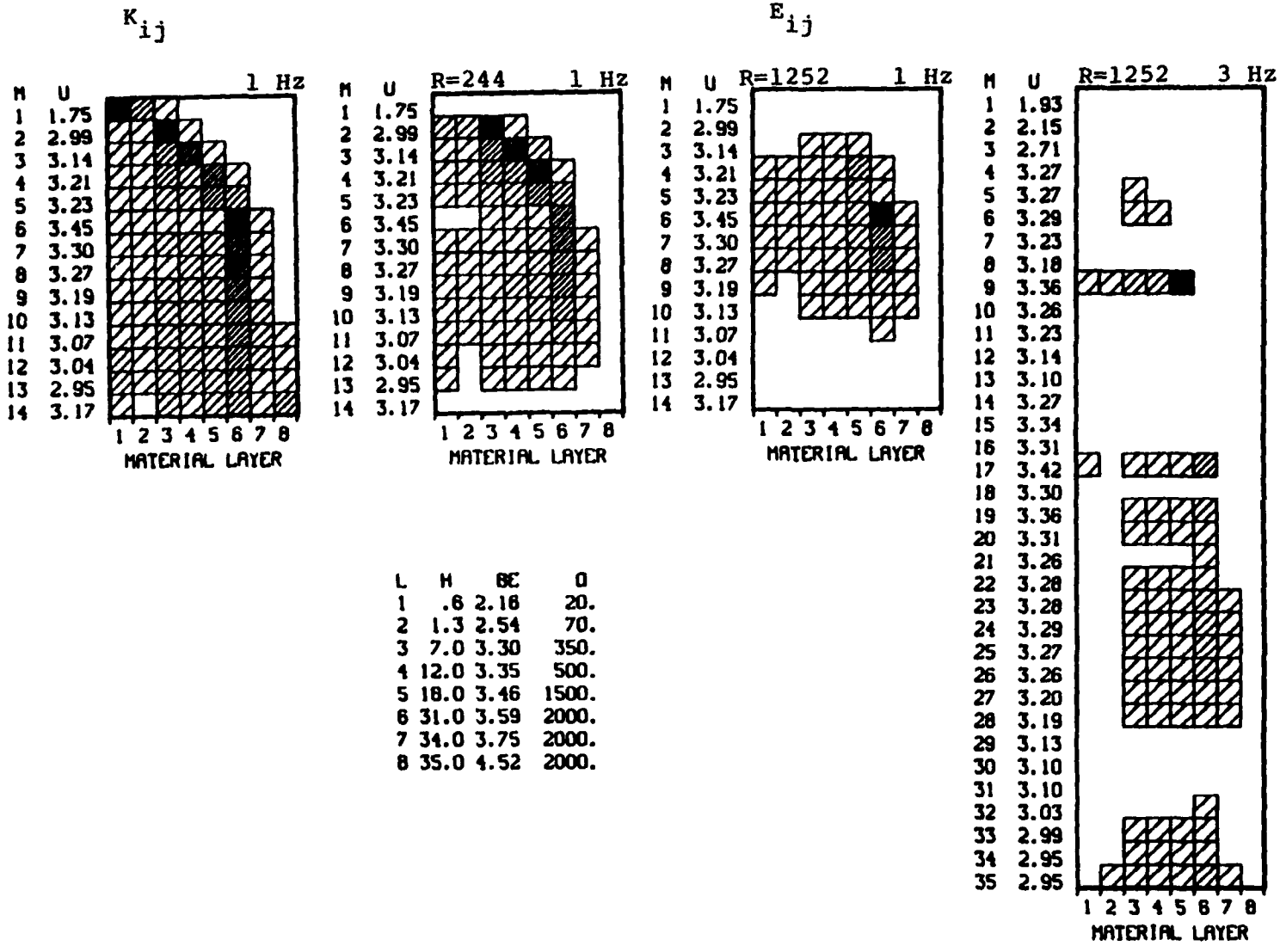

L	M	BE	Q
1	.6	2.16	20.
2	1.3	2.54	70.
3	7.0	3.30	350.
4	12.0	3.35	500.
5	18.0	3.46	1500.
6	31.0	3.59	2000.
7	34.0	3.75	2000.
8	35.0	4.52	2000.

Figure 34. The K_{ij} and E_{ij} distributions are plotted for the model S4.

TABLE 13

WEIGHTED KINETIC ENERGY DISTRIBUTION (Γ_i)
BY LAYER FOR THE MODEL S4

R = 244 KM

I	H	BE	Q	1 Hz Energy	2 Hz Energy	3 Hz Energy
1	0.6	2.16	20	21.2	11.2	10.4
2	1.3	2.54	70	13.0	4.7	5.6
3	7.0	3.30	350	93.1	68.9	51.7
4	12.0	3.35	500	75.5	64.1	50.6
5	18.0	3.46	1500	73.9	82.5	67.1
6	31.0	3.54	2000	100.0	100.0	100.0
7	34.0	3.75	2000	12.8	11.2	8.8
8	∞	4.52	2000	1.0	1.5	0.3

R = 1252 KM

I	H	BE	Q	1 Hz Energy	2 Hz Energy	3 Hz Energy
1	0.6	2.16	20	6.3	3.4	5.5
2	1.3	2.54	70	4.0	1.2	3.9
3	7.0	3.30	350	24.1	23.3	37.3
4	12.0	3.35	500	27.0	23.6	37.7
5	18.0	3.46	1500	40.0	36.3	100.0
6	31.0	3.54	2000	100.0	100.0	96.3
7	34.0	3.75	2000	5.5	9.0	21.7
8	∞	4.52	2000	0.2	0.2	0.5

frequency character of the data is not reproduced by the synthetic seismograms for any of the models.

The high Q models S5, S6 and S7 were selected to reduce the γ to a value closer to that observed in the eastern United States (section 3.4). The models S1 and S4 have γ values of about 0.34 deg^{-1}, much higher than the 0.07 to 0.10 deg^{-1} values observed. The models S5 and S7 do reduce the γ to 0.21 deg^{-1}, which is an improvement, but still much too high. These two models are quite different, even though they result in the same Lg amplitudes (Table 10), which match the SALMON observation at 1252 km, but are a factor of 4 larger at 244 km. The S5 model has relatively high Q values in the top 2.6 km, which allows too much fundamental mode energy at the closer range (Figure 27). The S7 model is elastic below 13 km and has very high Q below 4 km. However, it also has a very low Q near surface layer which does succeed in damping the fundamental mode.

Thus, we are left with the deficiencies we discussed in connection with Model S1 and Section 3.3. These are:

1. The synthetic seismograms have too little high frequency energy at velocities less than 2.9 km/sec.

2. The synthetic Lg spectra (windowed between 3.5 and 2.9 km/sec) have too little high frequency energy.

3. The γ for the synthetic seismograms is much larger than observed.

Our parametric studies are certainly far from complete. We have not yet looked at much different velocity-depth profiles, particularly with a different crustal thickness. There are many variations on the Q model that also could be tried. However, these parametric studies are enough to strongly indicate that we will not be able to remove the listed deficiencies with plane-layered, constant Q, laterally homogeneous models. The late-arriving high frequency energy may be largely due to scattering and multipathing.

But the most important upgrading of the models is likely to be the introduction of a frequency dependent Q. Recent results (Mitchell, 1980) indicate that this is important to match amplitude attenuation data in the eastern United States.

IV. THE DEPENDENCE OF Lg ON SOURCE DEPTH

4.1 INTRODUCTION

An important question is how strongly the Lg phase depends on the source depth. To address this question, we compute synthetic seismograms in the model S1 of section 3.3 Table 6. While this model does not give seismograms that match the observed characteristics of Lg in all respects, it should be good enough to indicate the gross effects of varying source depth. Our initial set of seismograms were done with a center of dilatation source. This is not a realistic source representation for depths below a few kilometers, but does lead to some interesting results that are worth mentioning. In fact, these results show that the center of dilatation source gives an unrealistic estimate for the depth dependence of the higher modes that control Lg.

The main calculations to determine the depth-dependence of Lg were done with a point double-couple source at the three basic orientations (strike-slip, vertical dip-slip and 45° dip-slip) which can be combined to give the solution for a double-couple with arbitrary orientation (Burridge, et al., 1964).

4.2 DEPTH-DEPENDENCE OF Lg FOR A CENTER OF DILATATION SOURCE

Synthetic seismograms were computed at seven depths from 1 to 14 kilometers in the crustal model S1. These seismograms are shown in Figure 35. To compare amplitudes, the source was scaled to a common moment (1.7×10^{22} dyne-cm). Since the moment of a center of dilatation source is given by (e.g., Hudson, 1969)

$$M_0 = 4\pi\rho\alpha^2 \quad \Psi_\infty,$$

where Ψ_∞ is the static value of the reduced displacement potential, we fix Ψ_∞ to be 2960 m^3 and scale by $\rho\alpha^2$. The peak-to-peak amplitude is indicated at the left of each record.

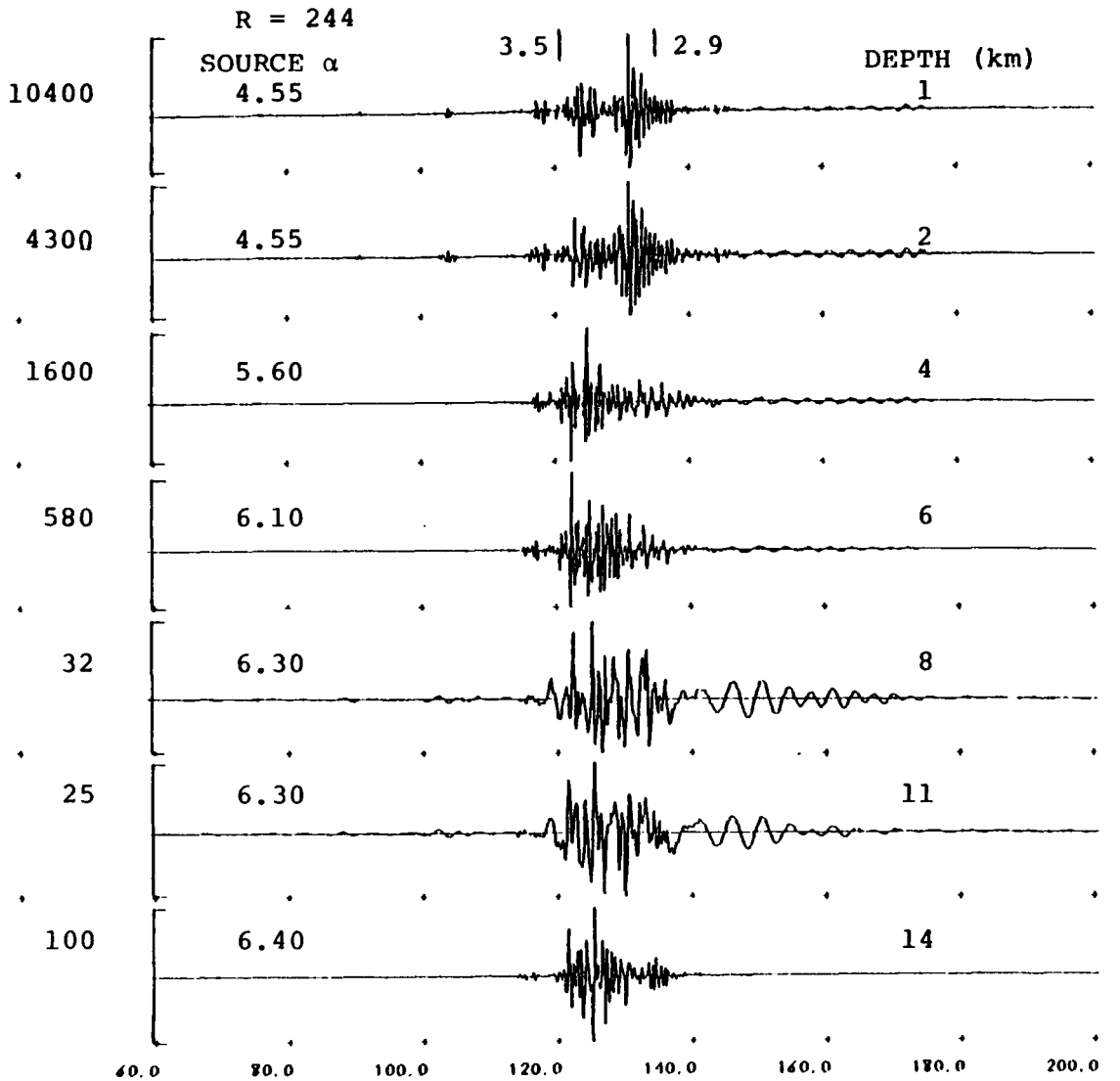

Figure 35. Synthetic seismograms are shown for the SALMON source at seven focal depths. The amplitude scale at left is in nanometers. The source moment, which is proportional to $\rho\alpha^2$, is held constant. The source region α is indicated with each record.

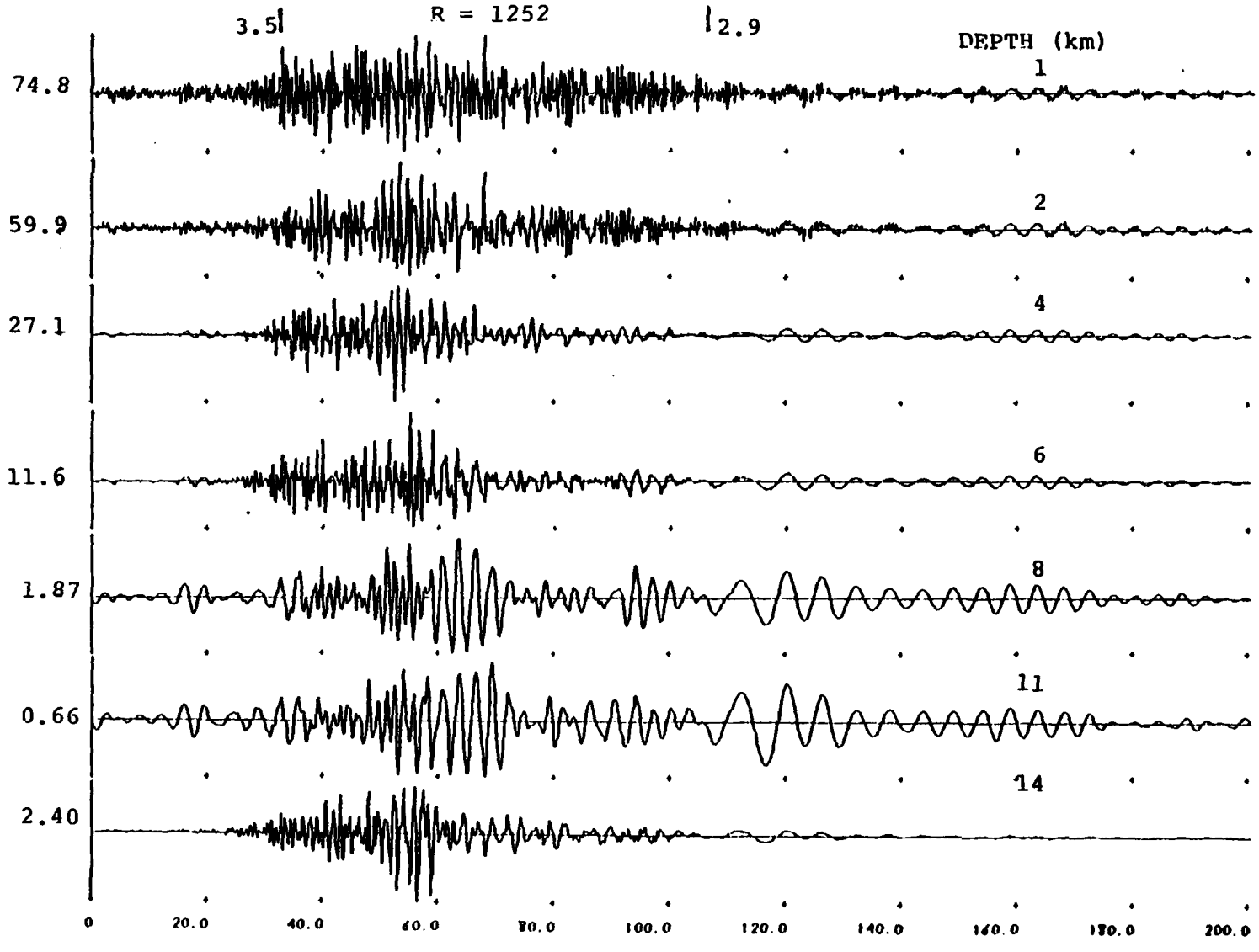

Figure 35. (continued)

The seismograms have a very strong, but irregular, dependence on depth. This is not a general characteristic of Lg, but occurs only for a center of dilatation source. The excitation of the high frequency, higher mode energy dies off rapidly away from layer interfaces for this P wave source. In the model S1, there are interfaces at depths of 6.2 and 13.2 km. Thus, the 8 and 11 km depths are near the center of this layer, while the 6 and 14 km depths are relatively near the interfaces.

From the seismogram comparison in Figure 35 it is obvious that the depth has a much stronger effect on the excitation of high frequency energy. This is also seen, of course, in the spectra of these seismograms. We plot these in the form of what we call "smoothed Lg spectra." These are obtained by first computing the Fourier spectra of the synthetic seismograms in the 3.6 to 2.9 km/sec group velocity window. These spectra are then smoothed by computing a thirty-one point moving average. A typical application of the smoothing is shown in Figure 36. The smoothed Lg spectra for the seismograms in Figure 35 are shown in Figure 37.

4.3 DEPTH-DEPENDENCE FOR A DOUBLE-COUPLE SOURCE

To investigate the depth-dependence of a double-couple source, synthetic seismograms were computed at various depths in the model S1 of Section 3.3, Table 6. The source is a point double-couple with a fixed moment of 10^{25} dyne-cm. The dislocation time history is a step function, so the source has no corner frequency. Seismograms were computed for this source oriented to represent strike-slip, vertical dip-slip and 45° dip-slip faulting. The solution at any other fault orientation can be obtained by summing solutions for these three basic orientations (Burridge, et al., 1964).

Synthetic seismograms which demonstrate the depth-dependence of Lg are shown in Figures 38 to 43. First, in Figures 38, 39 and 40, we show the seismograms at seven depths from 1 to 14 km for all three source orientations. The orientation of the source is given by dip (δ) and slip (λ) angles and the source-station azimuth is θ.

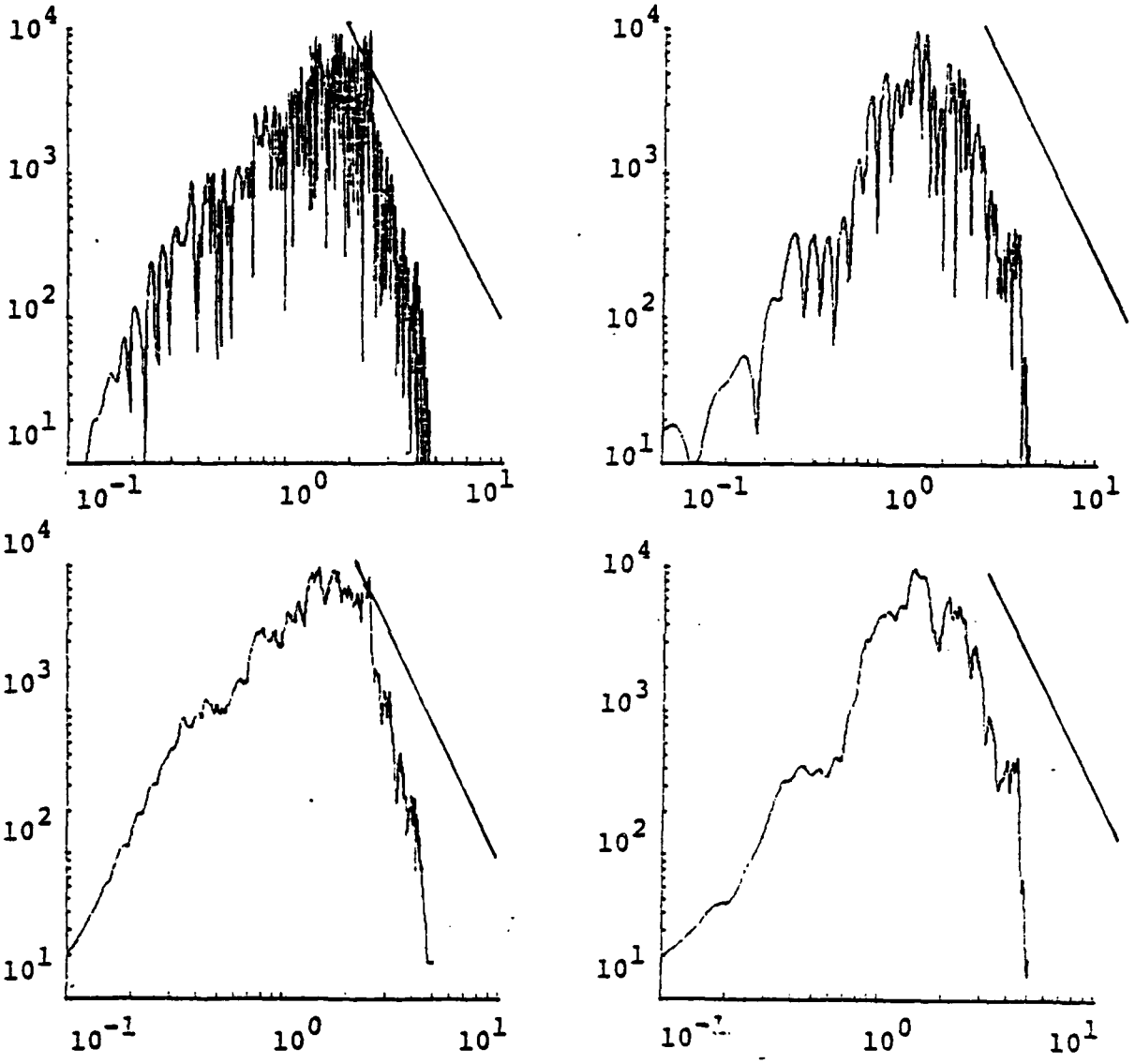

Figure 36. Examples of the application of the smoothing algorithm to Lg spectra. The top figures show the original spectra with the processed spectra just below.

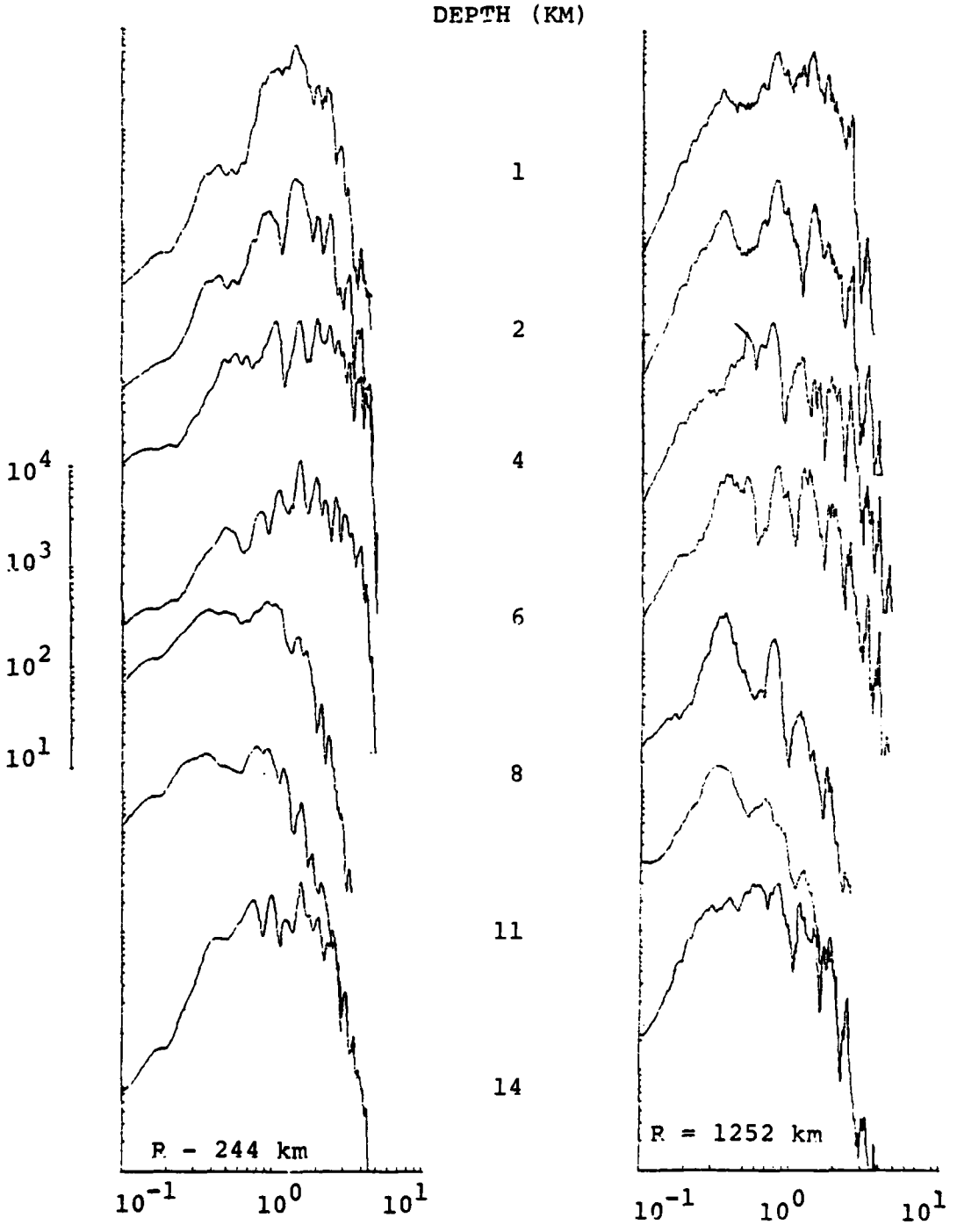

Figure 37. Smoothed Lg spectra for the center of dilatation source of Figure 35. These spectra are cosine tapered to zero between 4 and 5 Hertz.

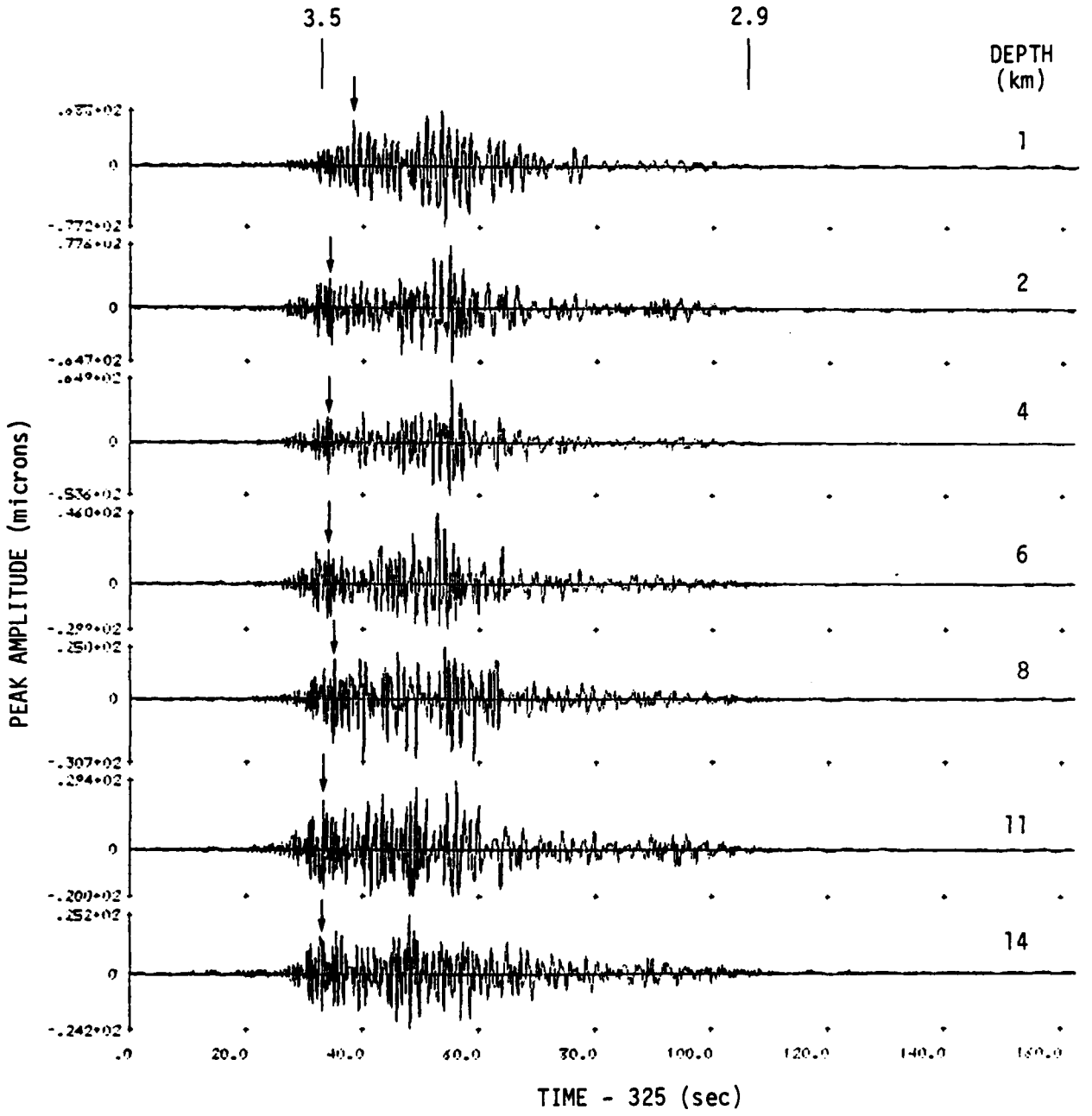

Figure 38. Synthetic seismograms for a strike-slip ($\lambda = 0°$, $\delta = 90°$, $\theta = 30°$) double-couple with a step dislocation time history with moment 10^{25} dyne-cm. The range is 1252 km and the LRSM short period instrument response is included. An amplitude measurement was made at the cycle marked with an arrow which is within 5 seconds of time associated with a group velocity of 3.5 km/sec.

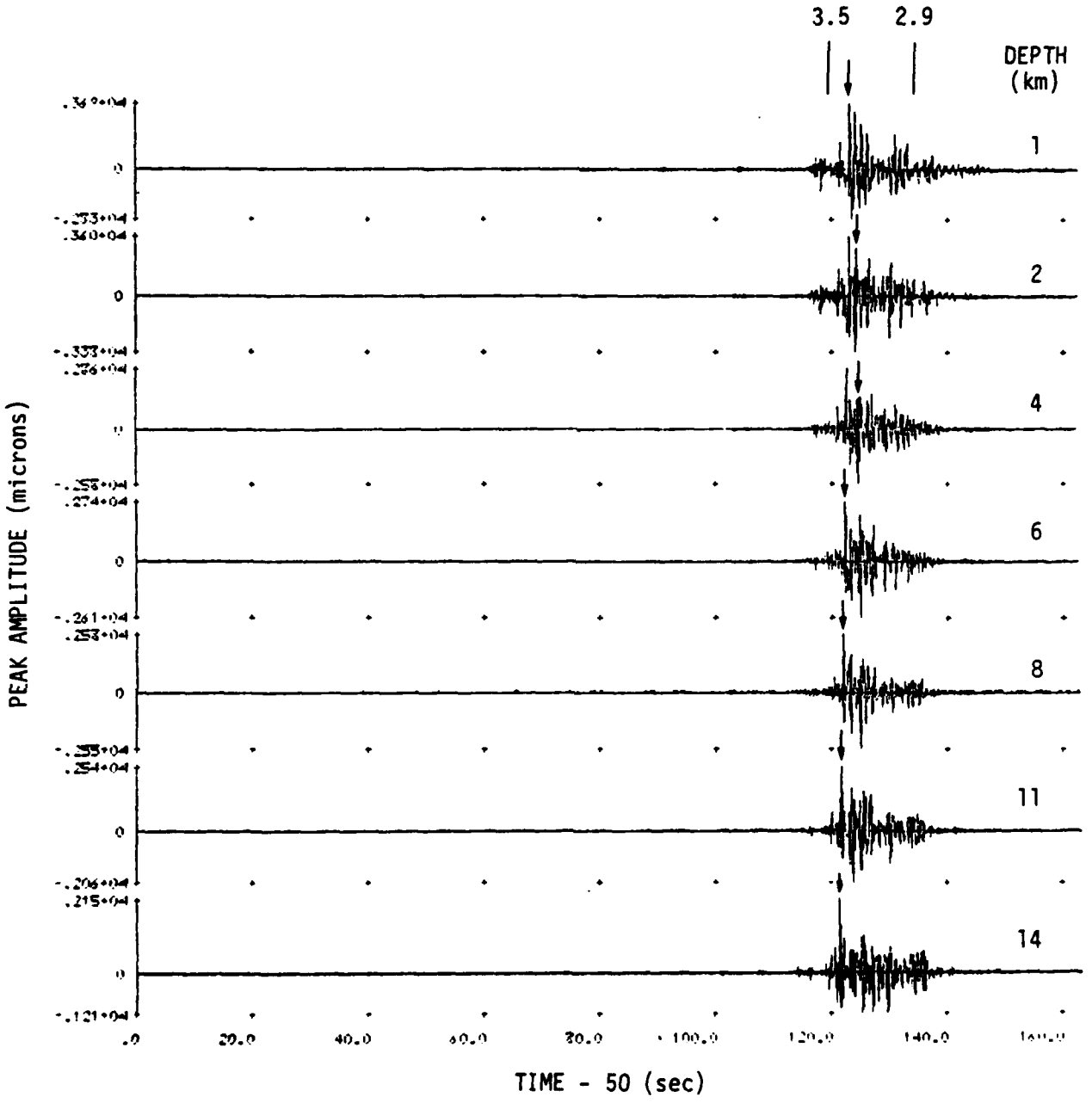

Figure 38. (Continued) The range is 244 km.

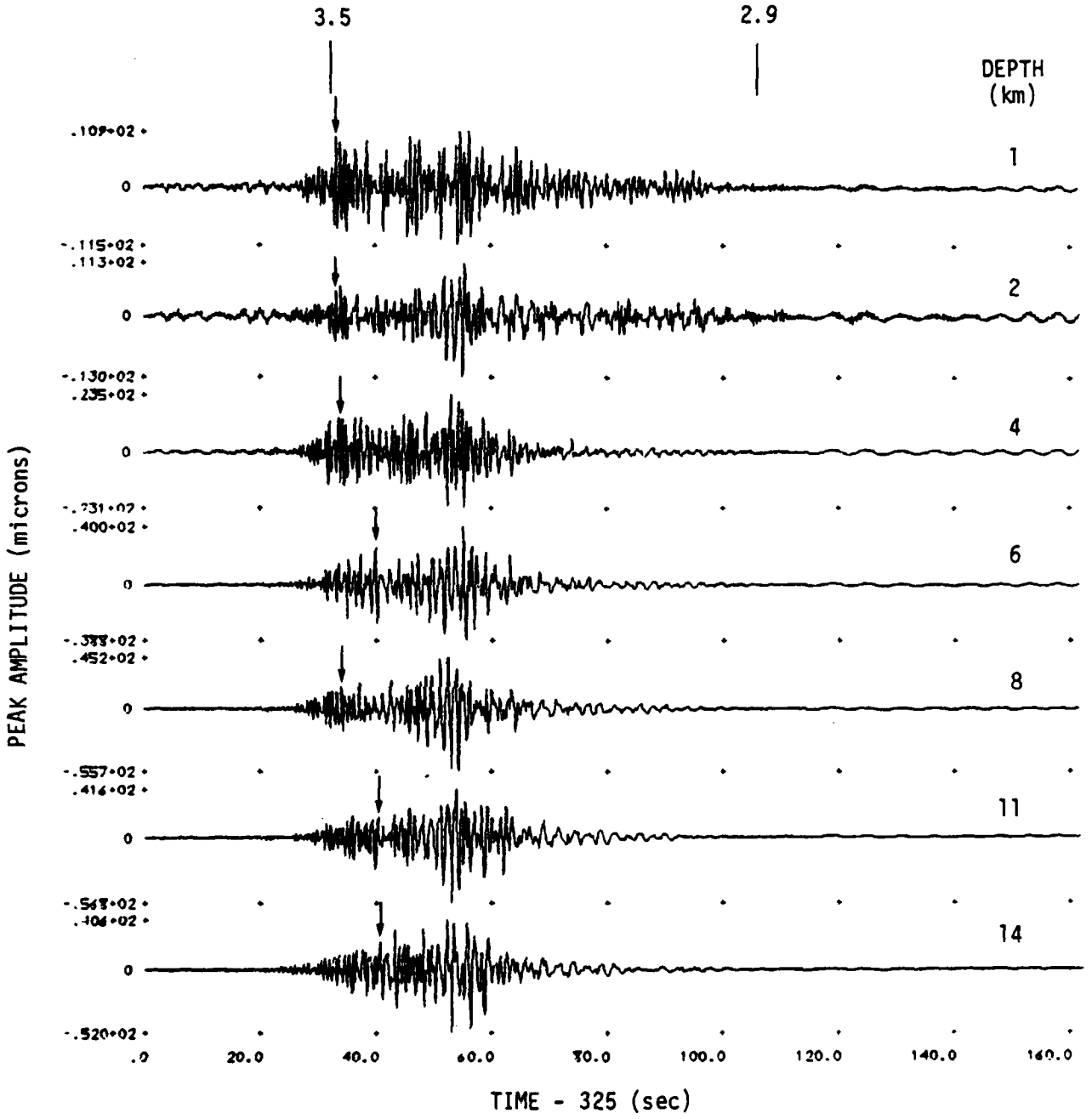

Figure 39. Synthetic seismograms for a normal dip-slip (λ = 90°, δ = 90°, θ = 22.5°) double-couple. The range is 1252 km and the LRSM short period response is included.

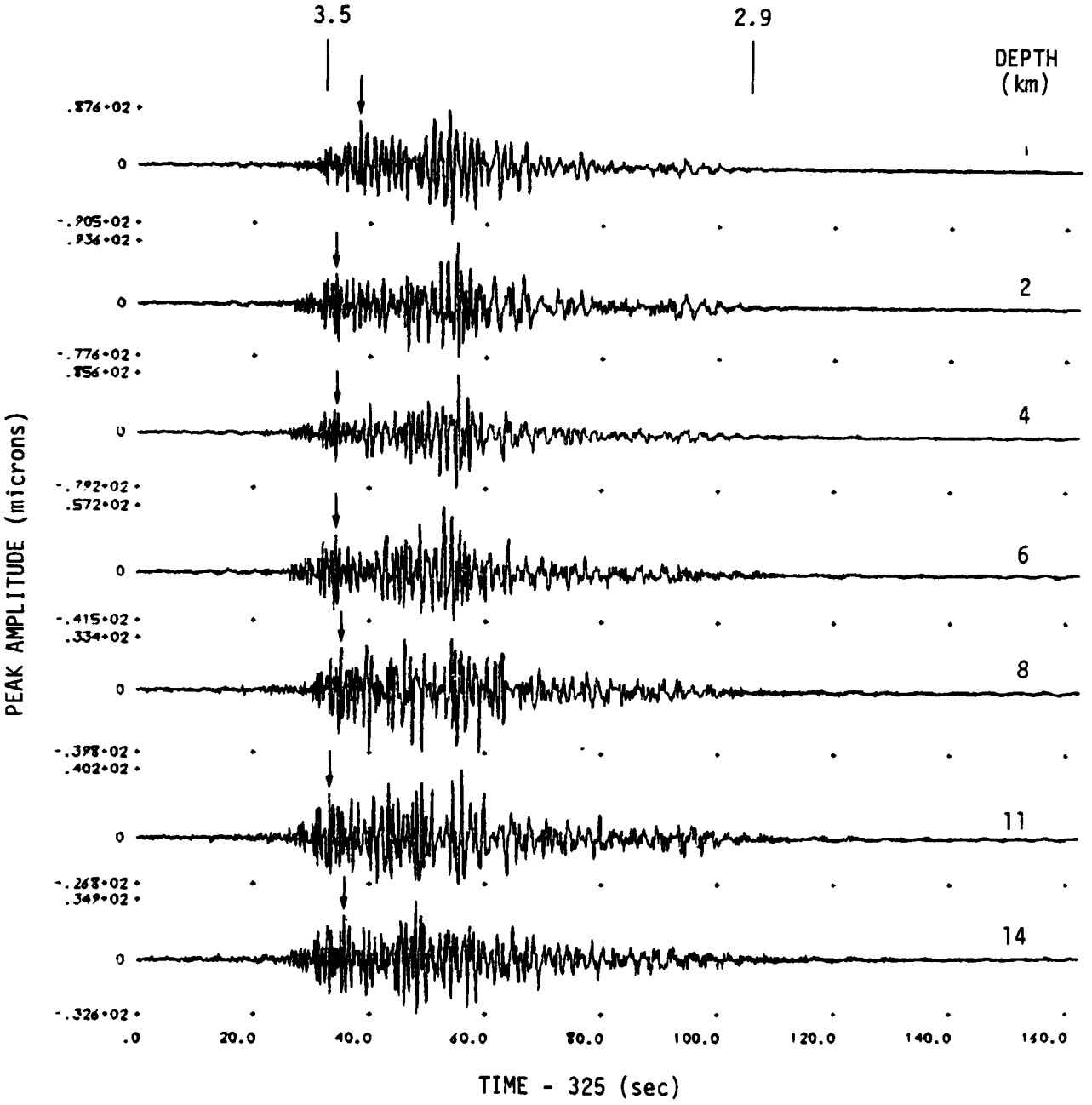

Figure 40. Synthetic seismograms for a 45° dip-slip (λ = 90°, δ = 45°, θ = 22.5°) double-couple. The range is 1252 km and the LRSM short period response is included.

These seismograms have been filtered by the LRSM short period instrument response. For all three orientations we show the seismograms at a range of 1252 km. For the strike-slip orientation (Figure 36), we also show the seismograms at a range of 244 km.

To demonstrate the dependence over a wider depth variation, a different set of seismograms is shown in Figures 41, 42 and 43. In this case, the range is 1000 km and the WWSSN short period instrument response is included. The depths are 5, 15 and 25 km.

There seems to be little systematic dependence of the waveforms on depth. The duration of the normal dip-slip synthetics appears to decrease with depth. Otherwise, the primary depth effect is that the amplitude changes. The Lg amplitude was measured on each record and these are plotted versus source depth in Figure 44. In this case, we measured the maximum peak-to-peak amplitude within five seconds of 3.5 km/sec. This phase is marked with an arrow on each seismogram. The amplitudes plotted in Figure 44 are the raw amplitudes from the seismograms; that is, no corrections were made for frequency dependent instrument response.

The depth of the layer interfaces is shown in the figure along with the Q_β at each depth. There is little, if any, indication that the amplitude depends on the layer in which the source occurs.

To see the depth dependence over the full range of depths, we need to scale the amplitudes from the two ranges and seismometers so they can be plotted together. To do so we scaled the WWSSN, R = 1000 km, Lg amplitudes so they fit on a line drawn between the 4 and 6 km depth points on the amplitude plots for the LRSM, R = 1252 km synthetics. The resulting composite curves are shown in Figure 45. There is a small break in the curve between the 14 and 15 km depth points, which is probably due to the range and seismometer differences, but this does not disturb the main trends apparent in the plot.

We conclude that the Lg amplitude decreases with depth at nearly the same rate for the strike-slip and 45° dip-slip source

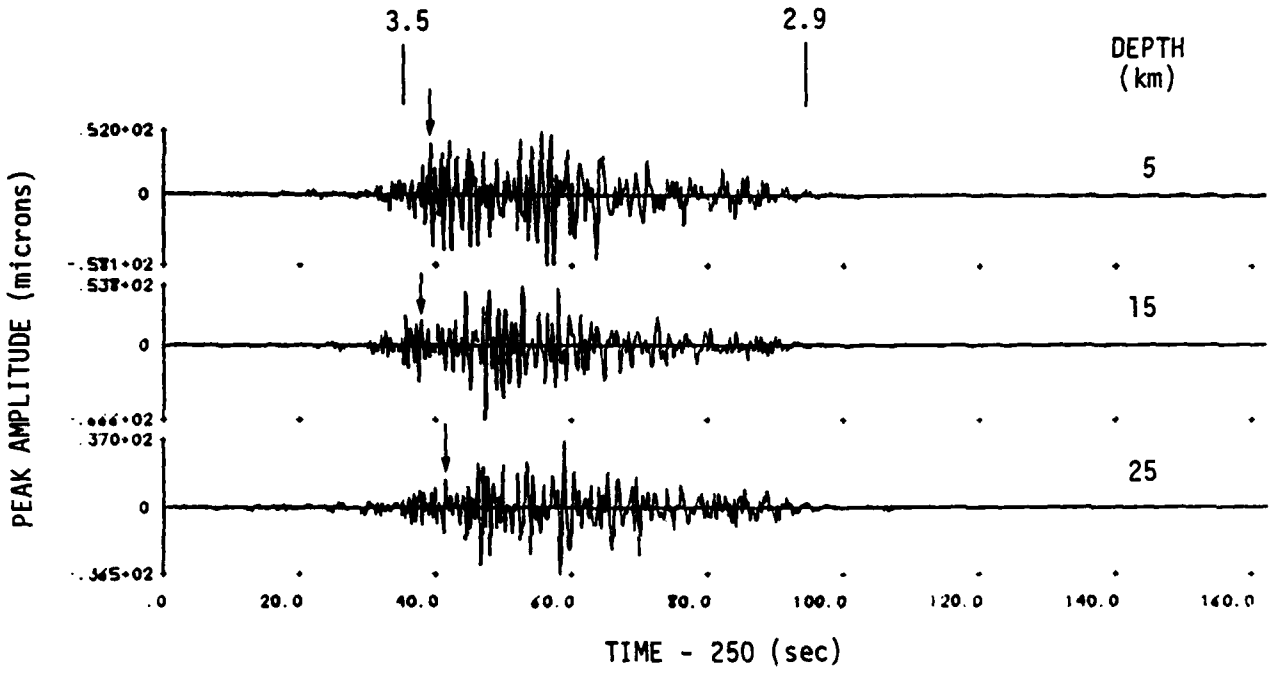

Figure 41. Synthetic seismograms for a strike-slip (λ = 0°, δ = 90°, θ = 30°) double-couple. The range is 1000 km and the WWSSN short period response is included.

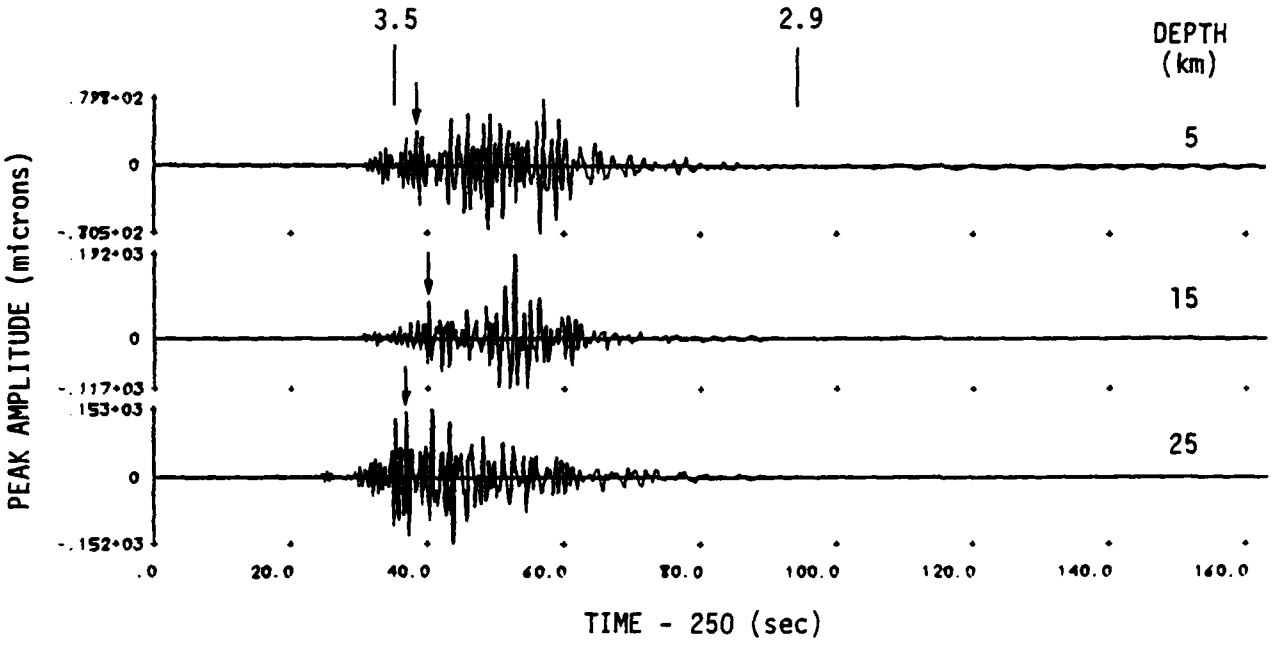

Figure 42. Synthetic seismograms for a normal dip-slip (λ = 90°, δ = 90°, θ = 30°) double-couple. The range is 1000 km and the WWSSN short period response is included.

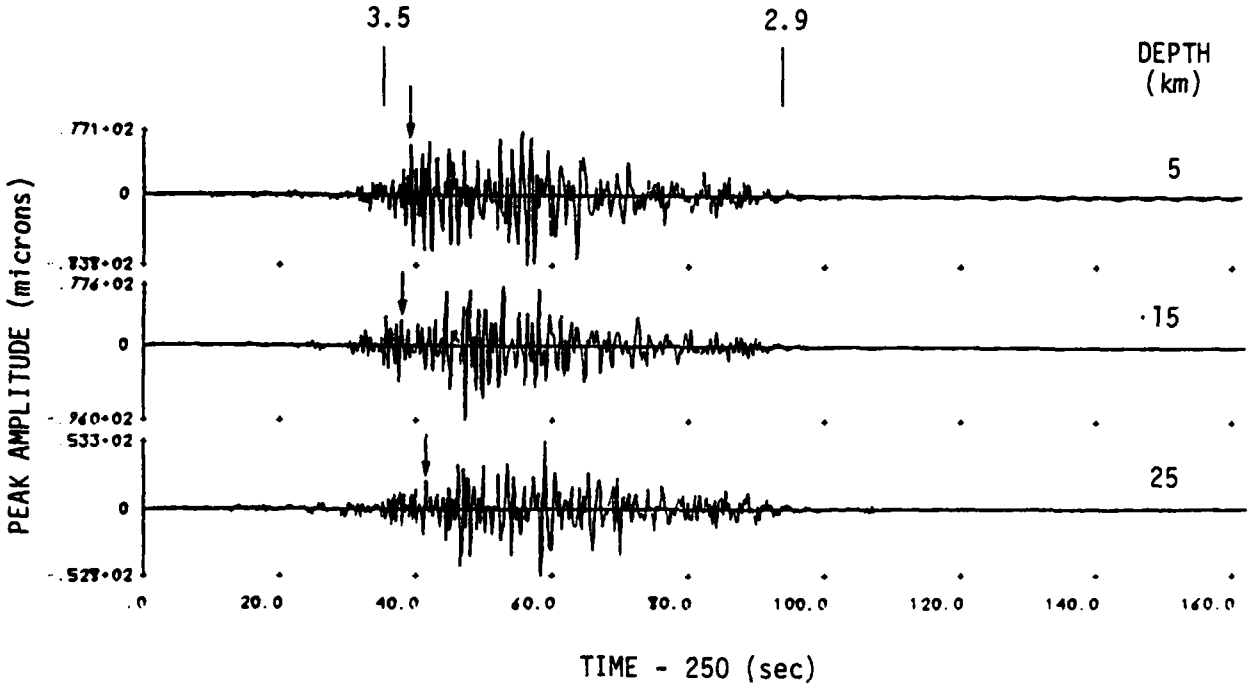

Figure 43. Synthetic seismograms for a 45° dip-slip (λ = 90°, δ = 45°, θ = 30°) double-couple. The range is 1000 km and the WWSSN short period response is included.

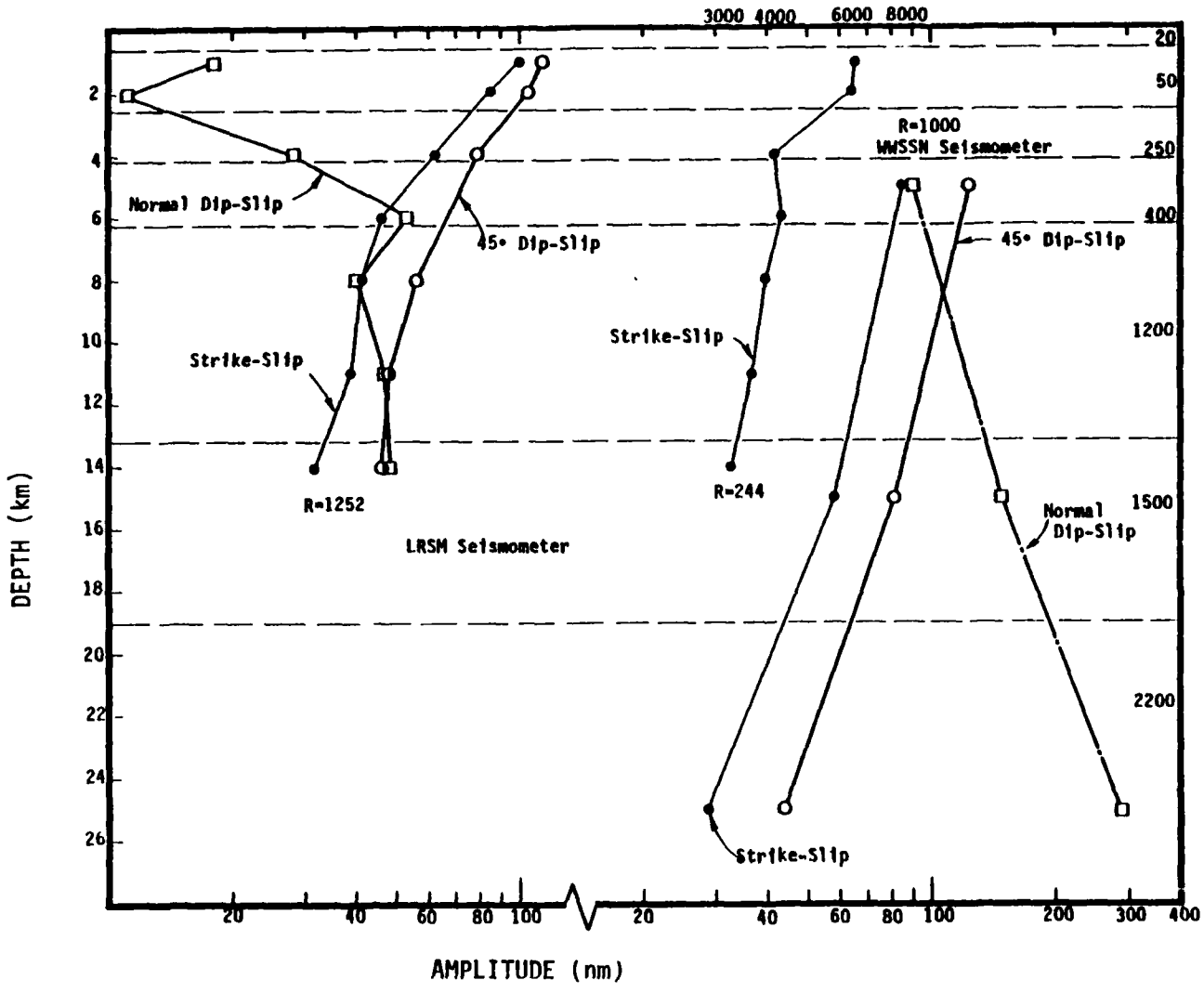

Figure 44. Lg amplitudes from the synthetic seismograms of Figures 38 to 43 are plotted versus source depth. The interfaces are indicated with a dashed line and the Q in each layer is listed along the right border of the plot. The amplitude scale for the R = 244 synthetics is at the top.

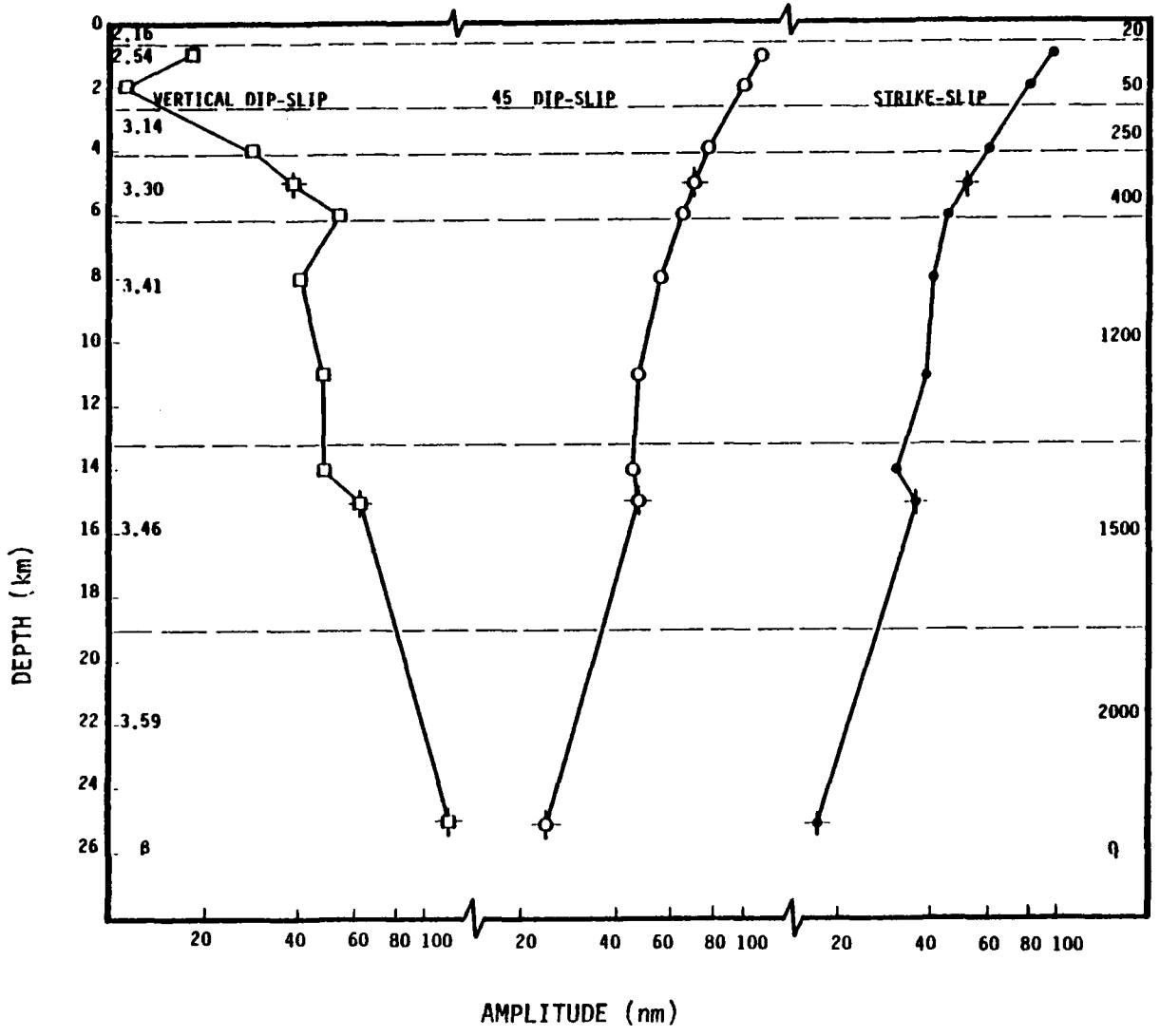

Figure 45. The data from Figure 44 are scaled to be comparable and replotted. The scaled points are at depths of 5, 15 and 25 and are marked. The format is like Figure 44, except the shear velocity is now listed along the left border.

orientations. This is a factor of four to five decrease in amplitude between 1 and 25 km depths. For vertical dip-slip faulting, the Lg amplitude increases with depth all the way to the deepest (25 km) computed. The rate of increase is a factor of five of six over the depths plotted.

THIS PAGE LEFT BLANK

REFERENCES

Anderson, D. L. and C. B. Archambeau (1964), "The Anelasticity of the Earth," JGR, 69. 2071-2084.

Apsel, R. J. (1979), "Dynamic Green's Functions for Layered Media and Applications to Boundary-Value Problems," Ph.D Thesis, University of California at San Diego, 380 pages.

Apsel, R. J., G. Rawson, G. A. Frazier, J. Fried, J. Sweet and P. Glover (1980), "Near-Source Phenomena and Their Manifestations on Signatures of More Distant Radiation of Seismic Energy," Del Mar Technical Associates Final Contract Report DELTA-R-79-0042, submitted to AFOSR, May, 431 pages.

Bollinger, G. A. (1973), "Seismicity of the Southeastern United States," Bull Seism. Soc. Amer., 63, 1785-1808.

Bollinger, G. A. (1979), "Attenuation of the Lg Phase and the Determination of m_b on the Southeastern United States," Bull. Seism. Soc. Amer., 69, 45-63.

Burridge, R., Lapwood, E. R. and Knopoff, L. (1969), "First Motions from Seismic Sources Near a Free Surface," Bull. Seism. Soc. Amer., 54, 1889-1913.

Harvey, D. J. (1980), "Seismogram Synthesis Using Normal Mode Superposition: The Locked Mode Approximation," Geophys. J., (in press).

Herrmann, R. B. (1969), "The Structure of the Cincinnati Arch as Determined by Short Period Rayleigh Waves," Bull Seism. Soc. Amer., 59, 399-407.

Herrmann, R. B. and B. J. Mitchell (1975), "Statistical Analysis and Interpretation of Surface Wave Anelastic Attenuation Data for the Stable Interior of North America," Bull Seism. Soc. Amer., 65, 1115-1128.

Hudson, J.A. (1969), "A Quantitative Evaluation of Seismic Signals at Teleseismic Distances -- II Body Waves and Surface Waves from an Extended Source," Geophys. J., 18, 353-370.

Jones, F. B., L. T. Long and J. H. McKee (1977), "Study of the Attenuation and Azimuthal Dependence of Seismic Wave Propagation in the Southeastern United States," Bull Seism. Soc. Amer., 67, 1503-1513.

Knopoff, L. (1964), "A Matrix Method for Elastic Wave Problems," Bull Seism. Soc. Amer., 54, 431-438.

Knopoff, L., F. Schwab and E. Kausel (1973), "Interpretation of Lg," Geophys. J. R. Astr. Soc., 33, 389-404.

Mantovani, E., F. Schwab, H. Liao and L. Knopoff (1976), "Generation of Complete Theoretical Seismograms for SH-II," Geophys. J. R. Astr. Soc., 48, 531-536.

Mitchell, B. J. (1980), "Frequency Dependence of Shear wave Internal Friction in the Continental Crust of Eastern North America," JGR, (in press).

Murphy, J.R. (1969), Discussion of a paper by D. Springer, M. Denny, J. Healy and W. Mickey, "The Sterling Experiment: Decoupling of Seismic Waves by a Shot-Generated Cavity," JGR, 74, 6714-6718.

Nakanishi, K., F. Schwab and L. Knopoff (1977), "Generation of Complete Theoretical Seismograms for SH-I," Geophys. J. R. Astr. Soc., 48, 525-530.

Nuttli, O. W. (1973), "Seismic Wave Attenuation and Magnitude Relations for Eastern North America," JGR, 78, 876-885.

Panza, G. F. and G. Calcagnile (1975), "Lg, Li and Ry from Rayleigh Modes," Geophys. J. R. Astr. Soc., 40, 475-487.

Springer, D. L., M. Denny, J. Healy and W. Mickey (1968), "The Sterling Experiment: Decoupling of Seismic Waves by a Shot-Generated Cavity," JGR, 73, p. 5995.

Schwab, F. and L. Knopoff (1972), "Fast Surface Wave and Free Mode Computations," Methods in Computational Physics, Vol. II, Ed. B. A. Bolt, Academic Press, New York, 87-180.

Street, R. L. (1976), "Scaling Northeastern United States/Southeastern Canadian Earthquakes by Their Lg Waves," Bull Seism. Soc. Amer., 66, 1525-1537.